



Calibration and Performance of the AEDC/VKF Tunnel C, Mach Number 4, Aerothermal Wind Tunnel

W. T. Strike, Jr.
Calspan Field Services, Inc.

June 1982

Final Report for Period May 15 – December 18, 1981

**PROPERTY OF U.S. AIR FORCE
AEDC TECHNICAL LIBRARY**

Approved for public release; distribution unlimited.

**ARNOLD ENGINEERING DEVELOPMENT CENTER
ARNOLD AIR FORCE STATION, TENNESSEE
AIR FORCE SYSTEMS COMMAND
UNITED STATES AIR FORCE**

NOTICES

When U. S. Government drawings, specifications, or other data are used for any purpose other than a definitely related Government procurement operation, the Government thereby incurs no responsibility nor any obligation whatsoever, and the fact that the government may have formulated, furnished, or in any way supplied the said drawings, specifications, or other data, is not to be regarded by implication or otherwise, or in any manner licensing the holder or any other person or corporation, or conveying any rights or permission to manufacture, use, or sell any patented invention that may in any way be related thereto.


Qualified users may obtain copies of this report from the Defense Technical Information Center.

References to named commercial products in this report are not to be considered in any sense as an endorsement of the product by the United States Air Force or the Government.

This report has been reviewed by the Office of Public Affairs (PA) and is releasable to the National Technical Information Service (NTIS). At NTIS, it will be available to the general public, including foreign nations.

APPROVAL STATEMENT

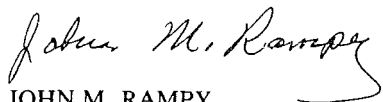
This report has been reviewed and approved.



LARRY M. DAVIS, 1Lt, USAF
Aerothermal and Aeropropulsion
Test Operations Manager
Deputy for Operations

Approved for publication:

FOR THE COMMANDER



JOHN M. RAMPY
Director of Aerospace Flight Dynamics Test
Deputy for Operations

UNCLASSIFIED

SECURITY CLASSIFICATION OF THIS PAGE (When Data Entered)

REPORT DOCUMENTATION PAGE		READ INSTRUCTIONS BEFORE COMPLETING FORM
1. REPORT NUMBER AEDC-TR-82-6	2. GOVT ACCESSION NO.	3. RECIPIENT'S CATALOG NUMBER
4. TITLE (and Subtitle) CALIBRATION AND PERFORMANCE OF THE AEDC/ VKF TUNNEL C, MACH NUMBER 4, AEROTHERMAL WIND TUNNEL		5. TYPE OF REPORT & PERIOD COVERED Final Report - May 15 - December 18, 1981
		6. PERFORMING ORG. REPORT NUMBER
7. AUTHOR(s) W. T. Strike, Jr., Calspan Field Services, Inc.		8. CONTRACT OR GRANT NUMBER(s)
9. PERFORMING ORGANIZATION NAME AND ADDRESS Arnold Engineering Development Center/DOF Air Force Systems Command Arnold AF Station, TN 37389		10. PROGRAM ELEMENT, PROJECT, TASK AREA & WORK UNIT NUMBERS Program Element 65807F
11. CONTROLLING OFFICE NAME AND ADDRESS Arnold Engineering Development Center/DOS Air Force Systems Command Arnold AF Station, TN 37389		12. REPORT DATE June 1982
		13. NUMBER OF PAGES 113
14. MONITORING AGENCY NAME & ADDRESS (if different from Controlling Office)		15. SECURITY CLASS. (of this report) UNCLASSIFIED
		15a. DECLASSIFICATION/DOWNGRADING SCHEDULE N/A
16. DISTRIBUTION STATEMENT (of this Report) Approved for public release; distribution unlimited.		
17. DISTRIBUTION STATEMENT (of the abstract entered in Block 20, if different from Report)		
18. SUPPLEMENTARY NOTES Available in Defense Technical Information Center (DTIC).		
19. KEY WORDS (Continue on reverse side if necessary and identify by block number) calibration pressure gages heaters Mach number wind tunnels cold flow interferograms dynamic pressure flow fields		
20. ABSTRACT (Continue on reverse side if necessary and identify by block number) The shakedown and calibrated characteristics of the new AEDC Mach Number 4 Aerothermal Wind Tunnel were experimentally identified at several test conditions. The nominal Mach number of the test core as defined by a 30-probe pitot pressure rake varied between nominally 3.95 and 4.0, depending on the test section Reynolds number and stilling chamber temperature. The overall variation in the stilling chamber pressure is nominally 15 to 180 psia, with		

DD FORM 1 JAN 73 1473

EDITION OF 1 NOV 65 IS OBSOLETE

UNCLASSIFIED

SECURITY CLASSIFICATION OF THIS PAGE (When Data Entered)

UNCLASSIFIED

SECURITY CLASSIFICATION OF THIS PAGE(When Data Entered)

20. ABSTRACT (Continued)

temperatures from 250 to 1,210°F for an overall Reynolds number range of 0.2 to 8.1 million per foot and true temperature-pressure altitude simulation from 56,000 to 105,000 ft.

UNCLASSIFIED

SECURITY CLASSIFICATION OF THIS PAGE(When Data Entered)

PREFACE

The work reported herein was performed by the Arnold Engineering Development Center (AEDC), Air Force Systems Command (AFSC) at the request of the Facilities Operations and Maintenance Division (DOFO), Directorate of Aerospace Flight Dynamics Test, AEDC. The tests and analysis were performed by Calspan Field Services, Inc./AEDC Division, operating contractor for the Aerospace Flight Dynamics testing effort at the AEDC, AFSC, Arnold Air Force Station, Tennessee. The test unit shakedown and initial calibration were performed in the von Kármán Gas Dynamics Facility (VKF), Tunnel C Mach 4 wind tunnel under AEDC Project Number C069VC and Program Element number 65807F during the periods of May 15 - 21, August 25 - 26, and October 23, 1981. Analysis of the calibration results was completed December 18, 1981. The Air Force Project Manager was Lt. L. M. Davis. The manuscript was submitted for publication on March 24, 1982.

The author gratefully acknowledges the supervision of the initial facility shakedown of the aerothermal unit provided by Mr. J. M. Langford (Project Engineer for the design and fabrication of the Aerothermal Wind Tunnel), Mr. P. G. Bryant (Wind Tunnel Installation Engineer), and Mr. D. T. Akers for providing the theoretical results which identified the structural and thermal limits of various components of this new test unit. Mr. D. W. Stallings provided background information and other useful suggestions in the preparation of this report.

CONTENTS

	<u>Page</u>
1.0 INTRODUCTION	
1.1 Background	7
1.2 Concept	8
1.3 Calibration Program	9
2.0 APPARATUS	
2.1 Plant Configuration	10
2.2 Test Facility	12
2.3 Test Articles	12
2.4 Test Instrumentation	13
2.5 Optical Systems	16
3.0 PROCEDURE	
3.1 Test Conditions	16
3.2 Test Procedures	16
3.3 Data Reduction	17
4.0 CALIBRATION RESULTS	
4.1 Operational Envelope	19
4.2 Test Section Calibration	21
4.3 Diffuser Performance	25
4.4 Mixing Chamber Performance	26
4.5 Bypass Line Characteristics	28
4.6 Control Valves	29
5.0 HEMISPHERE CYLINDER RESULTS	30
6.0 CONCLUDING REMARKS	31
REFERENCES	32

ILLUSTRATIONS

<u>Figure</u>	<u>Page</u>
1. Tunnel C Mach 4.0 Configuration	35
2. Definition of the Simulated Environment	36
3. Illustrated Aerothermal Problems	37
4. Altitude Duplication for Various Test Section Sizes and Mass Flow/Mach Number Ratios	38
5. The Mach 4 Aerothermal Wind Tunnel Circuit	39

<u>Figure</u>	<u>Page</u>
6. Test Section Survey Probes	41
7. Rake Installation and Orientations	42
8. Total Temperature Probe Locations in the Stilling Chambers	43
9. Bypass Line Flow Rate Control	44
10. Aerothermal Wind Tunnel Mixer Instrument Installation	45
11. Test Section and Diffuser Instrumentation	46
12. Hemisphere Model Instrumentation	47
13. True Temperature-Pressure Altitude Simulation	48
14. Aerothermal Wind Tunnel Reynolds Number Operating Envelope ($M = 4$)	50
15. Stilling Chamber Conditions for True Temperature - True Pressure Altitude Simulation	51
16. Thermal Heating Capacity in the Aerothermal Wind Tunnel Circuit	52
17. Aerothermal Wind Tunnel Power Consumption Rates	53
18. Summary of Mach Number Distributions Based on Pitot Probe Surveys	54
19. Lines of Constant Mach Number	58
20. The Effect of PT/\overline{PD} on the Test Section Rhombus at $X = 12$ in.	60
21. Typical Flow-Field Pictures	61
22. Test Rhombus Mach Number Calibration as a Function of Free-Stream Reynolds Number	63
23. Free-Stream Mach Number Axial Distribution	65
24. Mach/Flow Angularity Probe Results	69
25. Flow Angle Variations	71
26. Vertical Distribution of the Total Temperature Distribution in the Test Section	74
27. Lateral Survey of the Total Temperature Variation at $X = -18$ in., $M = 4.0$, $PT = 180$ psia, $TT = 1580^\circ R$, and $RE/ft = 3.3 \times 10^6$	75
28. Aerothermal (Tunnel C) Diffuser Performance	76
29. Variation of Pressure Ratio across the Aerothermal Wind Tunnel as a Function of PT	77
30. Effectiveness of the Thermal Insulation in the Mixing Chamber	78
31. Correlation between Mixing Chamber Baffle Temperature and the HB-3 Air Discharge Temperature	79
32. Pressure Drops through the Mixing Chamber	80
33. Mixing Chamber Dynamic Pressure Fluctuations	82
34. Power Spectral Density Distribution of a Typical Set of Mixing Chamber Pressure Fluctuation Measurements	84

<u>Figure</u>	<u>Page</u>
35. Pressure Fluctuations in HB-1 Bypass Air Supply Line	86
36. Power Spectral Density of the Pressure Fluctuations Recorded in the Bypass Line Downstream of Valve 554	87
37. Bypass Line and Valve Characteristics	89
38. Valve Performance in the Primary Flow Line Upstream of the Electric Heater HB-3	90
39. Shadowgram of the Hemisphere, $M = 3.95$, $PT = 180$ psia, and $TT = 1570^{\circ}R$	91
40. Interferogram of the Hemisphere, $M = 3.95$, $PT = 180$ psia, and $TT = 1570^{\circ}R$	92
41. Hemisphere Cylinder Pressure Distribution, Mach No. 3.95, $PT = 180$ psia, $TT = 1570^{\circ}R$, and $RE/ft = 3.3 \times 10^6$	93
42. Hemisphere Cylinder Heat Transfer Distribution, Mach No. 3.95, $PT = 180$ psia, $TT = 1570^{\circ}R$, and $RE/ft = 3.3 \times 10^6$	94

APPENDIXES

A. TEST SECTION FREE-STREAM PROPERTIES	95
B. REAL-GAS CORRECTION FACTORS	103
NOMENCLATURE	110

1.0 INTRODUCTION

The operating characteristics of a new AEDC test unit, the Mach Number 4 Aerothermal Wind Tunnel shown in Fig. 1, were recently evaluated at several operating conditions. The overall variation in stilling chamber pressure and temperature was 15 to 180 psia and 250°F to 1,200°F respectively, providing an overall Reynolds number capability of 0.2 to 8.1 million per foot. This operating range includes true temperature and pressure simulation at altitudes from 56,000 to 105,000 ft. This document contains a description of the background, calibration program, operating characteristics, and test section calibration of this aerothermal wind tunnel.

1.1 BACKGROUND

In the earlier years of wind tunnel testing in the supersonic flight regime, the major concern was the measurement of the aerodynamic characteristics (or performance) of flight vehicles. The primary total temperature requirement for these test units was that the total enthalpy of the flow in the wind tunnel be high enough to prevent air liquefaction. As the magnitude of the nozzle expansion (that is, the test section Mach number) increased, the total temperature of the wind tunnel flow was increased just enough to prevent air liquefaction, as noted in Ref. 1. Unfortunately, the resulting test section ambient temperature in a conventional wind tunnel varies from atmospheric temperatures at low supersonic speeds (Mach numbers less than 2) down to only 90 to 100°R (−360°F) at the higher supersonic/hypersonic speeds and therefore does not simulate flight conditions.

Until the recent decade, relatively little attention was given to aerothermal testing (true temperature – true pressure altitude simulation) in these so-called “cold-flow” facilities because of the low stagnation temperatures which were available. Prior to this decade, current aircraft development was primarily dependent on lower Mach number-altitude simulation. As shown in Fig. 2, the simulation requirements for current aircraft fall generally in the lower Mach number range where wind tunnel stagnation temperature requirements in the range of 300 to 600°F were adequate. In fact, a total temperature capability of only 300°F covered a large portion of the low supersonic flight envelope.

As high-temperature materials and more powerful propulsion systems were developed, flight at the higher supersonic speeds became more feasible. However, as aircraft and, particularly, missiles and reentry vehicles began to operate in this higher enthalpy flight regime, a variety of new aerothermodynamic problems appeared. As suggested in Fig. 2, it is apparent that an advanced aircraft capable of sustained flight at Mach number 3 will require a wind tunnel test simulation at stagnation temperatures greater than 700°F. Similarly, a missile carried and fired by such an aircraft flying at Mach 3 could be expected to operate at

Mach number 4 and require a wind tunnel simulation with an operating stagnation temperature in excess of 1,100°F. Besides the obvious structural problems which will occur under these conditions, many other problems will arise. For example, missile radomes or infrared (IR) domes may experience structural failures like those shown in Fig. 3a, or in less severe cases, the dome may transmit distorted information to the onboard sensors, resulting in the failure of the missile's mission. In another area, the performance of internal missile components such as the battery output shown in Fig. 3b may be degraded when the vehicle is exposed to high-temperature soaking for long periods of time. The problem of increased thermal loading at critical locations within the vehicle may involve a complex combination of convective, conductive, and radiation heat transfer rates. The complex geometries and combination of materials in the vehicle's construction may result in a situation which is not amenable to reliable numerical evaluations and for which testing must be accomplished under conditions duplicating the flight environment and hardware.

A ground testing unit with a known uniform test Mach number, flow angle, and total temperature distribution which is also free of undesirable flow contaminants (particles) is needed for this flight simulation. Most conventional wind tunnels are of reasonable size but cannot match the flight temperatures. Existing high enthalpy tunnels are usually impulse or blowdown facilities with limited run times, flow contaminants, and usually with nonrepeatable aerodynamic environments (flow field and thermal nonuniformities).

1.2 CONCEPT

In the late 1970's, a study was completed at AEDC to evaluate the existing test capabilities and to propose design modifications to add an aerothermal wind tunnel test capability. A major consideration was to make maximum use of existing compressor plant capability, ducting, heaters, model support equipment, tunnel instrumentation, computer support, and optical coverage. The von Kármán Facility (VKF) compressor plant, ducting, and heater capability were evaluated in terms of existing mass flow, pressure, and temperature availability. A proposal was conceived to use the mass flow rate and heater capabilities of the Mach 10 Hypersonic Wind Tunnel (Tunnel C) to produce test section flow conditions which would simulate the ambient pressure and temperature of a supersonic flight condition. Obviously, it was necessary to compromise between test section size and the duplicated altitude for a given Mach number. To aid in this decision, the continuity equation for isentropic flow of a perfect gas was formulated as follows:

$$\dot{m}/(M \cdot A) = 0.9188P/\sqrt{T} \quad (1)$$

The terms on the right, namely P and T, the ambient pressure and temperature, respectively, are a function of the simulated altitude. The terms on the left are dependent on the available

plant mass flow rate (\dot{m}), test core area (A), and the free-stream Mach number (M). This relationship is shown in Fig. 4. The inviscid area of the test core was assumed to be 4 percent smaller than the design geometric area and would account for the growth of a nozzle wall turbulent boundary layer.

The AEDC plant consists of 13 compressors driven by ten motors with a total power of 92,500 hp (Ref. 2). The machines are arranged to provide up to nine stages of compression. For a Mach number 3 or 4 nozzle in the existing Tunnel C circuit, the optimum plant configuration produces a mass flow rate of nominally 110 lbm/sec as shown in Fig. 4. Superimposing this plant operating condition on these results shows that increasing the tunnel Mach number increases the simulated altitude for a given test section size; alternately, decreasing the test section size reduces the simulated altitude. As a compromise between altitude and model size (or more precisely, test section size), a 25-in.-diam test section size with a Mach number 4 nozzle was selected to produce test conditions equivalent to an altitude of 56,000 ft. The results of this design study were implemented and ultimately resulted in the present aerothermal 25-in.-diam test core, Mach 4.0 nozzle test unit which was fabricated and installed in the existing Tunnel C circuit for evaluation under the present shakedown and calibration program.

1.3 CALIBRATION PROGRAM

The Mach Number 4 Aerothermal Wind Tunnel provides a unique, continuously operating test facility for simulating environmental pressures and temperatures existing at altitudes above 56,000 ft. The test unit provides a clean air, low turbulence, reasonably sized test core (maximum diameter of nominally 23 in.) Mach 4 free-stream testing capability for: (1) simulating the true, forced convective external heat transfer and internal conduction rates experienced by flight hardware components; (2) providing more accurate heat transfer measurements at supersonic speeds because of the higher total enthalpy of the free-stream flow; and (3) improving the evaluation of cold-wall (model) aerodynamic effects by providing a test unit where it will be more feasible to simulate, in some cases, the more realistic lower ratios of reentry body wall to free-stream stagnation enthalpy. The purpose of this study is to evaluate the overall performance of this aerothermal wind tunnel and to document the results and existing capabilities of this facility as defined by the shakedown and initial calibration. A detailed description of the shakedown and calibration program is given in Ref. 3.

The shakedown/calibration program objectives were to identify, establish, and evaluate the operational characteristics of the Tunnel C Mach 4 Aerothermal Wind Tunnel installation. The shakedown phase of the program included the establishment of safe, reliable, and repeatable tunnel starting procedures, confirmation of the normal wind tunnel

running modes, and tunnel shutdown procedures. Also, structural corrections were made as failures and weak elements in tunnel circuit components were identified during the shakedown. These problems are detailed in Ref. 3 and will not be discussed in depth in this report. For tunnel flow modeling purposes, the performance or calibration of major flow controlling devices such as valves, orifices, and mixing chambers in the circuit, was identified and documented, and air heating capabilities in the tunnel circuit were established.

The calibration phase includes surveys of the free-jet Mach number 4 test core to establish the test core size and shape, the Mach number uniformity, the local flow angle variations, and the test section total temperature distribution. The flow-field surveys were obtained by using a single rake containing an array of 30 pitot probes across a 44-in. span, three equally-spaced Mach/flow angularity probes spanning 8 in., and 13 equally-spaced total temperature probes spanning 24 in. This rake was translated axially 32 in. and laterally from the centerline 7 in.; therefore, the overall dimensions of the survey envelope were 32-by 7- by 44-in. (based on the array of pitot probes). The calibrations were conducted at several test conditions covering a Reynolds number range of 0.2 to 8.1 million per foot, stilling chamber pressure and total temperature ranges of 15 to 180 psia, and 710°R (250°F) to 1660°R (1,200°F), respectively.

To demonstrate that the Tunnel C testing techniques, instrumentation, and data acquisition systems could be used in this new aerothermal wind tunnel installation, a few sets of surface pressure and heat transfer rate distributions on a hemisphere were also obtained. This short sequence of tests also demonstrated that no problems were encountered with the free-jet test core when a model was injected into the test core using the existing Tunnel C model inject/retract system. In addition, a few holographic interferograms were recorded to check on the tunnel flow quality as revealed by the uniformity of the fringe patterns and to demonstrate the quality of the optical coverage available in the aerothermal installation.

2.0 APPARATUS

2.1 PLANT CONFIGURATION

Either seven or nine stages of compression can be used to produce the pressure ratio and mass flow requirements needed to operate the continuous flow aerothermal supersonic wind tunnel. The maximum discharge air pressure and temperature from the seventh stage are nominally 1,200 psia and 720°R, respectively. The corresponding maximum mass flow rate produced by this plant configuration is about 110 lbm/sec. An alternate plant configuration using nine stages of compression normally used for the Mach 10 nozzle operation was also evaluated. This configuration produces a maximum ninth stage discharge pressure of 2,700 psia, temperature of 780°R (320°F), and mass flow rate of 62 lbm/sec.

There are two air heaters in the plant circuit: a gas-fired heat exchanger (designated HB-1) and an electric heater (designated HB-3). The rated heating capacity of the gas-fired heater is 17,000 Btu/sec, and the electric heater is rated at 10,000 Btu/sec. In the normal operating mode with seven stages of compression, these two heaters are operated in parallel as shown in Fig. 5a; with nine stages of compression, these two heaters operated in series, as shown in Fig. 5b.

2.1.1 Parallel Heater (or Standard) Circuit

The parallel heater mode of operation provides a maximum mass flow rate of 110 lbm/sec and aerothermal stagnation temperatures up to nominally 1660°R (1,200°F). A simplified schematic of this plant configuration (Fig. 5a) shows that the flow from the seventh stage of compression passes through Valve 441 to a point just upstream of HB-1 and divides into two paths. Some of the flow passes through the HB-1 heater, while the remainder proceeds directly to the Tunnel C HB-3 heater. The maximum allowable flow rate through HB-3 is nominally 62 lbm/sec. The control valve in the discharge (bypass) line of HB-1, Valve 554, and/or the valve upstream of the HB-3, Valve 454, determine how much of the total flow rate passes through each leg of this parallel heater circuit. Although the flow rates through the two branches of the parallel circuit can be adjusted by setting valves 454 and 554 properly, the normal operational mode puts nominally one-fourth of the flow through HB-3 (primary flow) and three-fourths through HB-1 (bypass flow).

Prior to entering the mixing chamber, the bypass flow from HB-1 is again divided (trace the bypass line in Fig. 5a) into three streams. The two bypass flow lines enter the mixing chamber directly opposite each other, and the primary flow from HB-3 intersects these two opposing streams as it flows along the mixer axis. A set of two baffles and five screens within the mixing chamber is used to mix these three air streams, two of which are at different temperatures (the maximum difference is 600 to 800°F), and to attenuate the pressure fluctuations (turbulence) of the flow entering the stilling chamber. This aerothermal circuit is completed when the flow discharges as a free jet from the Mach number 4 nozzle into the existing Tunnel C test section and then returns to the first stage inlet as shown in Fig. 5a. In this mode of operation, the maximum pressure in the Mach 4 stilling chamber is presently 180 psia.

2.1.2 Series Heater (Tunnel C) Circuit

An alternate tunnel circuit system which places both heaters in series (i.e., the same circuit presently used to operate the Mach 10 nozzle) was also evaluated with the Mach 4 aerothermal test unit in the circuit as shown in Fig. 5b. The line to Valve 554, used in the parallel heater operation, is manually switched and reconnected to Valve 254 with Valve 454

closed. This puts the two heaters in series. All the flow enters HB-1 where it is heated to 1350°R (900°F) and then passed through Valve 254 to the electric heater, which boosts the air flow up to nominally 1660°R (1,200°F). In this mode of operation, the maximum pressure in the Mach 4 stilling chamber is 100 psia.

2.2 TEST FACILITY

The Mach 4 Aerothermal Wind Tunnel is a closed-circuit, high-temperature, supersonic free-jet wind tunnel with an axisymmetric contoured nozzle and a 25-in.-diam nozzle exit. The tunnel utilizes parts of the Tunnel C circuit (for example, the electric air heater and the Tunnel C test section) and presently operates continuously over a range of pressures from nominally 15 psia at a minimum stagnation temperature of 710°R to 180 psia at a maximum temperature of 1570°R. Using the normal Tunnel C Mach 10 circuit (heaters in series), the Aerothermal Mach 4 nozzle was operated at a maximum pressure and temperature of 100 psia and 1660°R, respectively. The air temperatures and pressures are normally achieved by mixing high-temperature air [up to 2250°R (1,790°F)] from the electric heater with the bypass flow from the natural gas-fired air heater [up to 1420°R (960°F)]. The primary and bypass air flows discharge into a mixing chamber just upstream of the aerothermal tunnel stilling chamber. The entire aerothermal nozzle insert (the mixing chamber, throat, and nozzle sections) is water cooled by integral, external water jackets. Since the test unit utilizes the Tunnel C model injection system, it permits the removal of the model from the test section while the free-jet tunnel remains in operation. A description of the Tunnel C equipment may be found in Ref. 2.

2.3 TEST ARTICLES

A rake used to survey the test section flow field was instrumented with thirty 0.093-in.-diam pitot probes, thirteen 0.065-in.-diam single-shielded total temperature Chromel®-Alumel® thermocouple probes, and three 0.312-in.-diam blunt 20-deg half-angle cone Mach/flow angularity probes (see Fig. 6). The orientation of the rake and the numbering system adopted to identify the probe locations are shown in Fig. 7. All probes were numbered in sequence starting with the lower probes (the ones closest to the model inject/retract tank). Pitot probe number 16 was located on the nozzle axis and was the rake reference point for all other probe locations.

2.3.1 Survey Hardware

The X-Y probe drive mechanism designed and fabricated at AEDC is a nonretractable system with a nominal survey envelope of 35 in. in the axial direction and up to 7 in. in the lateral direction. This mechanism can be mounted on the top port of Tunnel B or C. Any

probe pitch and vertical alignment must be made manually with the tunnel vented to atmospheric conditions.

An electric motor with a digitized potentiometer readout is used to drive and monitor the location of the X-Y mechanism. This unit is used primarily to survey the wind tunnel test section flow.

2.3.2 Single-Shielded Thermocouple Probes

As shown in Fig. 6b, the stainless steel tube shield for the thermocouple junction had an 0.065-in. OD with a 0.009-in. wall thickness, and the junction was located nominally 0.5 in. from the probe tip face. Two vent holes located diametrically opposite each other were 0.016 in. in diameter. Strength was added to the probe by encasing it in two larger tubular sleeves, one 0.093-in.-diam and the other 0.125-in.-diam as shown in Fig. 6b. No correction for total temperature probe recovery factor was applied to the present total temperature data since the primary purpose of these probes was to assess the tunnel total temperature uniformity within the test core. The uniformity did not deviate by more than 3 percent from the aerothermal stilling chamber total temperature measurement. All flow-field total temperature probes were designed and fabricated at AEDC.

2.3.3 Mach/Flow Angularity Probes

The stainless steel Mach/flow angularity probes were also designed, fabricated, and calibrated at AEDC and consisted of blunt 20-deg half-angle cone-cylinders instrumented with one nose or pitot pressure tap and four cone surface static pressure taps (see Fig. 6c). These surface pressure taps were located 0.150 in. from the probe nose and spaced circumferentially in 90-deg increments. The circumferential taps are sensitive to variations in local flow direction while the average of these static pressures ratioed to the cone nose probe pitot pressure is sensitive to the local free-stream Mach number (see Ref. 4). In this calibration, the variation in the cone surface static pressure differentials between two diametrically opposite surface pressures was used to evaluate the changes in flow field angle sensed by each of the three probes on the rake. The vertical spacing between the three probes was nominally 4 in. and displaced laterally from the reference pitot probe (No. 16) 1.18 in. (see Fig. 7).

2.4 TEST INSTRUMENTATION

The measuring devices, recording equipment, and calibration methods for all measured parameters are documented in Ref. 3, along with the estimated uncertainties. To minimize

the pressure stabilization time, the tunnel circuit and probe pressure transducers were mounted, whenever practical, as close to the probes as possible. The locations of the more significant pressure and temperature measurements in the tunnel circuit are summarized in the following sections.

2.4.1 Primary Supply Line

The discharge pressure and temperature from the seventh stage of the plant which supplies both the primary and bypass air systems were recorded. The flow-field properties (PTC and TTC) in the primary line were measured downstream of HB-3 in the Tunnel C Mach 10 nozzle stilling chamber instrument ring. Two total pressures (which are actually wall statics that are not shown) and seven total temperatures were recorded (see Fig. 8) and used to compute the mass flow through the Mach 10 throat which has a cross-sectional throat area of 2.39 sq in.

2.4.2 Bypass Supply Line

In the May entry of this test program, the total pressure and temperature upstream of a sonic valve (V554) were recorded. Since the effective area of this valve was not known, the mass flow through the valve was deduced by subtracting from the flow rate through the Mach 4 nozzle (the aerothermal test unit), the Mach 10 nozzle flow rate (that is, $\dot{m}_B = \dot{m} - \dot{m}_C$).

Prior to the August 1981 tunnel entry, as shown in Fig. 9, Valve 554 (V554) was removed and found to be structurally defective; it was subsequently replaced by a sonic orifice which simulated the condition when V554 was fully open. The total pressure and temperatures were still measured upstream of the orifice, but the mean and fluctuating pressures were also recorded upstream of the first and second baffles in this bypass supply line. The baffles were added to this line to force the flow leaving the valve or sonic orifice to fill the 11.8-in.-diam bypass line and therefore reduce the intense pressure fluctuations produced by the flow discharging from V554 which were observed in the initial bypass line geometry. The mean and fluctuating pressure transducers located immediately upstream and downstream of the baffles in the mixing chamber (see Section 2.4.3) were removed and reinstalled in the bypass line as described previously.

The final geometry of the bypass line in the region of V554 is shown in Fig. 9c. The total pressure and temperature upstream of the valve will continue to be part of the basic instrumentation setup for the aerothermal wind tunnel operation to aid in the evaluation of the flow rate in the bypass line.

2.4.3 Mixing Chamber

Figure 10 shows a cross section of the mixing chamber illustrating the location of all instrumentation in the region where the primary and bypass flows mix. Six thermocouples were tacked to the downstream section of the first baffle to monitor the temperature gradient along this baffle and also to detect any thermal nonuniformity of the airstream in the mixer. The remaining seven thermocouples were located at various points on either side of the insulation between the inner and outer shell of the mixer.

The mean and fluctuating pressure levels were recorded at four points along the mixer. These points were located where the primary flow discharged into the mixer, upstream of the first baffle, downstream of the second baffle (upstream of the first screen), and downstream of the last screen, that is, in the Mach 4 aerothermal stilling chamber instrument ring (see Fig. 10). This instrument ring also contains ten thermocouple probes (shown in Fig. 10), but it was necessary to record only seven of these temperatures in this shakedown/calibration, as indicated in Fig. 8.

2.4.4 Test Section

Four static pressure taps were flush-mounted to the discharge end of the Mach 4 nozzle (see Fig. 11a). Also, the surface pressure and temperature on the flange between the Mach 4 nozzle and the exiting 50-in.-diam Tunnel C section were recorded (see Figs. 7 and 11a).

Downstream of the test section, in the initial portions of the diffuser, four wall static pressure measurements were recorded to detect any changes in the diffuser pressure which would indicate possible blockage problems. Relative to the midpoint between the two test section windows, these taps were located 152.3, 201.1, 252.3, and 302.1 in. downstream (see Fig. 11b).

2.4.5 Hemisphere

A stainless steel hemisphere, designed and fabricated at AEDC, was instrumented with 28 pressure taps, 17 coaxial surface thermocouples, three thermopile heat-flux gages (Gardon type), and one Schmidt-Boelter heat-flux sensor. The instrumentation locations on this 5.8-in.-diam hemisphere are shown in Fig. 12. Prior to the test entry, the nose surface roughness was at least 11 $\mu\text{in.}/\text{in.}$ Following the entry, it increased to more than 27 $\mu\text{in.}/\text{in.}$, still an acceptable model finish.

2.5 OPTICAL SYSTEMS

The standard single-pass optical flow visualization system was used to record shadowgraph pictures of selected test conditions. In addition, a few selected holographic results were obtained to reconstruct finite fringe interferograms of the flow through the test section and around the 5.8-in.-diam hemisphere. These results are discussed in Section 5.0.

3.0 PROCEDURE

3.1 TEST CONDITIONS

A summary of the primary test conditions is given below.

Mach	PT, psia	TT, °R	P, psia	T, °R	RE/ft $\times 10^{-6}$
3.93	13	1,334	0.094	315	0.3
3.94	26	1,461	0.184	348	0.5
↓	29	1,673	0.200	423	0.5*
	56	1,556	0.385	373	1.0
	99	1,659	0.677	418	1.7*
	110	1,570	0.759	377	2.0
	166	1,573	1.146	378	3.0
↓	179	1,567	1.230	376	3.3**
3.95	40	973	0.280	230	1.5
3.96	132	711	0.881	169	8.1

*Conditions established with the two heaters operated in series

**Hemisphere cylinder data acquired at this test condition only

Test section flow-field surveys (i.e., tunnel calibrations) were made at each of these test conditions, and the tunnel circuit parameters (i.e., operating condition) were recorded at these and other intermediate test conditions. Plots of nominal free-stream conditions as a function of stilling chamber pressure, PT, are given in Appendix A.

3.2 TEST PROCEDURES

The initial shakedown and calibration of the Mach 4 Aerothermal Wind Tunnel was conducted in a series of distinct steps. Basically, two types of data were recorded as the program progressed. Once an intermediate test condition was reached, the mean pressure

and temperatures of various tunnel components, the air flow through the duct, and the four mixer section fluctuating pressure measurements were recorded. At each final test condition in the operating envelope, the flow in the test section (in the free jet from the Mach 4.0 nozzle) was surveyed with the X-Y probing mechanism supporting the rake which contained 30 pitot probes, 13 total temperature probes, and three flow angularity probes. The survey rake was translated laterally 8 in. from the tunnel centerline and docked; then the hemisphere cylinder was injected into the test rhombus to record hemisphere pressure and heat transfer results. A detailed description of the test procedure is documented in Ref. 3.

3.3 DATA REDUCTION

The mass flow rates, pressure, and temperature in the primary and bypass lines, and the test section conditions were recorded and computed as follows. These equations include the known cross-sectional areas of the Mach number 10 and Mach number 4 nozzle throats:

1. Primary mass flow rate (2)

$$\dot{m}_C = 1.2730 \text{ PTC} / \sqrt{\text{TTC}}, \text{ lbm/sec}$$

2. Aerothermal tunnel mass flow rate (3)

$$\dot{m} = 23.471 \text{ PT} / \sqrt{\text{TT}}, \text{ lbm/sec}$$

3. Bypass flow rate (4)

$$\dot{m}_B = \dot{m} - \dot{m}_C, \text{ lbm/sec}$$

The effective discharge area of V554, a sonic valve, or the sonic orifice which was later substituted for this valve was defined as follows:

$$\text{Area} = 1.881 \dot{m}_B \sqrt{\text{TTB}/\text{PTB}}, \text{ in.}^2 \quad (5)$$

The Mach 4 test section conditions, like the Mach 10 Tunnel C conditions, were adjusted for real-gas effects (Appendix B) as follows:

$$\text{Real Gas Property}/(\text{Perfect Gas Property}) = \sum_{i=1}^2 \sum_{j=1}^3 A_{ij} \text{PT}^{i-1} \text{TT}^{j-1} \quad (6)$$

Perfect gas relationships were used to define the free-stream parameters in terms of the stilling chamber properties; then the results were adjusted to include the real-gas effects. The real-gas properties are based on the Beattie-Bridgeman equation of state for air which was used to define the coefficients A_{ij} (see Table 1, Appendix B) of the curve fits.

3.3.1 Flow-Field Surveys

At each point in the survey (that is, for each X position), the data were sampled once, and the results were recorded and reduced to final form. The pitot probe pressures were normalized by the Mach 4 nozzle stilling chamber. The real gas-to-perfect gas ratio based on the stilling chamber parameters (PT and TT) was used to interpret the corresponding perfect gas ratio before the adiabatic perfect gas relationships were used to define the local Mach number.

$$(PP/PT)_{\text{perfect}} = (PP/PT)_{\text{measured}}/R(PP/PT) \quad (7)$$

where $R(PP/PT) = (\text{Real-gas value of } PT_2/PT)/(\text{Perfect gas value of } PT_2/PT)$

No corrections for Reynolds number effects or radiation were applied to the total temperature measurements made by the probes on the test section rake.

The Mach/flow angularity results, namely the surface static pressures, were used in the following manner to compute the local flow angle:

$$ALPHAO = -\left\{ (P_1 - P_3)/PPS \right\}_0 / \text{ETA}, \text{ the first point in the survey.}$$

Therefore,

$$ALPHAF = \left\{ (P_1 - P_3) / PPS \right\} / \text{ETA} - ALPHAO \quad (8)$$

PSIO = $\left\{ (P_2 - P_4)/PPS \right\}_0 / \text{ETA}$, also the first point in the survey, and PSIF is defined in the same manner as ALPHAF.

ETA = $0.033 (0.8894 \text{ MACH} - 2.5574)$, a curve fit of the theoretical variation in the cone surface pressure differential (two pressure taps 180-deg apart) across a 20-deg sharp cone at small angles of attack (see Ref. 4) as a function of small changes in free-stream Mach number relative to Mach = 4.0. These probes can only be used to define the relative variation in the local flow angle, since the absolute alignment of each probe relative to the nozzle axis was not evaluated. See Fig. 6 for probe pressure identification.

3.3.2 Hemisphere Data

The surface-mounted coaxial thermocouple time histories were reduced as described in Ref. 5 to produce the heat transfer results. The sampling interval for these data was 0.058 sec between data points, starting from the time when the model lifted off from the inject/retract position and ending 4 to 5 sec after the model reached the tunnel centerline.

The equilibrium pressure prediction technique (Ref. 6) was used to process the transient pressure time history results. As in the case of the heat transfer results, the data were scanned at a rate of 0.058 sec per point until 40 points in the pressure time history were obtained. Using this time history, the stable pressure (PW) was computed and tabulated.

4.0 CALIBRATION RESULTS

4.1 OPERATIONAL ENVELOPE

The existing and proposed operating envelope of the Aerothermal Mach Number 4 Wind Tunnel is shown in Fig. 13 in terms of the measured stilling chamber pressure (PT) and temperature (TT). The solid line denotes the present operating envelope. If the structural limits under the present thermal loading of 1,200°F are subsequently found to be adequate at 1,440°F* and a lower stilling chamber pressure, the present operating envelope will be extended as shown by the dashed curve. The maximum stilling chamber pressure is a function of the ratio of the flow rates through the primary and bypass lines, the heater efficiencies, and the maximum mass flow rate produced by the plant.

The solid symbols in Fig. 13 indicate the stilling chamber conditions at which flow-field surveys were made in the test section. In general, these calibrations were made close to the outer limits of the operating envelope. Superimposed on the envelope are the corresponding true altitude (ambient pressure and temperature) conditions that can be simulated in the aerothermal wind tunnel. At the elevated stagnation temperatures, the average test core Mach number is closer to 3.95 than 4.0. Also note that there is a break in the curve and ordinate between the minimum temperature level 720°R and 1500°R in Fig. 13.

Presently, the normal minimum operating ratio of \dot{m}_B/\dot{m}_C for a mixture of bypass flow (\dot{m}_B) with primary flow (\dot{m}_C) is nominally 3.0. Under these conditions, with both heaters operating within their maximum output capability, the maximum total temperature attained in this initial calibration was nominally 1580°R at a total pressure of 180 psia. Since the heaters are performing as anticipated, a reduction of the mass flow mixture ratio to a value

less than 3.0 and a slight increase in the HB-3 heater output will increase the maximum stilling chamber operating conditions by about 6 percent beyond the levels reached in this calibration and produce total pressure and temperature conditions equal to the design values for parallel heater circuit operation ($PT = 190$ psia and $TT = 1580^{\circ}\text{R}$ ($1,120^{\circ}\text{F}$) shown in Fig. 13. With both heaters operating at the maximum heating capacity, the variation in the mass flow rate with an optimum reduction in the mixture ratio (\dot{m}_B/\dot{m}_C) defines the upper nonlinear right-hand side of the operating envelope shown in Fig. 13.

The decrease in PT with TT that defines the right side of the envelope ($PT = 190$ psia, $TT = 1580^{\circ}\text{R}$ to $PT = 125$ psia, and $TT = 720^{\circ}\text{R}$) is attributable to the mass flow rate limitations of the seven-stage compressor plant configuration. The present wind tunnel shakedown indicates that the minimum operating conditions are nominally atmospheric pressure (the left vertical boundary) and the plant heat of compression which is normally 720°R (260°F), the lower horizontal boundary.

Most of the test section surveys were made using the parallel heater circuit with seven stages of compression. The two surveys at nominally 1660°R were obtained with the series heater circuit with nine stages of compression, which is the normal Tunnel C operating mode. In this series heater circuit operating mode, less thermal strain is placed on the electric heater, but the operating envelope does not extend beyond a PT of 100 psia.

Figure 13 shows that the Aerothermal Mach 4 Wind Tunnel has an actual average test section Mach number closer to 3.95 and can simulate a true pressure and temperature altitude from 56,000 to about 105,000 ft. This covers a Reynolds number range of 0.3 to 3.4 million per foot.

The test section free-stream Reynolds number envelope of the aerothermal tunnel is summarized in Fig. 14. The test conditions at which test section surveys were made are again indicated by the solid symbols. Note that the maximum Reynolds number of nominally 8 million per foot was achieved at the minimum stagnation temperature which was actually lower than the expected minimum stagnation temperature. It is conceivable that on any given day, depending on the prevailing atmospheric conditions and the size of the model in the tunnel, the minimum operating conditions can be lower than those already identified in Figs. 13 and 14.

The stilling chamber conditions required to produce true ambient temperature - pressure conditions at a given altitude for the calibrated average test section Mach number in the aerothermal wind tunnel are given in Fig. 15. For example, an altitude simulation of 80,000 ft based on the tables in Ref. 7 requires a stagnation pressure of 58 psia and temperature of 1574°R ($1,114^{\circ}\text{F}$) for a Mach number of 3.95. Real-gas effects are included in the results given in Fig. 15.

The heating capacity of the two heaters, HB-1 and HB-3, is given in Fig. 16. As shown, the upper mass flow limitation through the electric heater (HB-3) is 60 to 62 lbm/sec, whereas 110 lbm/sec can be passed through the gas-fired heater. The discharge temperature of the air from these heaters is dependent upon the temperature of the air entering the heater and the air heater exchange efficiency. As noted by the solid symbols, the maximum air temperature of 2260°R was achieved at a mass flow rate of 22 lbm/sec in HB-3, and 1420°R at 80 lbm/sec in HB-1. As noted earlier, the heating capacity of HB-3 is 10,000 Btu/sec, and of HB-1, 17,000 Btu/sec. For parallel heater circuit operations, the inlet temperature normally varies somewhat between 710 and 760°R for both heaters.

The power required to operate this facility is given in Fig. 17. The power usage is a function of the mass flow requirement and/or plant staging configuration and the power needed to heat the air. These curves are based on actual power usage rates recorded during the present shakedown and calibration of the aerothermal wind tunnel. An equation for computing the mass flow rate in terms of the required test stilling chamber pressure and temperature is included in the figure.

4.2 TEST SECTION CALIBRATION

All results presented are for the heaters in parallel unless otherwise noted.

4.2.1 Test Rhombus

The Mach number results of four typical pitot probe flow-field surveys are presented in Fig. 18 to show that the shape of the free-jet test section rhombus is independent of the stilling chamber operating conditions. These are carpet plots of the Mach number distribution at six selected stations through the test section. Each profile has been shifted in proportion to the axial location of the profile. Superimposed on the plots is the location of the Aerothermal Mach 4 nozzle exit and the existing Tunnel C test section windows. The midpoint between the test section windows was arbitrarily selected as a zero station.

The pitot pressure flow-field surveys normalized by the measured stilling chamber pressure were used to evaluate the corresponding real-gas local stream Mach numbers presented in Fig. 18. As suggested by these results, the Mach number variation within the supersonic core of this free jet is quite uniform. Outside the core, the flow is expanding rapidly to higher velocity. The overall length of the surveyed rhombus is 32 in., and varies in diameter from 23 in. at the forward survey station (− 19.5 in.) to slightly less than 8 in. at the aft station (12 in.).

A comparison of the four carpet plots given in Figs. 18a through 18d shows that the general shape of the test rhombus is not significantly affected by tunnel operating conditions. The average Mach number within the test core tends to be slightly higher at the lower stilling chamber temperatures (compare Fig. 18a with Figs. 18b through 18d). The results in Fig. 18a were obtained at the maximum free-stream Reynolds number; the results in Fig. 18b at the minimum Reynolds number; and the results in Fig. 18c at the maximum stilling chamber pressure and temperature. The results in Figs. 18a-c were obtained during the parallel heater circuit calibration, whereas the result presented in Fig. 18d was obtained at a higher stilling chamber temperature during the series heater circuit operations.

The variation in the local stream velocity outside the test rhombus is shown in Fig. 19. The local Mach numbers defined between the test rhombus and the free-jet imbedded shock (see discussion of Fig. 20) were based on the ratio of the stilling chamber pressure (PT) to the locally measured pitot probe pressure. Outside of the imbedded shock region, the local Mach numbers were based on the ratio of the measured static pressure or the minimum probe pitot pressure recorded in the quasi-ambient region surrounding the free jet to the locally measured pitot probe pressure. This technique provided a reasonable experimentally based estimate of the velocity distribution outside of the test rhombus. Lines of constant Mach number in the flow field outside the test rhombus have been connected to show the variation in Mach number in the expanding supersonic portion of the free jet. These results illustrate the effect of varying the pressure ratio across the nozzle, that is, the ratio of the tunnel stilling chamber pressure to the average static pressure in the wind tunnel diffuser (PT/\overline{PD}). In Fig. 19a, the maximum pressure ratio, PT/\overline{PD} , is 474 and in Fig. 19b, a lower pressure ratio, PT/\overline{PD} , is 44, or ten times smaller. Although the test rhombus size and shape remained fairly constant, the free-jet plume outside this rhombus at the higher nozzle-to-diffuser pressure ratio expanded to higher local stream velocities.

Figure 20 is a plot of the pitot pressure profile obtained at the aft test section station for various ratios of PT/\overline{PD} . This figure clearly shows, as expected, the variation in PT/\overline{PD} affects only the expanding supersonic flow field outside of the free-jet supersonic test core rhombus. The abrupt increase in the pitot pressure, for example, at $Z = 12$ in. for the profile where $PT/\overline{PD} = 44$, indicates the expected presence of an imbedded shock wave in the free-jet plume. A reduction in this ratio PT/\overline{PD} to 36.4 causes the flow from the Mach 4 nozzle to break down; the test rhombus decreases in size and the Mach number within the rhombus begins to decrease. As shown in Fig. 20, the diameter of the aft section of the test rhombus where the Mach number was nominally 3.94 decreased from nominally 8 in. to less than 2 in. when PT/\overline{PD} was reduced from 44 to 36.4. There was an abrupt increase in pitot pressure from $Z = 1$ in. to $Z = 2$ in. when PT/\overline{PD} equaled 36.4.

An attempt was made to operate the aerothermal wind tunnel with the first stage of compression removed (i.e., at increased backpressure). The results in Fig. 21 (a comparison of Fig. 21a with 21b) show that the removal of the first stage and the associated increase in pressure downstream of the nozzle caused the flow to become partially blocked. These photographs were made in the aft window of the Tunnel C test section. Figure 21b illustrates the type of flow field blockage encountered in the aerothermal free-jet wind tunnel. Compared to the shocks on the probes in Fig. 21a, those in Fig. 21b are more irregular and suggest a lower test core Mach number (the included bow shock waves are slightly larger). Also, the shock in the upper and lower edge of the schlieren (Fig. 21b) indicates the flow has already separated from the nozzle ahead of the nozzle exit. The pitot pressure distribution for the blockage shown in Fig. 21b would be similar to the profile shown in Fig. 20 for $P_T/\overline{P_D} = 36.4$.

4.2.2 Mach Number

The flow-field Mach number variation and uniformity in the test core rhombus are summarized in Fig. 22. The variation in the average free-stream Mach number with Reynolds number for the maximum and minimum stilling chamber temperatures (namely, $TT \approx 1580^\circ R$ and $TT < 800^\circ R$) is shown in Fig. 22a. This is a plot of the deviation in the calibrated mean Mach number relative to the designed nozzle Mach number ($M = 4$) as a function of free-stream Reynolds number. A plot of the test section average Mach number as a function of tunnel stagnation pressure is given in Fig. A-1.

In general, the maximum divergence in the value of the average Mach number at any given free-stream Reynolds number between cold and hot flow within the aerothermal wind tunnel operating envelope is less than 0.4 percent. Thus, the empirical curve fits given in Fig. 22a for defining the test section Mach number should be adequate for most tests.

The maximum overall variation in the free-stream Mach number distribution or the flow nonuniformity at RE/ft greater than or equal to 0.5×10^6 in the free-jet test rhombus, is nominally 0.4 percent or less as shown in Fig. 22b. The value $\sigma(M)$ represents the standard deviation in the Mach number distribution relative to the average Mach number, M_{AVG} . Naturally, a portion of the $\sigma(M)$ value includes the uncertainty associated with the basic measurements (pitot and stilling chamber pressure) used to compute the Mach numbers in the distribution.

A typical set of axial variations in the free-stream Mach number distributions is given in Fig. 23. These surveys were made in the vertical plane along the tunnel axis. In each axial distribution, the average and standard deviation in the local Mach number is listed. In general, the average Mach number at $Z = 4$ in. is slightly higher (0.6 percent) than the value

of $Z = -4$ in. for all test conditions; that is, the Mach number level is slightly higher above the tunnel axis.

4.2.3 Flow Angularity

The flow angularity variation through the test section was evaluated using three Mach/flow angularity probes. A plot of the average (or mean) and the standard deviation, $\sigma(M$ or $\alpha)$, in the variation of the flow angle along the nozzle axis as a function of free-stream Reynolds number is given in Fig. 24. In general, the flow angularity variation in the pitch and yaw plane appears to be conservatively on the order of ± 0.2 deg or less.

Typical examples of the axial variation in flow angularity are given in Fig. 25 for three typical tunnel operating conditions. The pressure tap or instrumentation used to detect flow angularity variations in the yaw plane for the centerline probe behaved erratically at times and these values in most cases are deleted from Fig. 25. It must be emphasized that these plots describe the change in flow angularity relative to the first point in the distribution. There is no reliable way at this time to define accurately the probe and probe support system orientation with respect to the tunnel axis under an aerodynamic load.

4.2.4 Test Section Total Temperature Uniformity

Total temperature surveys were made with a rake containing 13 single-shielded thermocouples equally spaced 2 in. apart. This rake is supported parallel to the pitot probe rake and displaced laterally (Y-direction) from the array of pitot probes. The individual probe sensitivity to a force-convective flow field, (the probe total temperature recovery factor) may vary by ± 1.5 percent. A known uniform total temperature flow field was not available to establish the individual calibration of these probes; therefore, these results were used only to establish quantitatively the uniformity and not the absolute level of the flow-field total temperature distribution.

The total temperature distribution at the forward ($X = -18.0$ in.) and aft ($X = 12.0$ in.) ends of the test rhombus are shown in Fig. 26 for TT values of 711 to 1580°R. In the forward portion of the test section, total temperature probes at $Z = \pm 12$ in. lie in the shear layer which is mixing with the lower temperature, initially quiescent, air enclosing the free jet. Thus, the total temperatures at $Z = \pm 12$ in. tend to approach from the higher values sensed in the test core. At the aft station, the free jet expands, enveloping the outer probes (at $Z = \pm 12$ in.), and the overall variation in the total temperature diminishes and approaches the anticipated variation (of ± 1.5 percent) expected because of the probable variation in the total temperature probe calibrations.

In general, as shown by the results in Fig. 26, the overall variation in the total temperature was nominally ± 1.5 percent. Some of the variations in the distributions can be attributed to differences in the recovery factors of the individual probes. Also, there were some difficulties in keeping these probes operational, as indicated by the questionable or erratic results obtained from a few individual probes. Throughout the program various probes obviously failed, and these data, when identified, were deleted. These test section distributions appear to be consistent with the stilling chamber distribution, which did not vary by more than one percent from the norm (average value).

The lateral variation in the total temperature distribution, as indicated in Fig. 27, was obtained by translating the survey rake 8 in. at the forward axial survey station. Each probe shows that the overall variation in the total temperature survey is less than 2 percent. This survey is probably the best indication of the actual variations in the free-jet stream flow total temperature.

4.3 DIFFUSER PERFORMANCE

An indication of the variation in pressure ratio across the Aerothermal Wind Tunnel nozzle and diffuser as a function of the nozzle exit conditions is summarized in Figs. 28 and 29. In Fig. 28, the stilling chamber pressure (PT) upstream of the nozzle normalized by the mean diffuser duct pressure \overline{PD} is correlated with the ratio of the computed average free-stream static pressure of the free-jet supersonic core divided by the flange pressure (see Fig. 11a) for various tunnel circuit operating conditions. The mean diffuser duct pressure is the average of four wall static pressure measurements (see Fig. 11b). For most operating conditions, this local flow in the diffuser duct is supersonic. The results suggest that as the ratio PT/\overline{PD} falls below 40, there is an abrupt shift in the relationship between PT/\overline{PD} versus P/PF which probably indicates that the flow in the diffuser shocks down to a subsonic condition.

At the ratios of $PT/\overline{PD} \gg 40$, the number of stages of compression, the nominal stream total temperature, and other conditions which affect the inlet pressure to the first stage of compression in the plant alter the relationship between PT/\overline{PD} and P/PF . Actually, the result of increasing the inlet pressure (PIN) to the first stage of compression as a function of the total operating pressure upstream of the Mach number 4 nozzle, namely PT, is shown in Fig. 29. As expected, it is a little easier to reduce the pressure ratio across the tunnel circuit (PT/PIN) at the lower operating conditions (lower PT's). Additional studies or test results may be needed to establish the optimum pressure ratio to operate the Aerothermal Wind Tunnel in an energy efficient manner.

4.4 MIXING CHAMBER PERFORMANCE

The effectiveness of the thermal insulation and the water cooling in the mixing chamber (see Fig. 10) is illustrated in Fig. 30. These are typical results which show that the maximum temperature between the inner shell and the insulation (in this case TWC13) increases with the temperature of the air (TTC) supplied from HB-3 (the electric heater). On the other side of the insulation, between the insulation and the outer water jacket, the local temperature (in this case TWC12) is fairly constant and independent of the air temperature (TTC) supplied by HB-3.

Several thermocouples were spot-welded to the back side of the first baffle in the mixer (see Fig. 10). The effect of the air flow through the HB-3 heater on the uniformity of the temperature distribution over the surface baffle is summarized in Fig. 31. In the case where hot air at 1380°R from the gas-fired heater (HB-1) was mixed with room temperature air through the primary line (HB-3 was not activated), the cooling process was uniform across the baffle.

As heated air flows through HB-3 into the mixer and mixes with the bypass air, the overall temperature level of the first baffle increases with the supply air (TTC) from HB-3. The bypass air temperature in this case is nominally 1380°R and the mass ratio of primary air (from HB-3) to bypass air (from HB-1) is on the order of 3. The overall variation across the baffle at any given value of TTC is within $\pm 50^\circ\text{F}$ of the mean value. This variation in temperature across the baffle did not pose any potential structural problem as far as the baffles were concerned.

The initial pressure drop measurements across the baffles and screens were made in May and August 1981 and provided the most reliable pressure drop results; these are summarized in Fig. 32. As noted in the figure, the data uncertainty for these measurements is nominally ± 0.2 psi. The transducer size and range were originally dictated by the estimated design limits for the pressure drops across the screens and baffles which, fortunately, turned out to be considerably smaller than anticipated.

In general, the pressure drop as shown in Fig. 32a increases linearly with the increase in mixing chamber pressure, nominally equal to PT. The maximum pressure drop occurs from the entrance of the mixer, where the local chamber diameter is 11.4 in., to where the maximum chamber diameter is 37.7 in. The pressure drop across the baffles is nominally 0.6 percent of the mixing chamber pressure, while the drop across the screens falls within the uncertainty of the measurements, or less than 0.1 percent. These results were obtained with no flow through the electric heater (no primary flow).

The effect of opening V454, which allows the flow to enter the primary line (through HB-3) is shown in Fig. 32b. These results were obtained at a constant chamber pressure and simply show that detouring a portion of the flow through the primary line (through HB-3) which then flows along the axis of the mixer reduces the pressure drop when V454 is opened more than 40 or 45 percent. In this condition when the pressure drop decreases, the flow through HB-3 is approaching one-half the amount of air entering through the bypass lines.

The mixing of the airstreams from the primary (HB-3) heater and bypass (HB-1) heater lines also has a pronounced effect on the dynamic pressure levels in the mixing chamber. These results are summarized in Fig. 33. The root-mean-square (RMS) of the pressure fluctuations evaluated over a total bandwidth from dc to 5 KHz is normalized by the nominal mixing chamber total pressure, in this case PT. Reading from left to right, the curves show the effects of passing flow only through the primary line, next the effect of mixing the primary and bypass streams in the mixing chamber, and finally operating the test unit with air passing only through the bypass line. As noted earlier and shown in Figs. 4 and 5, the bypass air coming from the gas-fired heater, HB-1, enters through two 8-in.-diam lines diametrically opposite each other while the primary flow enters through an 11.4-in.-diam line along the mixer axis. These airstreams mix upstream of the first baffle in the conical segment of the mixer shown in Fig. 10. The minimum turbulence levels are obtained when air enters only from the bypass lines (Fig. 33 on the right). There is a relatively smooth transition in these turbulence levels as the flow changes from an air source obtained from the primary line to one from the bypass lines. This trend is generally true for the heated (Fig. 33a) and unheated (Fig. 33b) airstreams.

The expected systematic reduction or attenuation in the turbulence levels as the flow expands from the 11.4-in.-diam entrance to the mixer into the 37.7-in.-diam section upstream of the first baffle is observed. As flow proceeds through the baffles and screens, the turbulence levels are reduced even further. The lower curves indicated by the diamond symbols represent the measured turbulence in the Aerothermal Wind Tunnel stilling chamber. In comparison to the turbulence levels measured in Tunnel A, which also has a Mach number 4.0 contour, the minimum pressure fluctuation levels in the aerothermal stilling chamber are ten times greater. (The turbulence level, P/PT , at a PT of 20 psia in Tunnel A is 0.016 percent and decreases to 0.006 percent at a PT of 60 psia; see Ref. 8).

A comparison of the heated air turbulence (Fig. 33a) with the unheated air turbulence (Fig. 33b) in the mixing chamber at the same mass flow rate or mixing rate indicates the heated air turbulence is slightly less. This may be explained in part because the total pressure in the chamber at any given mass flow rate is higher in the heated flow, and usually the higher chamber pressure tends to attenuate (percentage-wise) the level of the pressure fluctuations (see Fig. 15 of Ref. 8).

Adding the baffles and the conical section in the bypass line downstream of V554 (see Fig. 9b) had a negligible effect on pressure fluctuations in the mixing chamber, as shown by the solid symbols in Fig. 33a.

The power spectral density plots of the pressure fluctuations recorded at the entrance and exit (or in the stilling chamber) of the mixer are shown in Fig. 34. The analysis was evaluated over a frequency range of 5 KHz with an analyzer aliasing filter set at 80 percent of the frequency range. The analysis was performed on a Spectral Dynamics SD360 Digital Signal Processor and the results were stored, processed, and plotted using the VKF standard DEC 10 computer. The response of these transducers as installed in the mixer was calibrated in the VKF 2.5-in.-diam shock tube and found to have flat response over the frequency range out to about 20 KHz.

The RMS level is in percent of the total pressure in the stilling chamber located at the discharge end of the mixing chamber. The parameter $F(NED = 0.99)$ is the frequency range of the fluctuating pressure containing 99 percent of the dynamic energy. Obviously, values beyond 4 KHz are influenced by the aliasing filter used in the analysis, but the smaller values for V454 settings less than 50 percent are valid. These results suggest that the fluctuations measured for mixing flow ratios ($\dot{m}_{HB-1}/\dot{m}_{HB-3}$) less than 4 extend over a wider frequency range than 4 KHz. In the mixing chamber, the geometry of the chamber attenuates (or filters) the fluctuation levels in the frequency band close to 200 Hz. There is some indication of a weak resonance in the mixing chamber acoustics at 120 and 240 Hz, but for mixing ratios ($\dot{m}_{HB-1}/\dot{m}_{HB-3}$) greater than 4, the spectral content of the fluctuation rolls off and is insignificant beyond 4 KHz.

4.5 BYPASS LINE CHARACTERISTICS

As a result of a structural failure in the line downstream of V554, the bypass line in this region was modified from the configuration shown in Fig. 9a to the one in Fig. 9b. Details concerning the nature and corrective action taken after these failures in the bypass line are documented in Ref. 3. Prior to the August 1981 entry, two dynamic pressure transducers were installed upstream of the baffles; results of these measurements are summarized in Figs. 35 and 36.

In Fig. 35, the RMS of the pressure fluctuations was normalized by the local mean pressure measured immediately upstream of the baffles. The magnitude of the pressure PT_b upstream of the first baffle was nominally 2.6 to 3.6 greater than the mixing chamber pressure (PT), and the ratio of the total pressure upstream of the first baffle to the one upstream of the second baffle was nominally 2.2. Thus, in terms of the total pressure in the Mach number 4 stilling chamber, these pressure fluctuation levels would reach 20 to 30

percent of PT. Heating the air tended to reduce slightly the overall RMS level of the pressure fluctuations in the bypass line (compare solid and open symbol data).

To illustrate the type of typical power spectral density distribution generated by the pressure fluctuations recorded in the bypass line, the results are presented in Fig. 36. These results were recorded at the same time as those previously shown in Fig. 34. Unlike the RMS data given in Fig. 35, the present results were normalized by the Mach number 4 stilling chamber pressure (PT) in lieu of the local pressure PT_b upstream of a given baffle.

There is an acoustical harmonic established in the modified bypass line which appears to be a function of the length of the cavity between the sonic orifice and the first baffle. This distance is nominally 1.02 ft long and would produce the first harmonic at about 441 Hz, as shown in Fig. 36a. These harmonics increase until the fifth harmonic is reached. A portion of this energy is transmitted through the first baffle and is detected ahead of the second baffle, as noted by comparing Figs. 36a and b. Note also that the first baffle plus the slight expansion in the bypass line reduced the pressure fluctuations by more than 50 percent. The addition of a cruciform or some equivalent structure between the sonic orifice and the first baffle might break up the existing harmonics and reduce the chance for certain elements in this line to fatigue structurally because of harmonic-induced vibration.

4.6 CONTROL VALVES

Two valves are used to regulate the flow rates through the primary and bypass lines. The valve located upstream of electric heater HB-3 in the primary line is V454. The other major valve, designated V554, is located downstream of gas-fired heater HB-1. Presently, a sonic orifice is temporarily in this line to simulate V554 100-percent open.

The measured flow coefficient of V554 and its temporary replacement, the sonic orifice, along with the total pressure drop from the seventh stage of the plant to a point just upstream of the V554 location are given in Fig. 37. The pressure drop ($PTB/PDIS$) shown in Fig. 37a for the unheated flow appears to be nominally 48 percent of the seventh stage discharge pressure which reaches a maximum of 1,200 psia. If the gas-fired heater (HB-1) is activated, the increase in air temperature reduces the realized pressure drop to nominally only 52 percent of the discharge pressure.

V554 has a designated flow coefficient of 360 which agrees fairly well with the experimental values shown in Fig. 37b. Although the sonic orifice was designed to simulate V554 when it was wide open, these results show that the corresponding flow coefficient of the sonic orifice was nominally 4 percent smaller.

The nonlinear operating characteristic of V454 which controls the flow rate through electric heater HB-3 is summarized in Fig. 38. This particular valve installation is essentially wide open once the valve setting reaches 78 percent. The curve of this valve performance shown in Fig. 38 is only valid for valve settings less than or equal to 0.78. Beyond this point the parameter $\dot{m}_C \sqrt{\text{TDIS}/\text{PDIS}}$ is equal to 1.095.

The results in Figs. 37 and 38 will be helpful in the preparation of any attempts to model the performance or operation of the aerothermal test unit.

5.0 HEMISPHERE CYLINDER RESULTS

To demonstrate that no unusual problems were encountered by injecting a model into the Aerothermal Wind Tunnel free jet using the existing Tunnel C model inject/retract system, the following very limited hemisphere cylinder results were obtained. As shown in Figs. 39 and 40, very good shadowgrams and interferograms can be obtained to visualize optically the flow-field patterns over a typical model configuration. The nominal uniformity in the spacing between the fringes upstream of the hemisphere suggests that the flow was fairly uniform through the test section rhombus. There are no severe density gradients in the free stream that resemble those produced by the flow downstream of the detached shock produced by the hemisphere. These results were obtained using existing operational Tunnel C optical capabilities.

Surface pressure measurements on the hemisphere cylinder were made using existing instrumentation and data acquisition techniques. The surface pressure measurements were normalized by the total pressure downstream of a normal shock in a flow field defined by the free-jet core mean Mach number obtained during the tunnel calibration. The abscissa is the surface distance from the stagnation point normalized by the hemisphere 2.90-in. nose radius. The experimental results presented in Fig. 41 are in good agreement with the empirical results from Ref. 9, represented by the solid line. The flagged symbols simply denote a repeat run which produced identical results. The reason for the difference in the experimental and inviscid theoretical results on the cylindrical section has not been identified.

The heat transfer results presented in Fig. 42 were obtained by using surface-contoured coaxial thermocouples. The measured or computed heat flux rate has been normalized by the corresponding classical Fay-Riddell laminar boundary-layer surface stagnation-point heat transfer rate based on the Aerothermal Wind Tunnel calibrated Mach number, stilling chamber properties, and local hemisphere wall temperature. The solid curve represents the theoretical heat transfer distribution for fully laminar flow and the dashed lines for fully

turbulent or transitional boundary-layer flows over the hemispheres as defined by theoretical results based on Refs. 10 and 11.

The zero roll ray of heat transfer results appears to be considerably higher than the theory based on an attached laminar boundary layer. In fact, these results suggest that the flow over the hemisphere is transitional for values of S/R_N greater than 1.0. The test data appear to be approaching the turbulent or transitional boundary-layer heat transfer rates. As noted in Section 2.4.5, model roughness did not change significantly and therefore is not considered to be responsible for the local change in boundary-layer transition.

6.0 CONCLUDING REMARKS

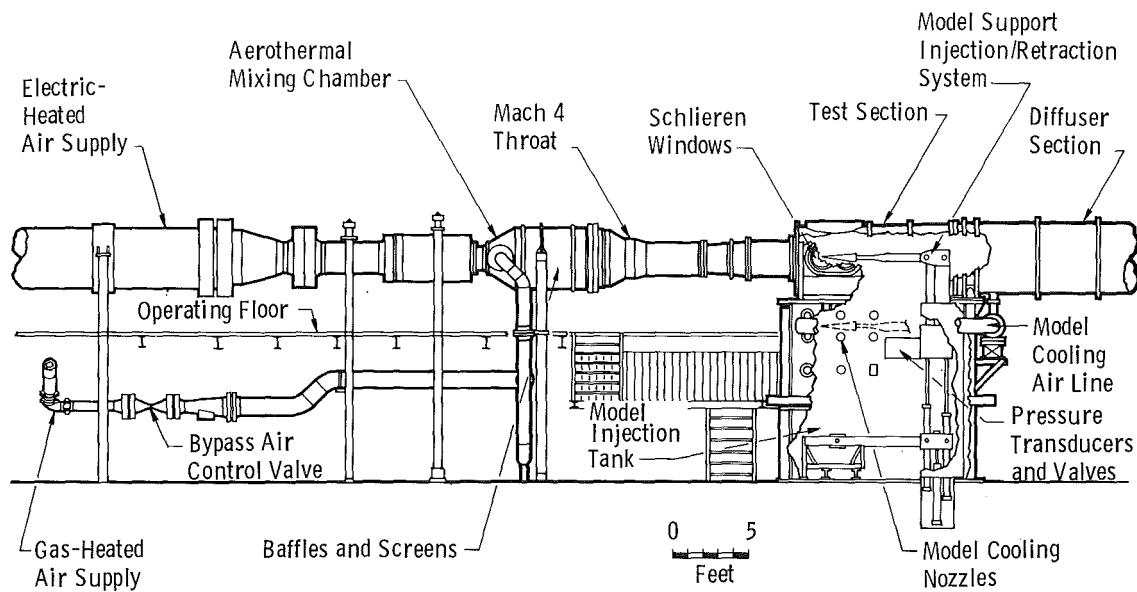
1. The Aerothermal Mach 4.0 Wind Tunnel was successfully operated over test conditions which simulate a true temperature - true pressure altitude condition from 56,000 to 105,000 ft. The shakedown and calibration program identified the operating limits, wind tunnel circuit performance, test section calibration, and the design or structural problems which were corrected as the program progressed.
2. The calibration phase revealed that the free-jet supersonic core of uniform flow in the test section is 32 in. long, with an upstream diameter of 23 in. tapering linearly to a downstream diameter of 8 in.
3. The mean Mach number within the test rhombus varies from 3.99 at the minimum operating temperature of 720°R at a pressure of 132 psia to a value of 3.95 at the maximum temperature of 1570°R. The uniformity of the Mach number distribution within the test core is less than ± 0.4 percent of the mean value for stilling chamber pressures above 50 psia.
4. The local flow angle variation within the test core is less than ± 0.2 deg in both the pitch and yaw planes of the flow.
5. Varying the diffuser pressure had no measurable effect on the test rhombus calibration, but did alter the expanding supersonic portion of the free-jet plume.
6. A stilling chamber-to-mean static diffuser pressure of approximately 40 was required to maintain the fully expanded flow through the Mach number 4 nozzle of the Aerothermal Wind Tunnel.

7. The operating envelope in terms of the stilling chamber properties of the Aerothermal Wind Tunnel is 20 to 132 psia for temperatures around 710°R, 20 to 180 psia at temperatures approaching 1580°R, and 20 to 100 psia for temperatures of 1660°R. The operational potential exists to increase the pressure level to 195 psia at a total temperature of 1580°R, and 20 to 100 psia for temperatures of 1660°R. The operational potential exists to increase the pressure level to 195 psia at a total temperature of 1580°R, and a study is presently underway to see if the test unit can be safely operated at temperatures up to 1900°R over a pressure range of 20 to 100 psia.
8. Real-gas corrections are needed to compute the test section properties which, at the higher stilling chamber temperatures, produce results that differ by 3 to 4 percent from the perfect gas values.

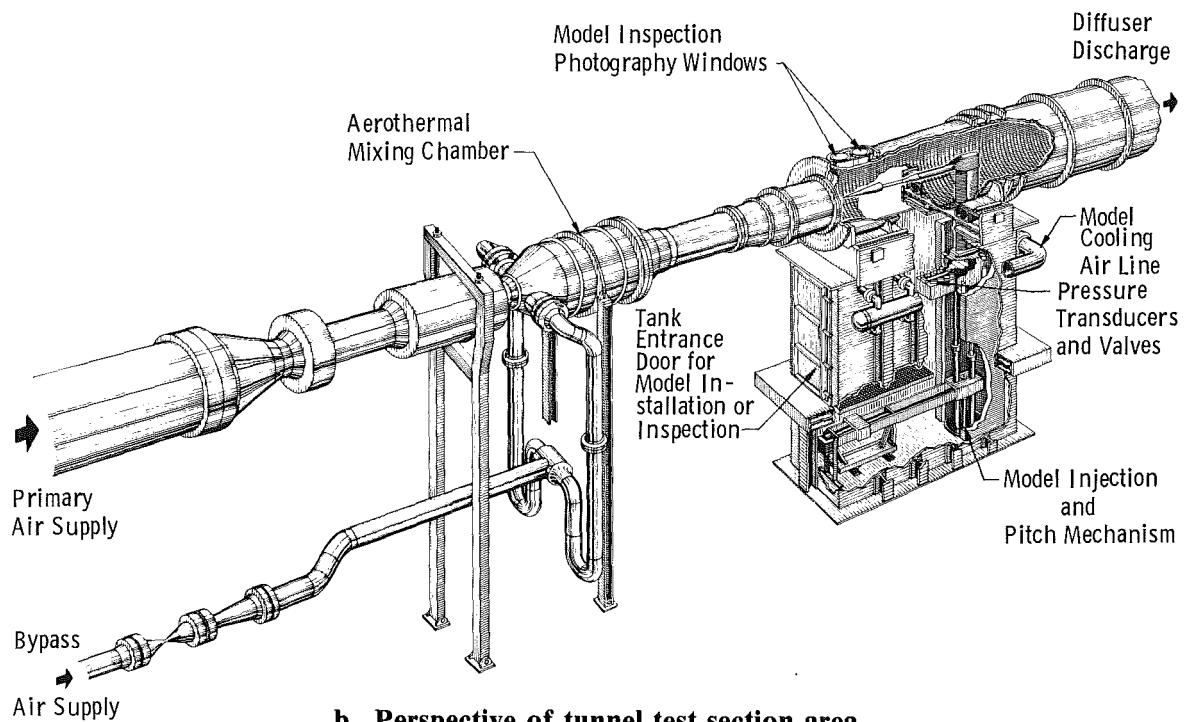
REFERENCES

1. Boudreau, A. H. "Performance and Operational Characteristics of AEDC/VKF Tunnels A, B, and C." AEDC-TR-80-48 (AD-A102614), July 1981.
2. *Test Facilities Handbook* (Eleventh Edition). "von Kármán Gas Dynamics Facility, Vol. 3." Arnold Engineering Development Center, April 1981.
3. Strike, W. T., Langford, J. M., and Davis, L. M., Lt., USAF. "VKF Aerothermal Supersonic, Mach 4 Wind Tunnel Shakedown and Calibration." AEDC-TSR-81-V42, November 1981.
4. Strike, W. T., Penny, T. R. and Porter, J. H. "The AFFDL-Nielson Flow-Field Study." AEDC-TR-76-18 (AD-A023755), April 1976.
5. Trimmer, L. L., Matthews, R. K., and Buchanan, T. D. "Measurement of Aerodynamic Heat Rates at the AEDC von Kármán Facility." *ICIASF Record*, IEEE Publication CHO 784-9AES, September 1973.
6. Brown, David L. "Predicting Equilibrium Pressures from Transient Pressure Data." Aerospace Research Laboratories, ARL-65-7 (AD614819), January 1965.

7. *U. S. Standard Atmosphere, 1962*. Prepared under sponsorship of National Aeronautics and Space Administration, U. S. Air Force, and U. S. Weather Bureau, December 1962.
8. Strike, W. T., Jr., Donaldson, J. C., and Beale, D. K. "Test Section Turbulence in the AEDC/VKF Supersonic/Hypersonic Wind Tunnels." AEDC-TR-81-5 (AD-A102615), July 1981.
9. Rohsenow, W. M. and Hartnett, J. P. *Handbook of Heat Transfer*. McGraw-Hill, Inc., New York, 1973.
10. Pantankar, S. V. and Spalding, D. B., *Heat and Mass Transfer in Boundary Layers*. CRC Press, Cleveland, 1968.
11. Mayne, A. W., Jr., and Dyer, D. F. "Comparisons of Theory and Experiment for Turbulent Boundary Layers on Simple Shapes at Hypersonic Conditions." *Proceedings of the 1970 Heat Transfer and Fluid Mechanics Institute*, Stanford University Press, 1970, pp. 168-188.



a. Tunnel assembly



b. Perspective of tunnel test section area
Figure 1. Tunnel C Mach 4.0 configuration.

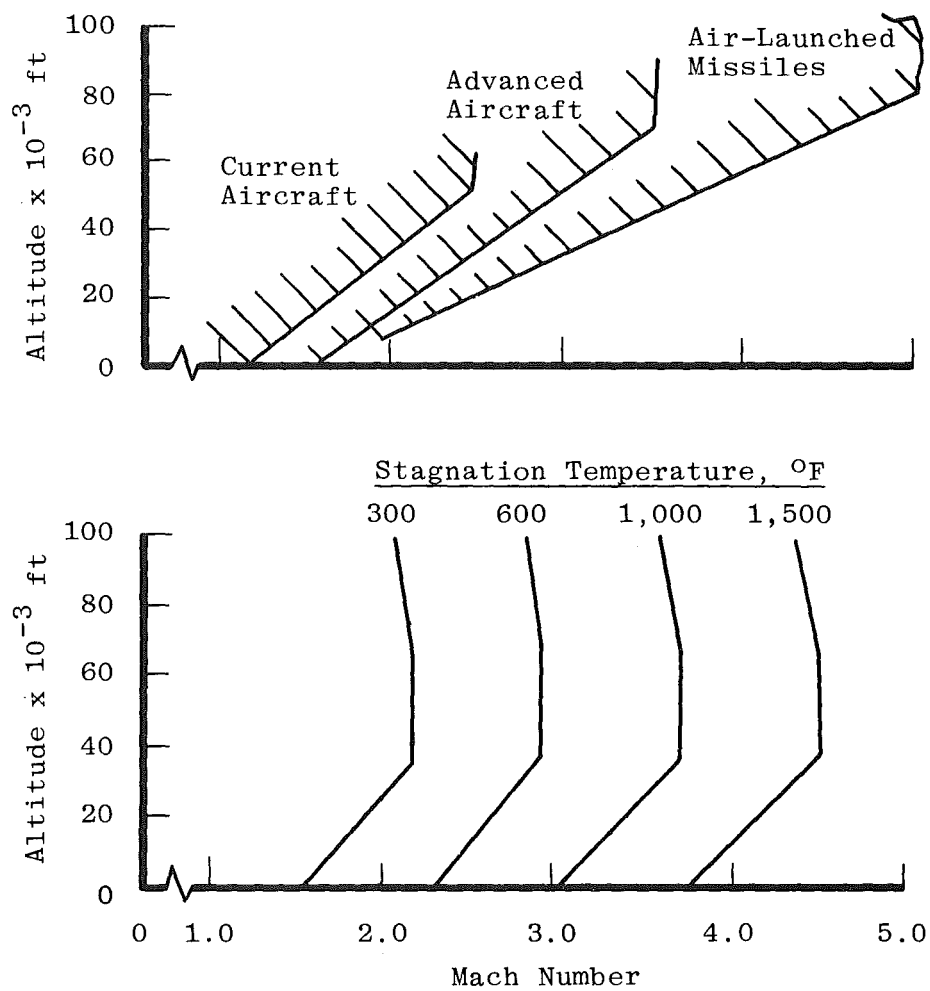
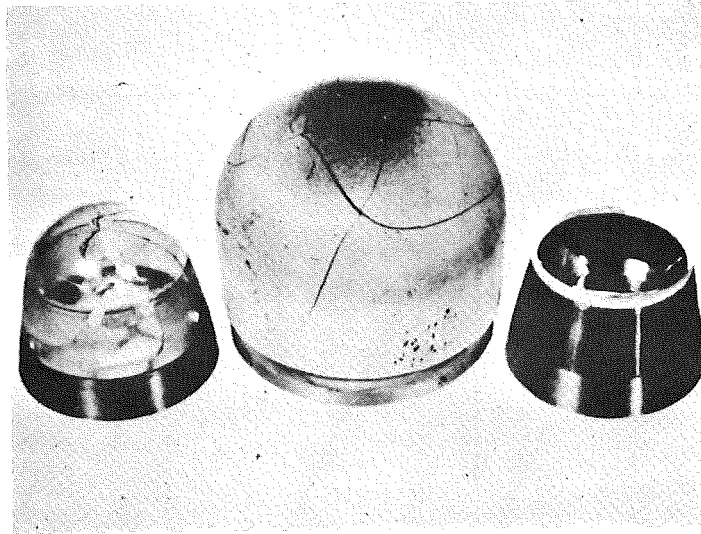
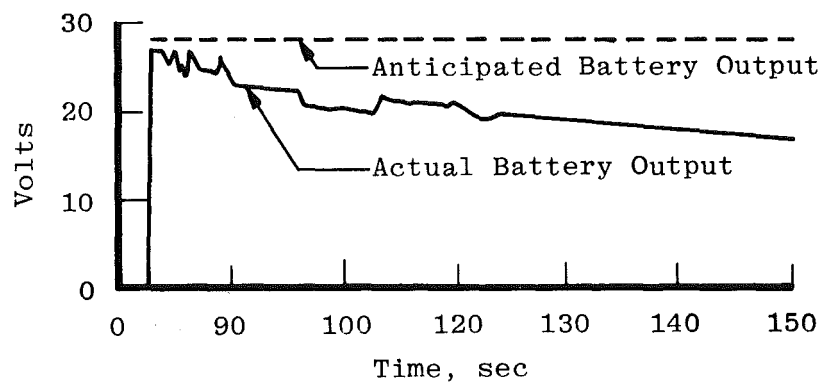


Figure 2. Definition of the simulated environment.



a. Radome failures



b. Battery performance

Figure 3. Illustrated aerothermal problems.

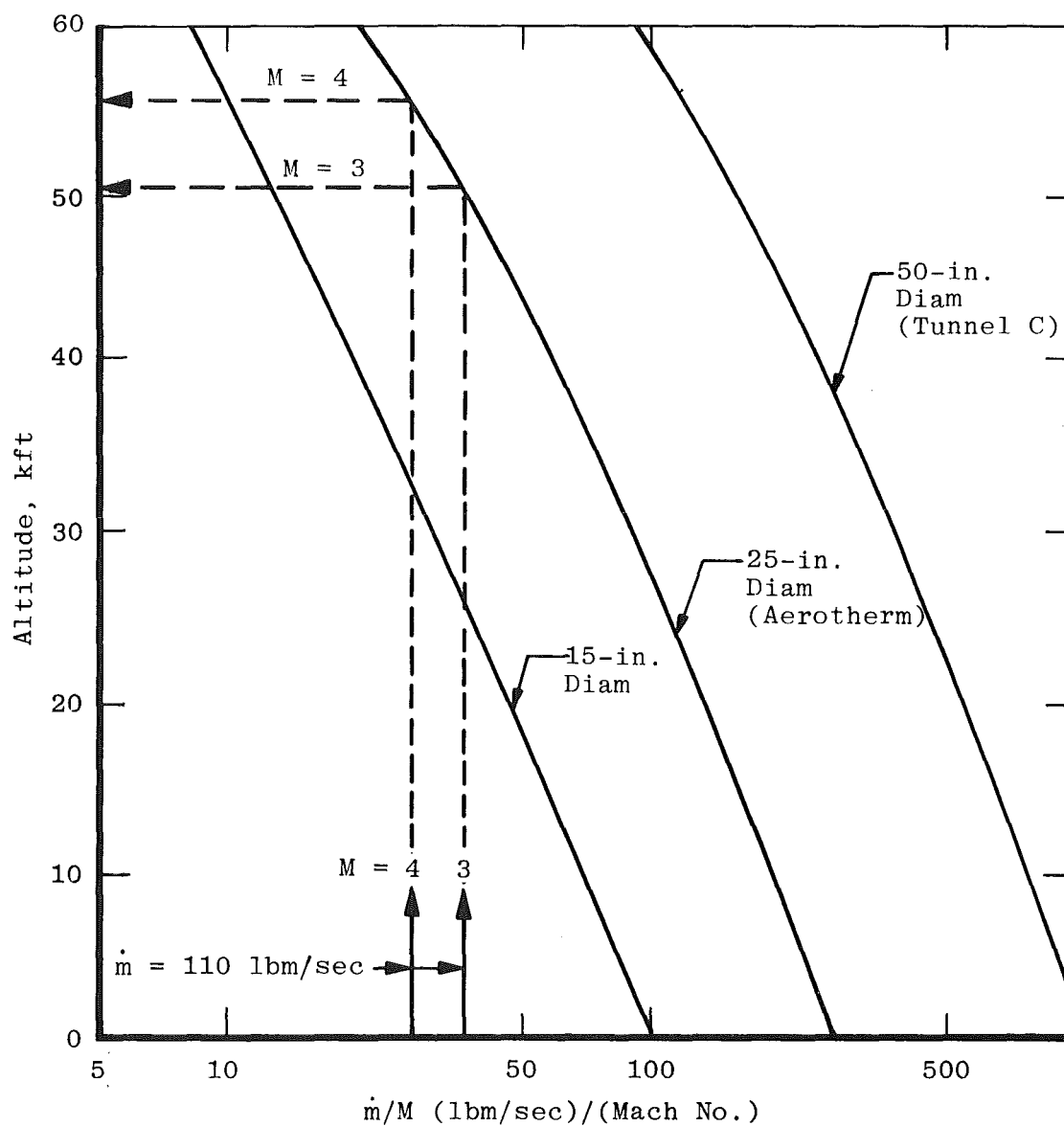
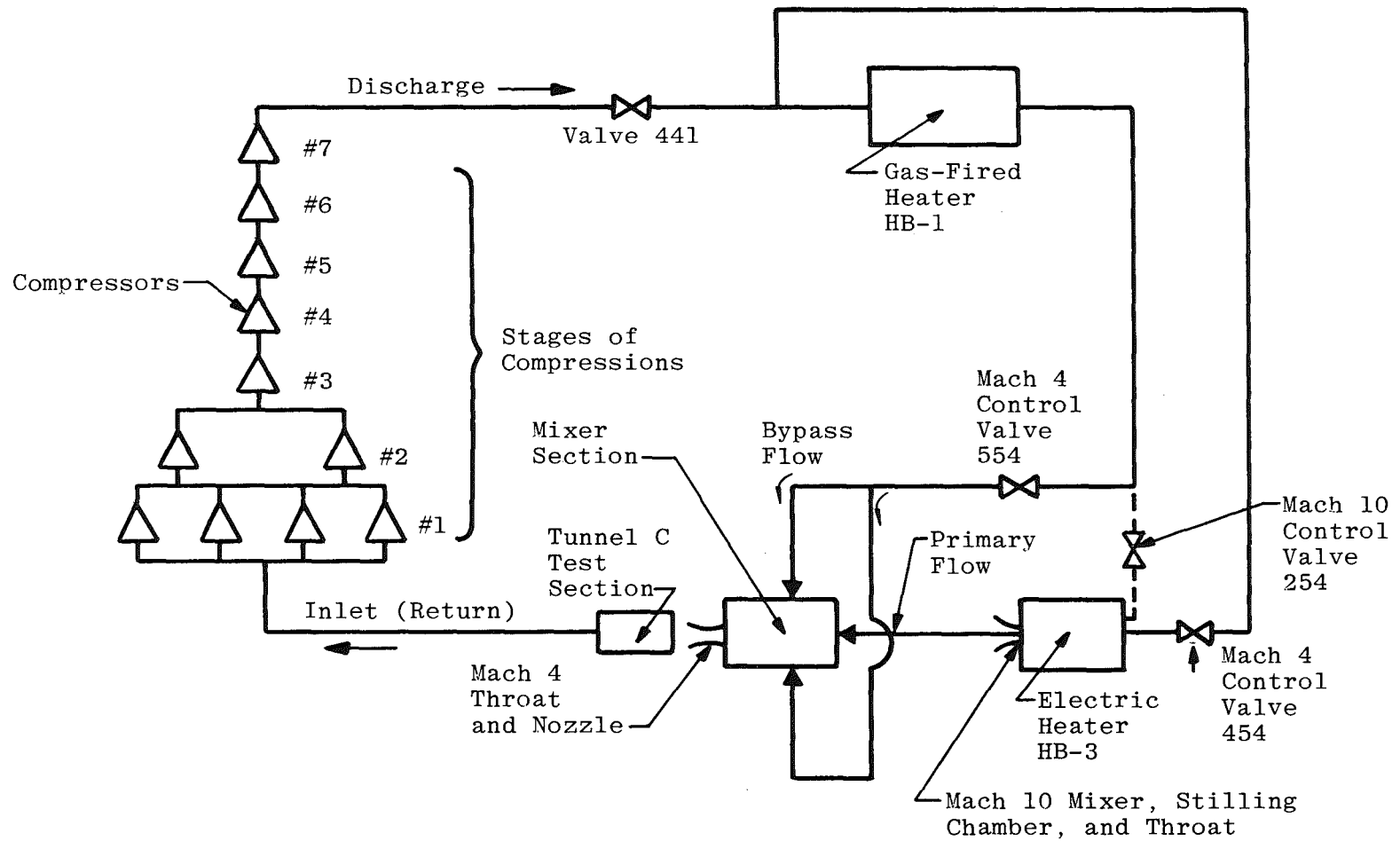
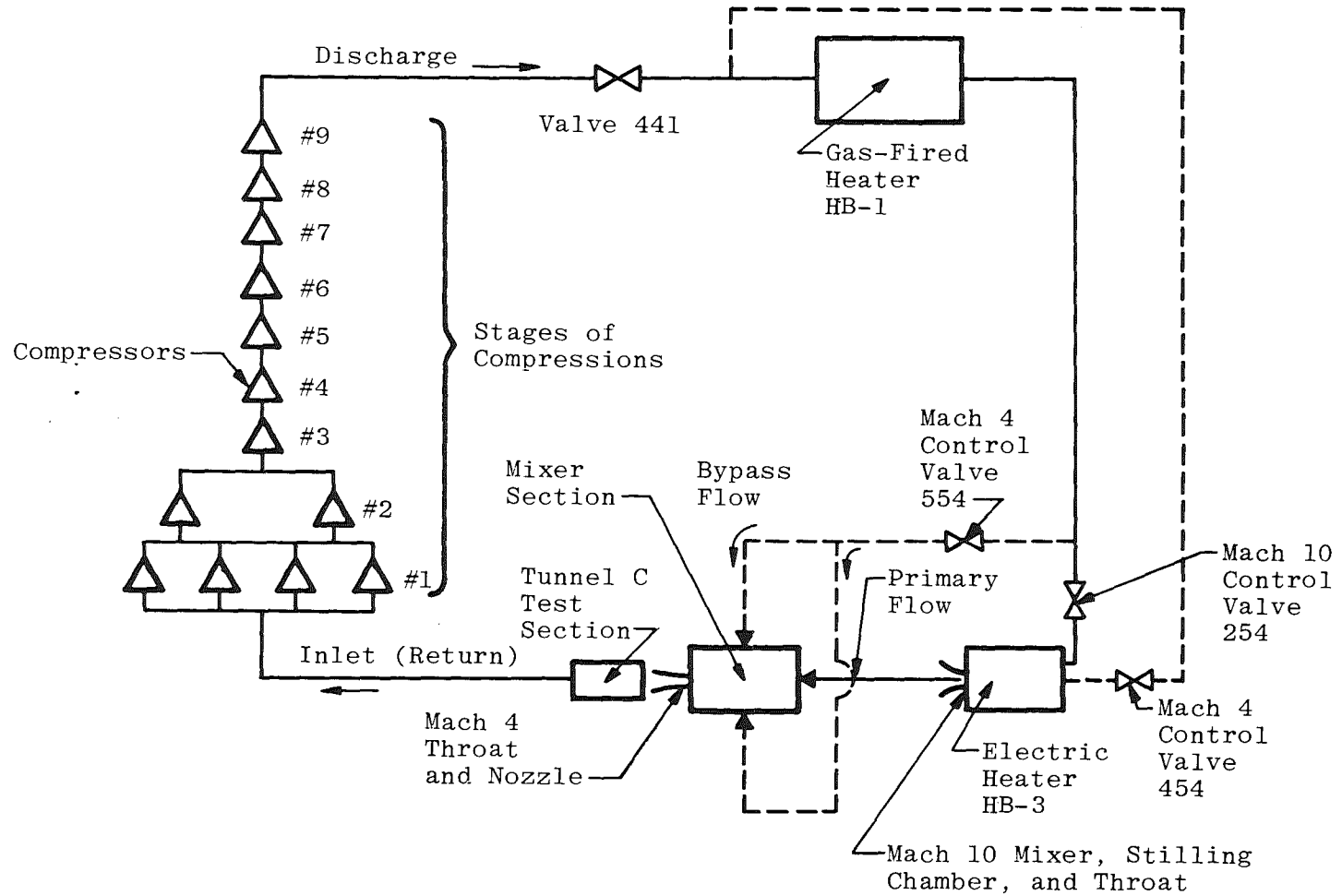


Figure 4. Altitude duplication for various test section sizes and mass flow/Mach number ratios.

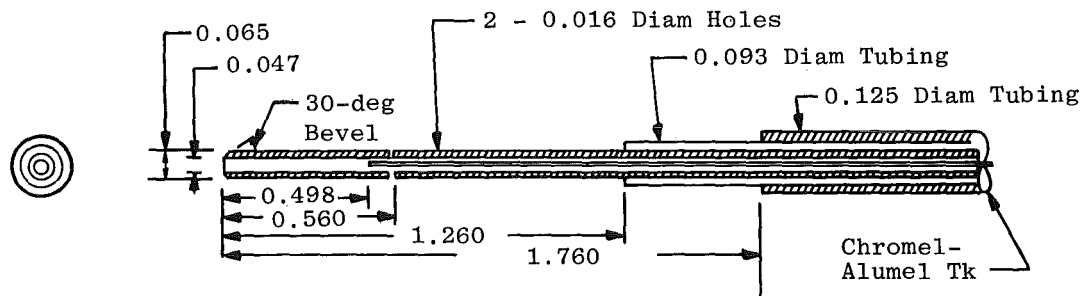
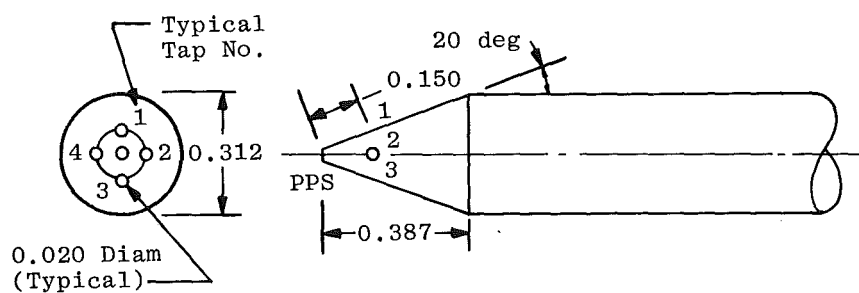


a. Parallel heater circuit
 Figure 5. The Mach 4 aerothermal wind tunnel circuit.



b. Series heater circuit (Tunnel C-type operation)
Figure 5. Concluded.

All Dimensions in Inches

**a. Pitot probe****b. Total temperature probe****c. Mach/flow angularity probe****Figure 6. Test section survey probes.**

Note:
PF and
TF Measurements

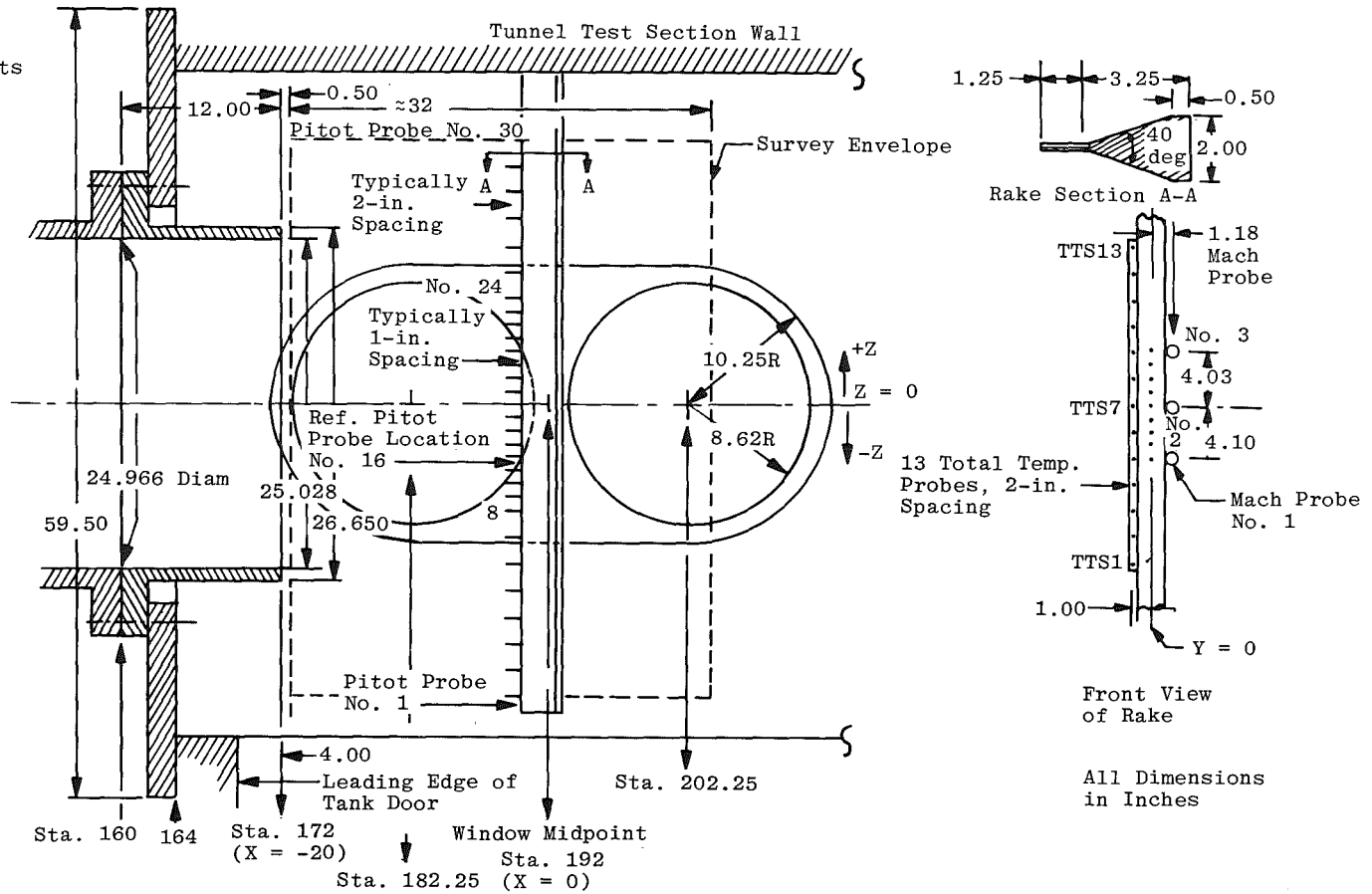
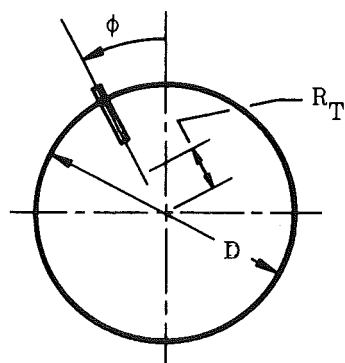


Figure 7. Rake installation and orientations.



View Upstream
Toward HB-3

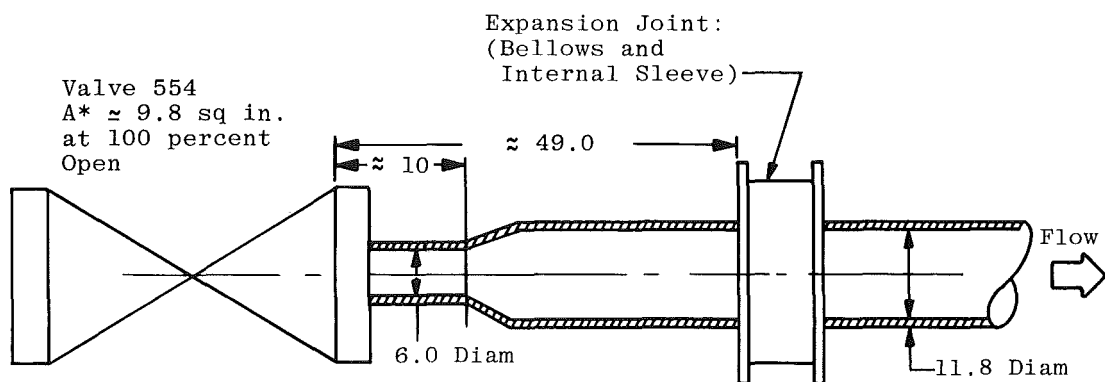
Electric Heater
(Mach 10 Stilling Chamber,
HB-3) $D = 12.0$ in.

	R_T , in.	ϕ , deg
TTC1	2.0	-22.5
TTC2	3.0	-45.0
TTC3	3.0	-90.0
TTC4	3.0	-135.0
TTC5	2.0	-202.5
TTC6	3.0	-225.0
TTC7	3.0	-292.5

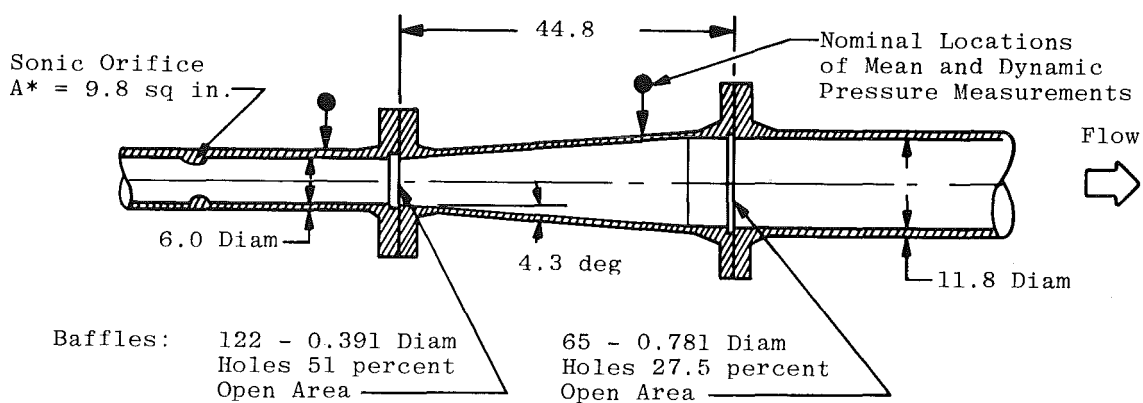
Mach 4 Stilling Chamber
 $D = 37.7$ in.

	R_T , in.	ϕ , deg
TT1	16.5	15
TT2	0.5	90
TT3	9.5	150
TT4	16.5	200
TT5	9.5	240
TT6	4.5	285
TT7	9.5	330

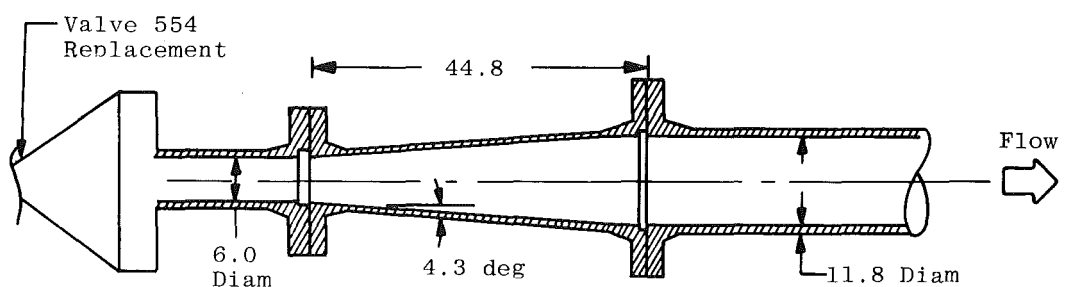
Figure 8. Total temperature probe locations in the stilling chambers.



a. May 1981 survey



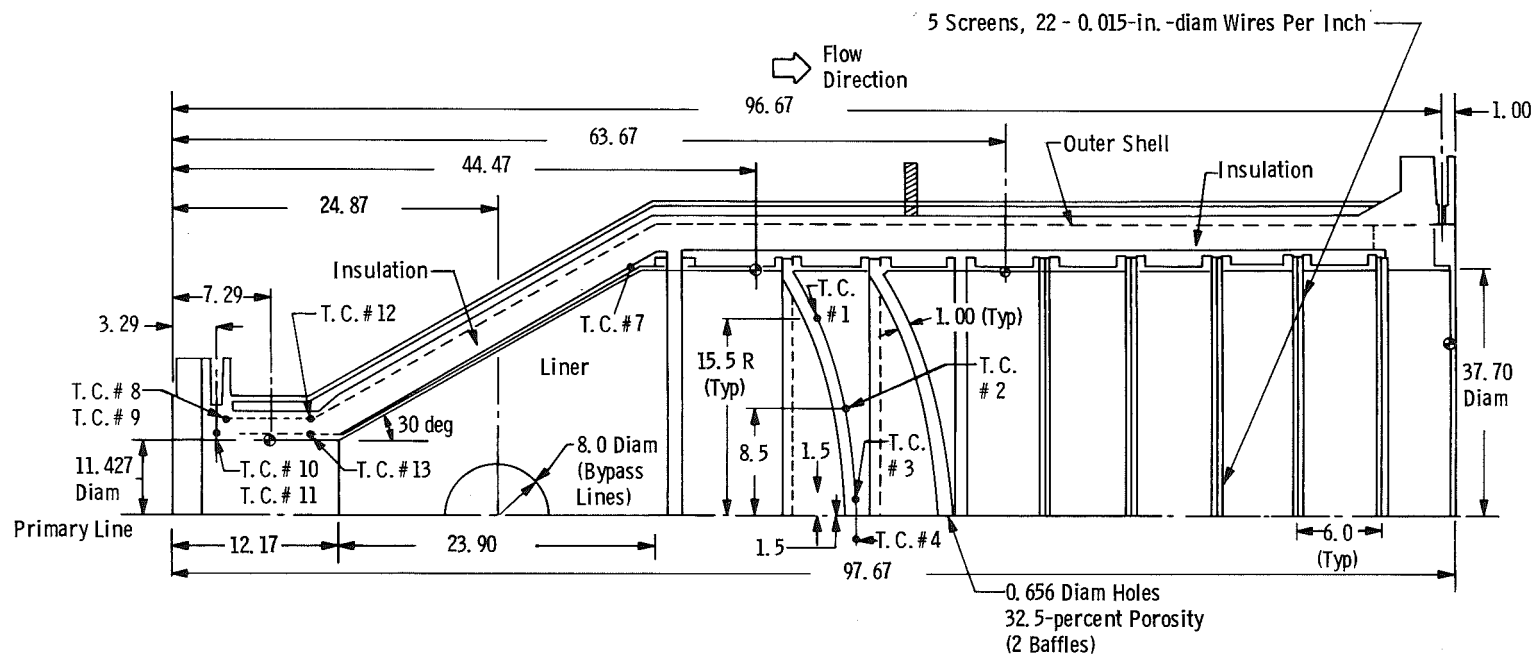
b. Aug. 1981/Oct. 1981 entries



All Dimensions in Inches

c. Planned modification

Figure 9. Bypass line flow rate control.



Mixing Chamber Instrumentation

TWC (T. C.) Location Position

1. Baffle R = 15.5
2. R = 8.5
3. R = 1.5
4. R = 1.5 (180 deg)
5. R = 8.5 (180 deg)
6. R = 15.5 (180 deg)
7. Insulation/Liner
8. Insulation/Outer Shell
9. Insulation/Outer Shell (180 deg)
10. Insulation/Liner
11. Insulation/Liner (180 deg)
12. Insulation/Outer Shell, Downstream Station
13. Insulation/Liner, Downstream Station

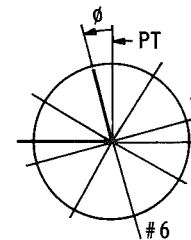
Dynamic Pressure

- 1 7.29
- 2 44.47
- 3 63.67
- 4 96.67 (Stilling Chamber)

Note: T. C. Thermocouple

⊗ Mean and Dynamic Pressure Tap Locations

Stilling Chamber Instrumentation

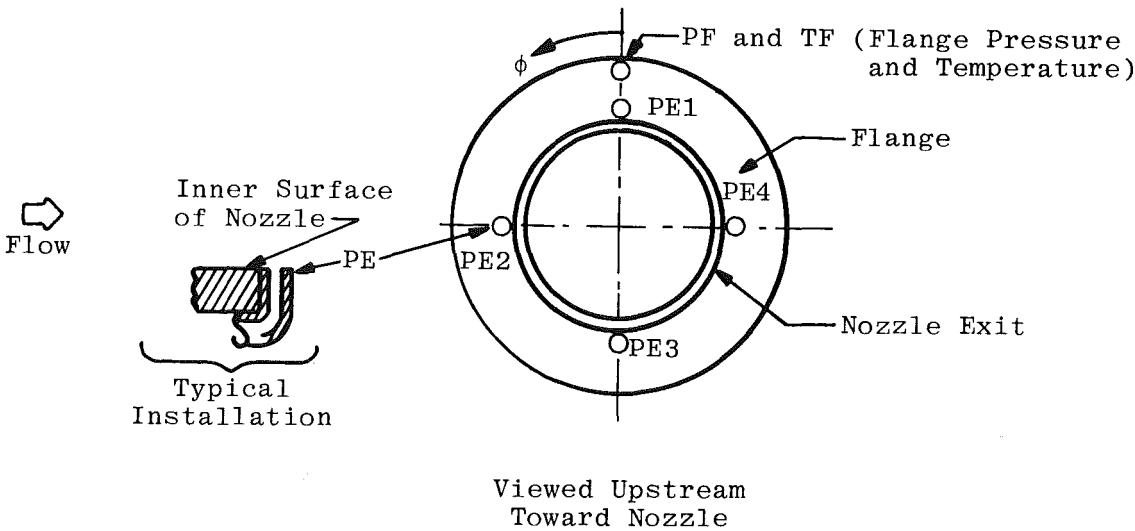


Looking Upstream
Toward HB-3

TT	ϕ	l (in.)
1	15	16.5
2	60	9.5
3	90	0.5
4	105	4.5
5	150	9.5
6	195	16.5
7	240	9.5
8	270	16.5
9	285	4.5
10	330	9.5

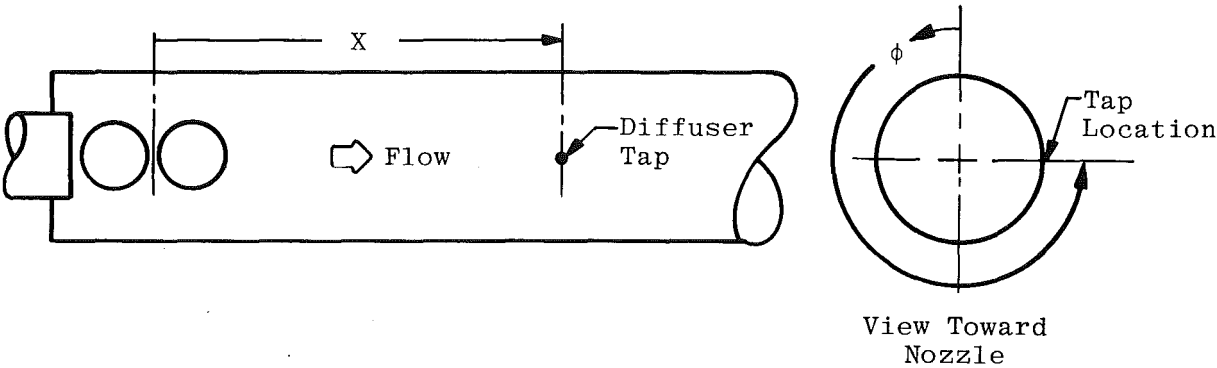
All Dimensions in Inches

Figure 10. Aerothermal wind tunnel mixer instrument installation.



Pressure Tap	PE1	PE2	PE3	PE4
Roll Position, ϕ (deg)	0	90	180	270

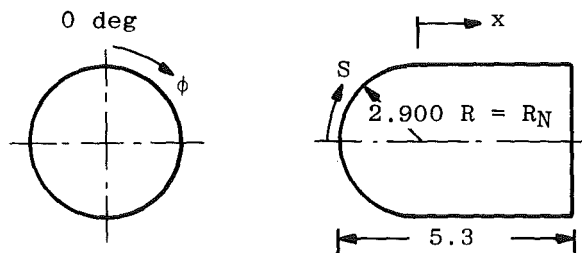
a. Nozzle exit instrumentation



Pressure Tap	ϕ , deg	X, in.
PD1	270	152.3
PD2	↓	202.1
PD3	↓	252.3
PD4	↓	302.1

b. Diffuser instrumentation

Figure 11. Test section and diffuser instrumentation.

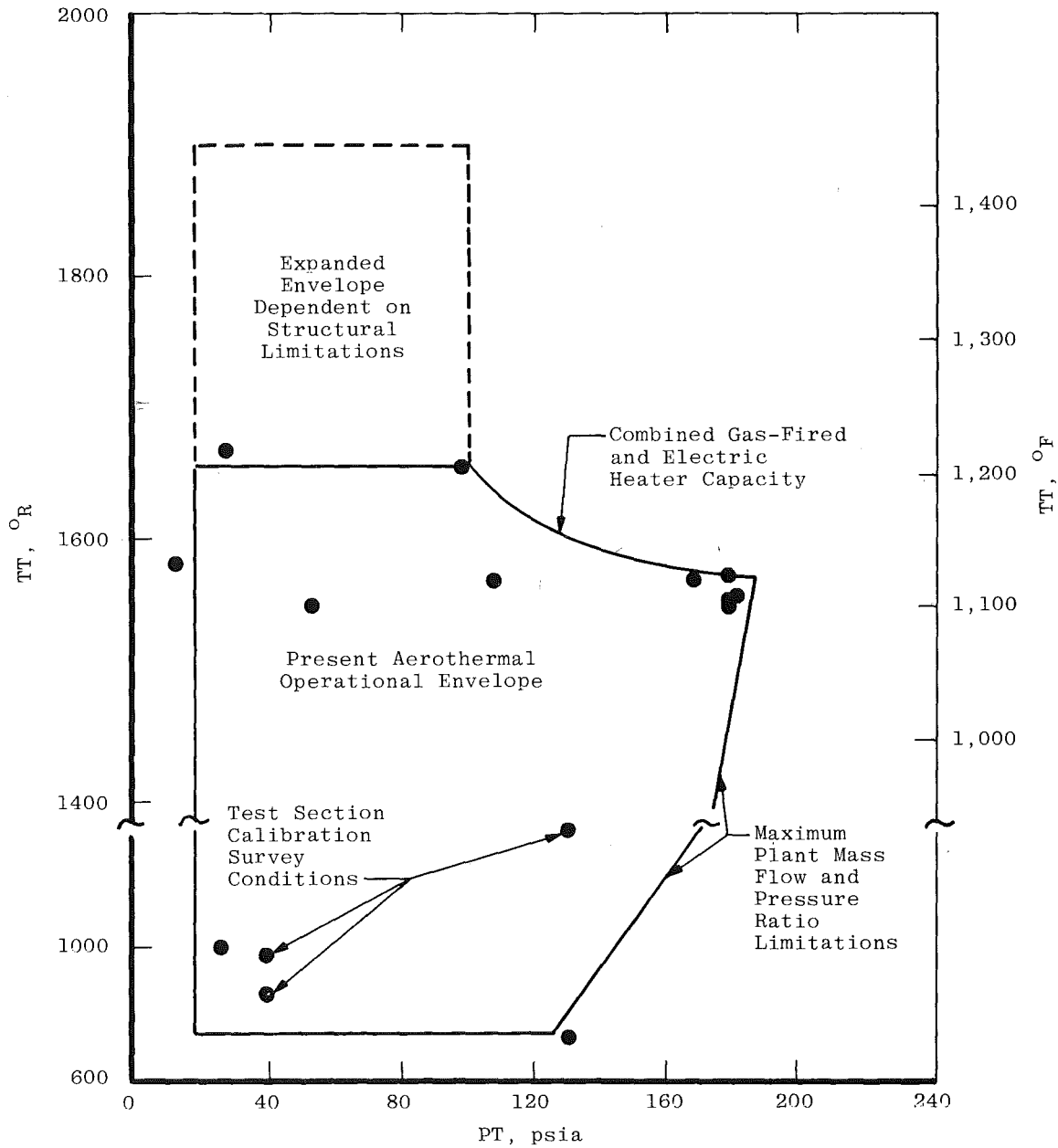


All Dimensions in Inches

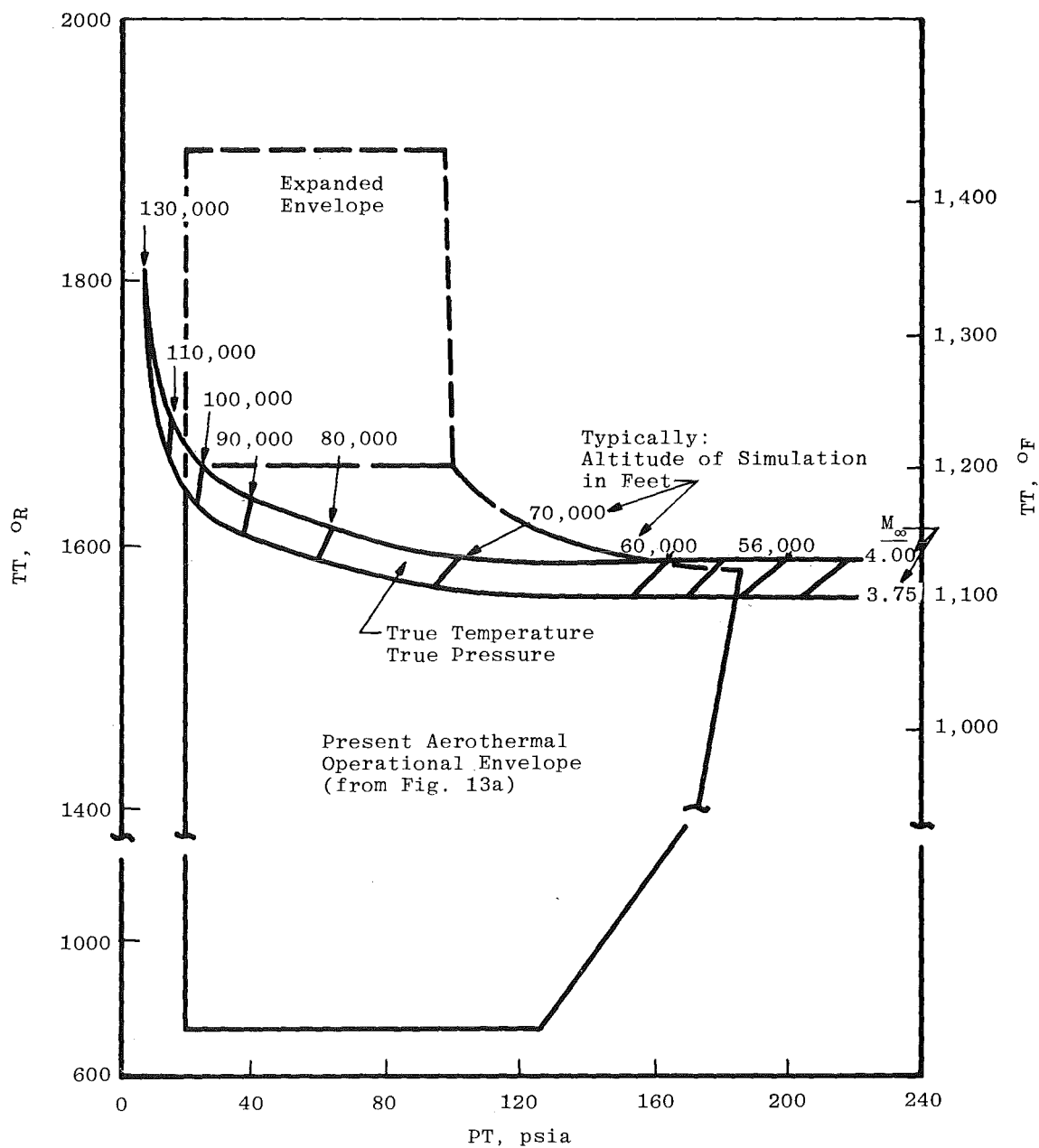
Sym	No.	Type Measurement
HC	~ 1.7	Coax Gages
GH	~ 3	Gardon Gages
SH	~ 1	Schmidt Boelter
PW	~ 28	Pressure Taps

Axial Sta.	S/R _N Station	x, in.	Roll Position, ϕ , (deg)			
			0	90	180	270
1	0	---	HC1	---	---	---
2	0.1745	---	HC2	PW1	HC13	PW14
3	0.3490	---	HC3	PW2	HC14	PW15
4	0.5236	---	HC4	PW3	HC15	PW16
5	0.6981	---	HC5	PW4	HC16	PW17
6	0.8727	---	HC6	PW5	---	PW18
7	1.0472	---	HC7	PW6	---	PW19
8	1.2217	---	HC8	PW7	---	PW20
9	1.3963	---	HC9	PW8	---	PW21
10	1.5708	0.0	HC10	PW9	---	PW22
11	1.9279	1.04	HC11	PW10	---	PW23
12	1.9840	1.20	---	PW11	---	PW24
13	2.285	2.07	HC12	PW12	HC17	PW25
14	2.370	2.32	SH1	GH1	GH2	GH3
15	2.642	3.11	PW27	PW13	PW28	PW26

Figure 12. Hemisphere model instrumentation.



a. Operating envelope — January 1982
Figure 13. True temperature - pressure altitude simulation.



b. True temperature - true pressure envelope
Figure 13. Concluded.

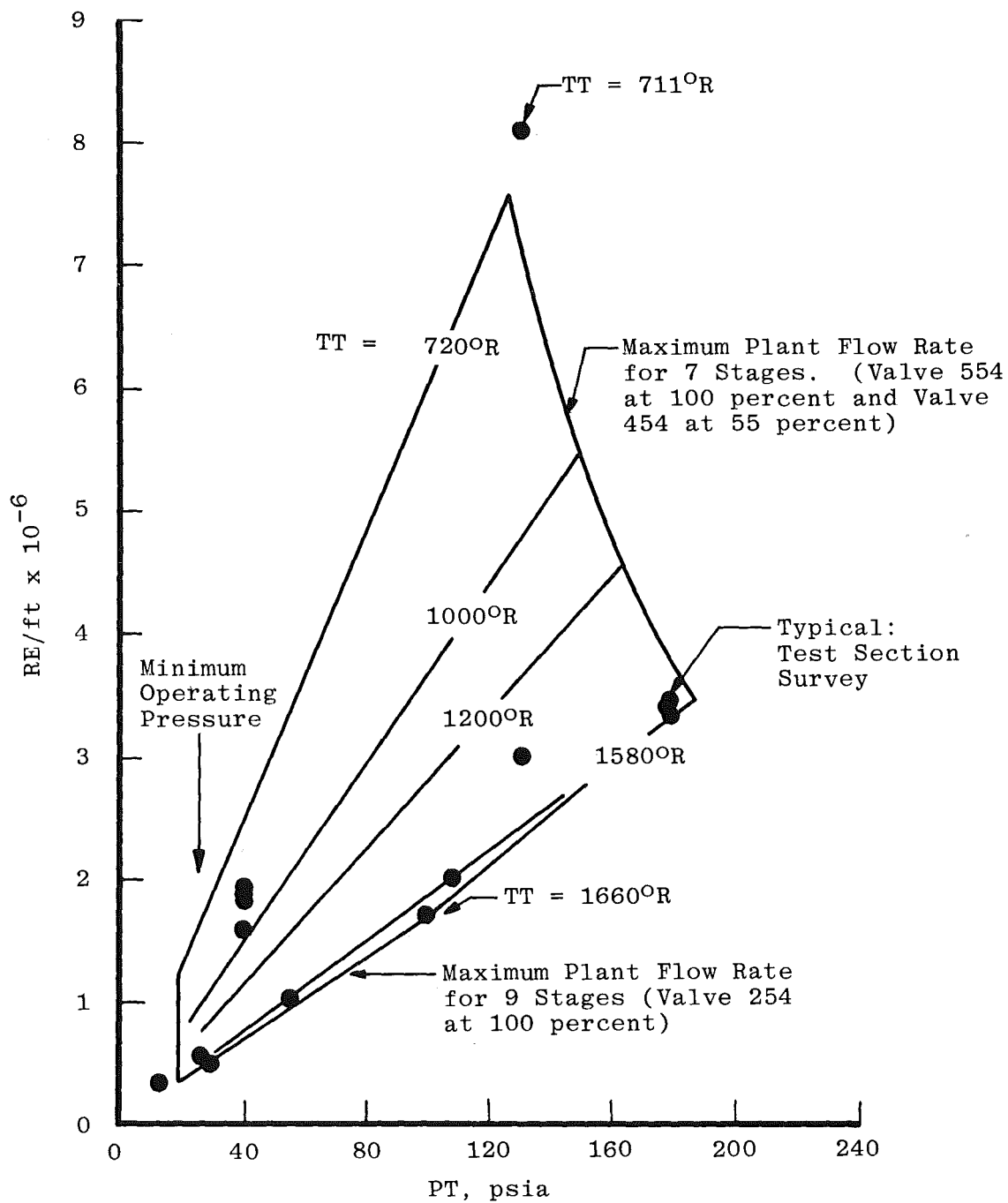


Figure 14. Aerothermal wind tunnel Reynolds number operating envelope ($M=4$).

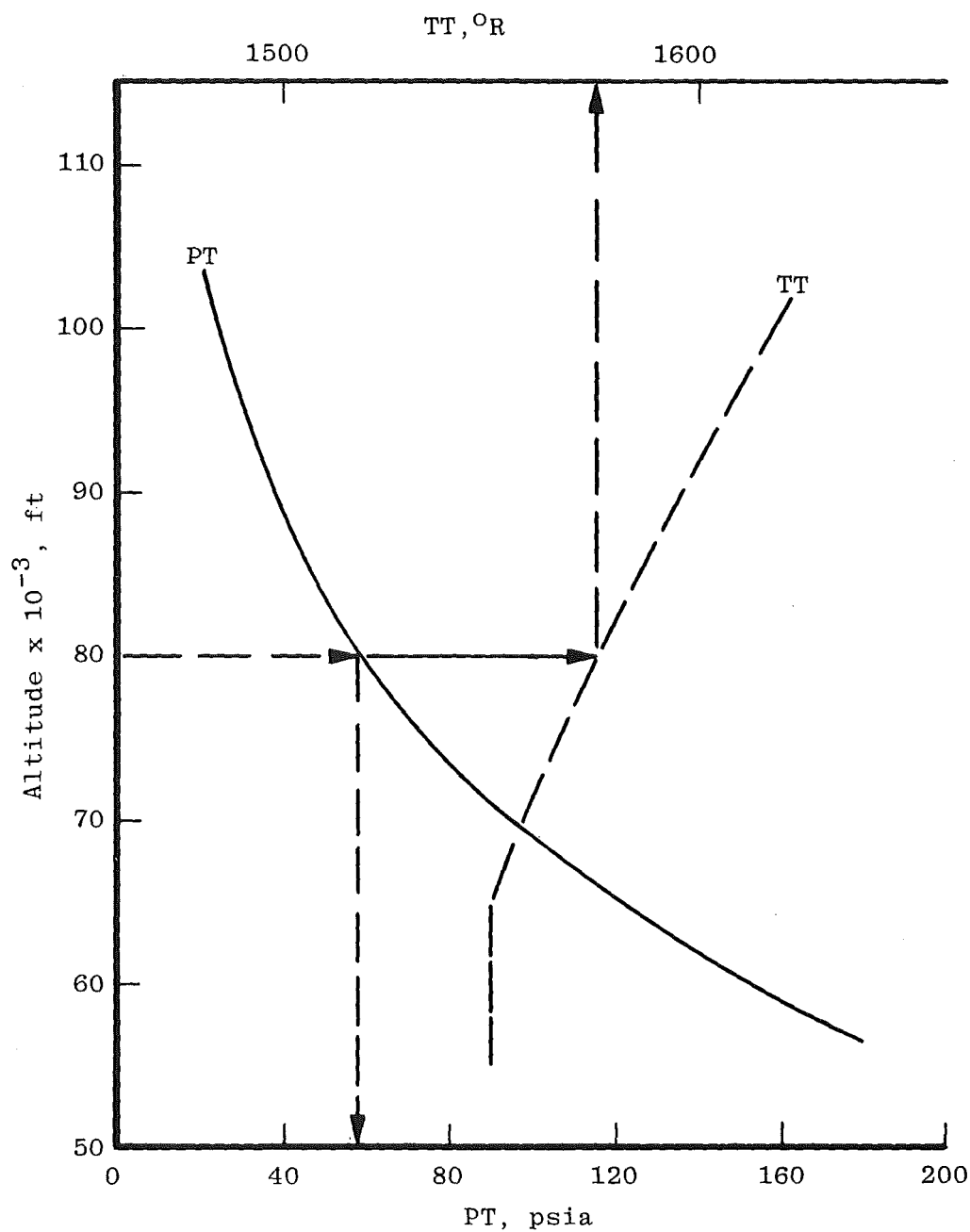


Figure 15. Stilling chamber conditions for true temperature - true pressure altitude simulation.

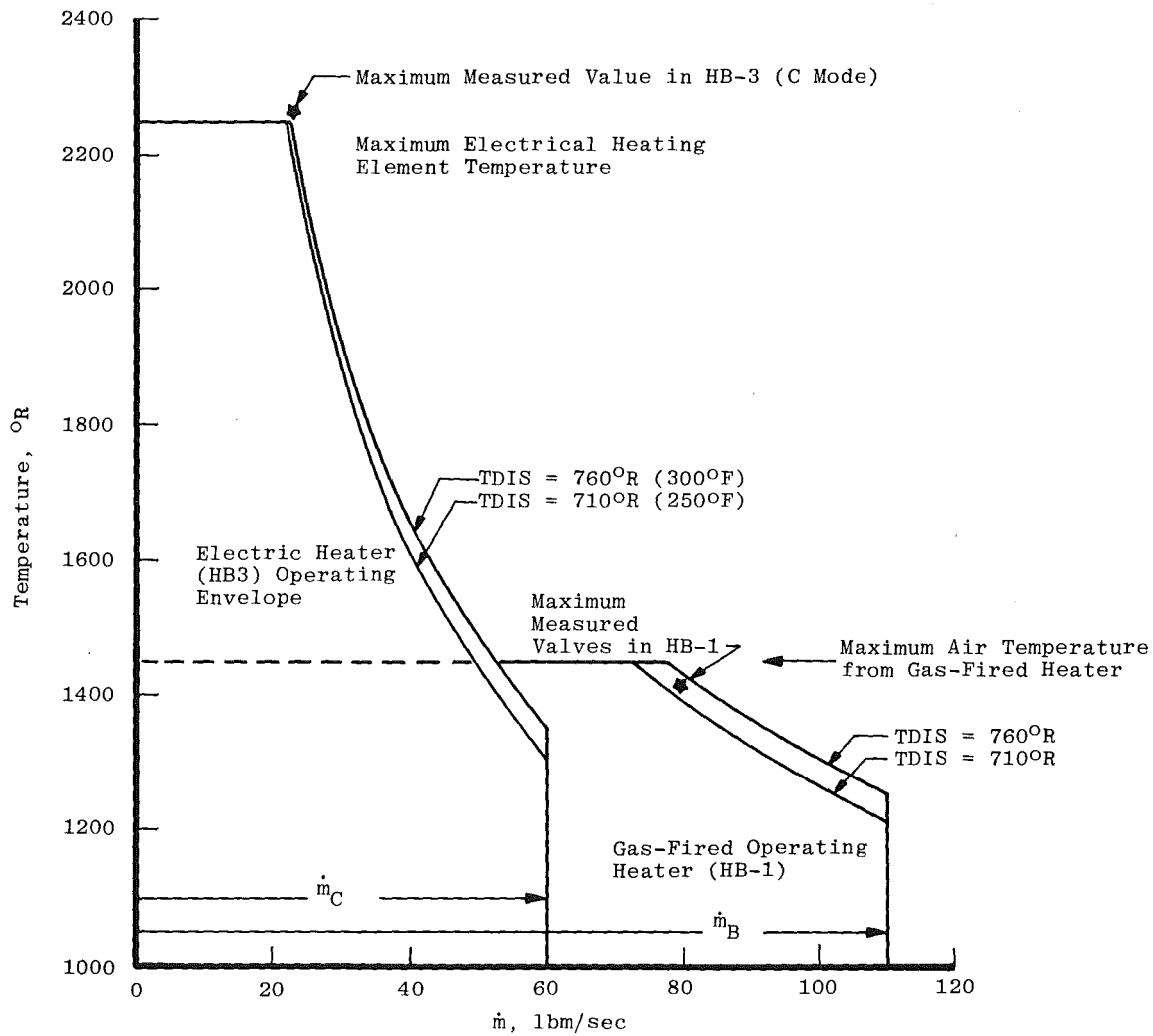


Figure 16. Thermal heating capacity in the aerothermal wind tunnel circuit.

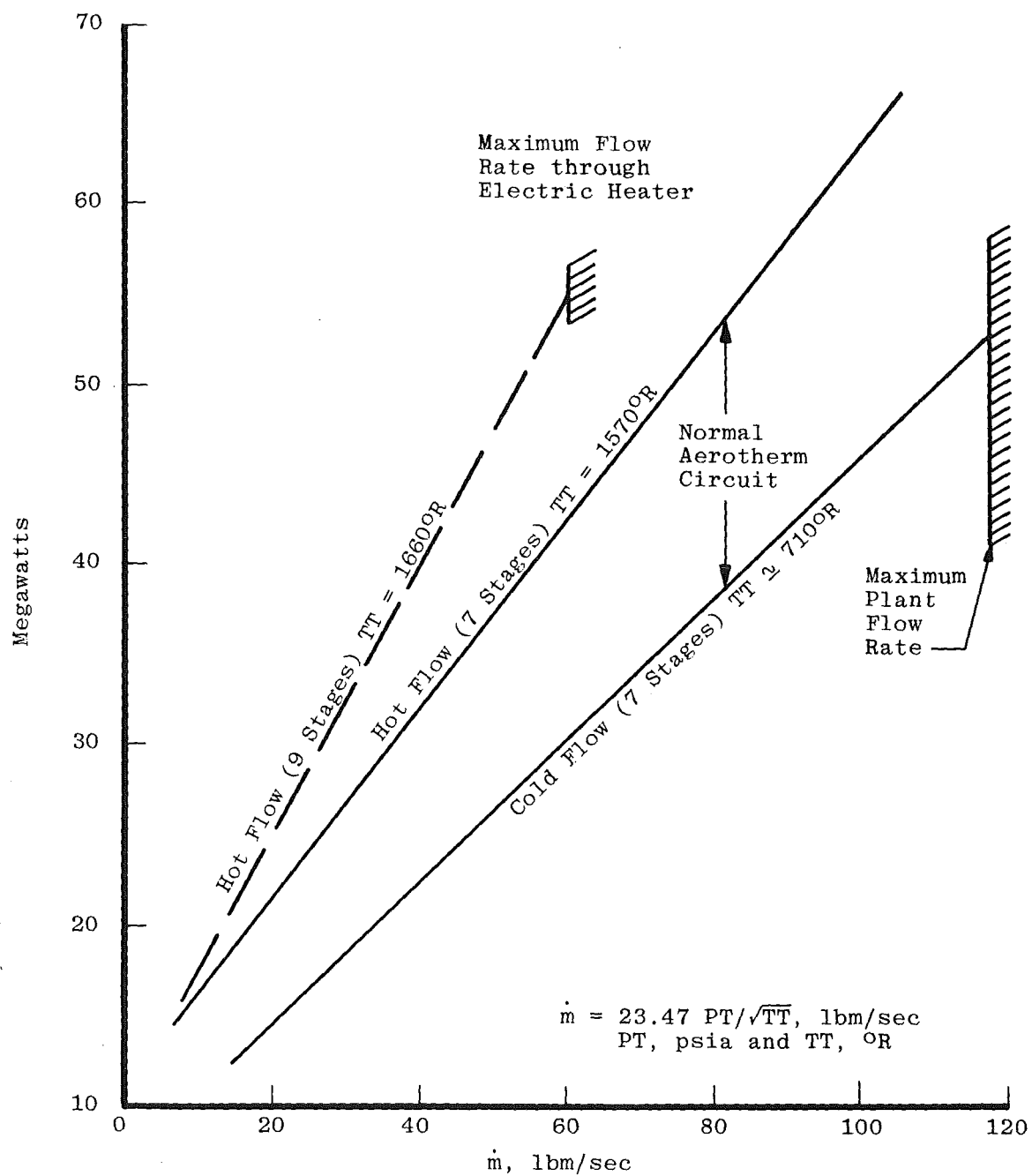
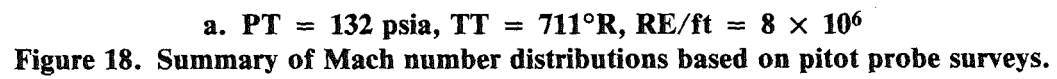
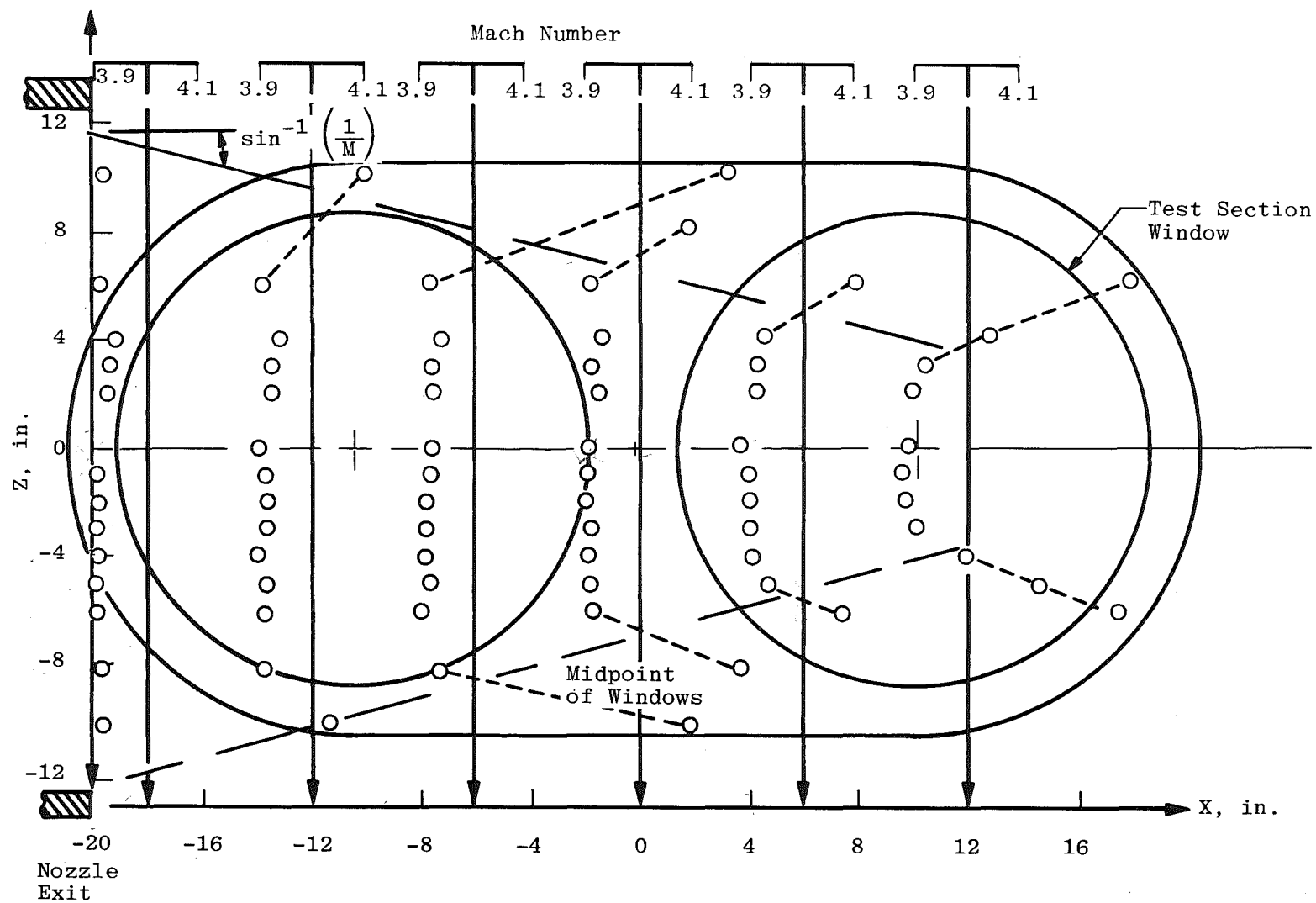


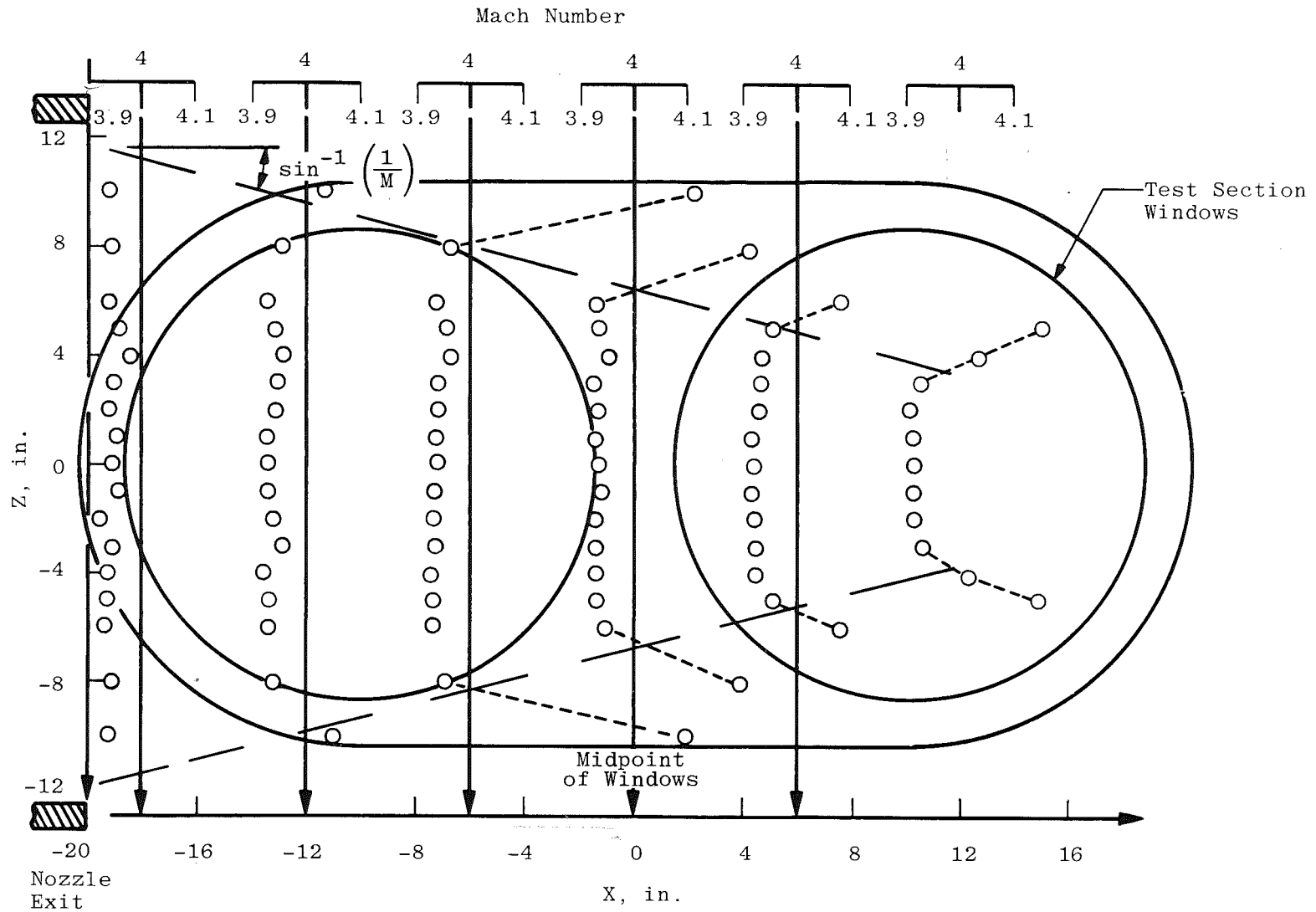
Figure 17. Aerothermal wind tunnel power consumption rates.



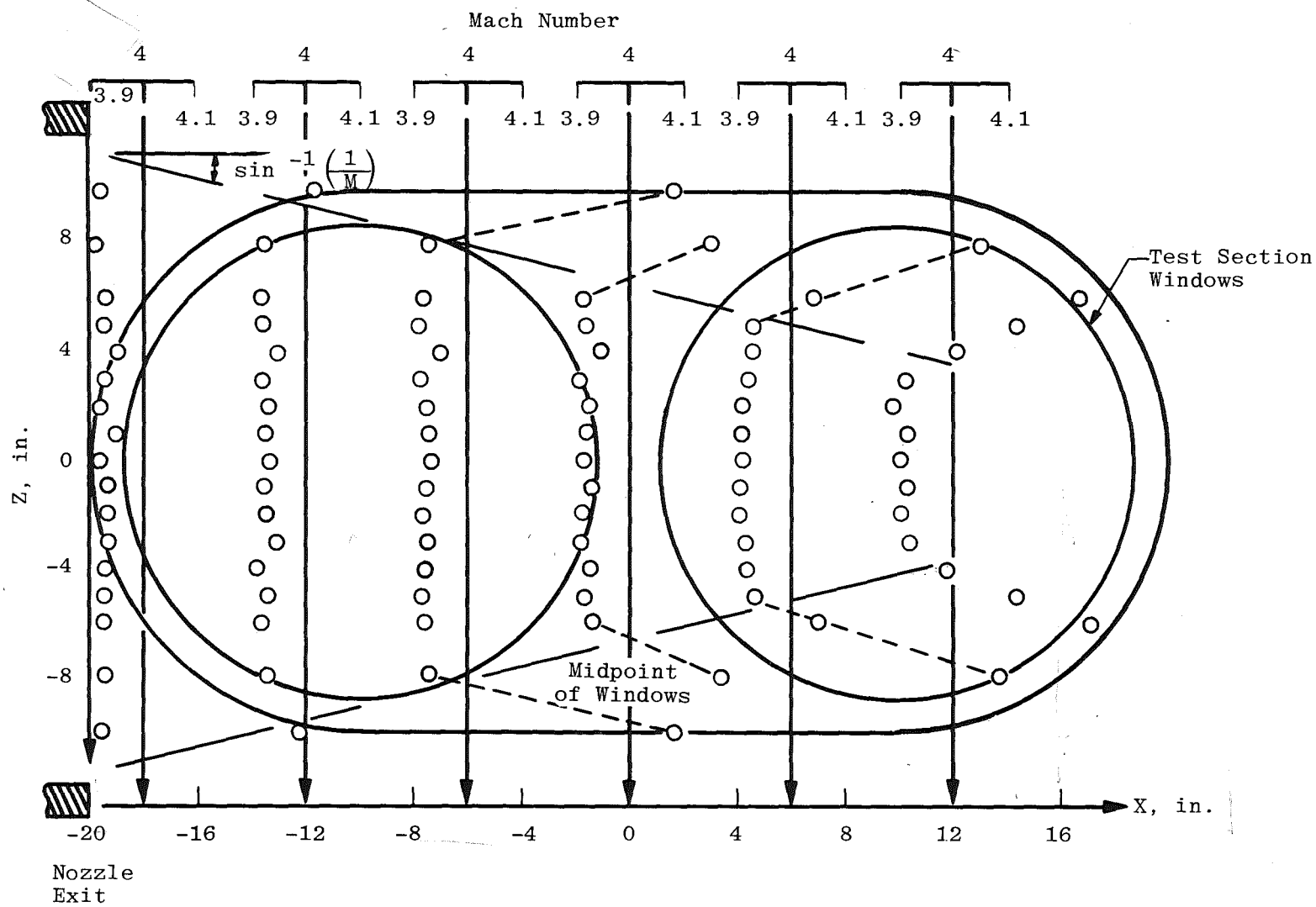


b. $PT = 26$ psia, $TT = 1461^{\circ}R$ and, $RE/ft = 0.54 \times 10^6$

Figure 18. Continued.

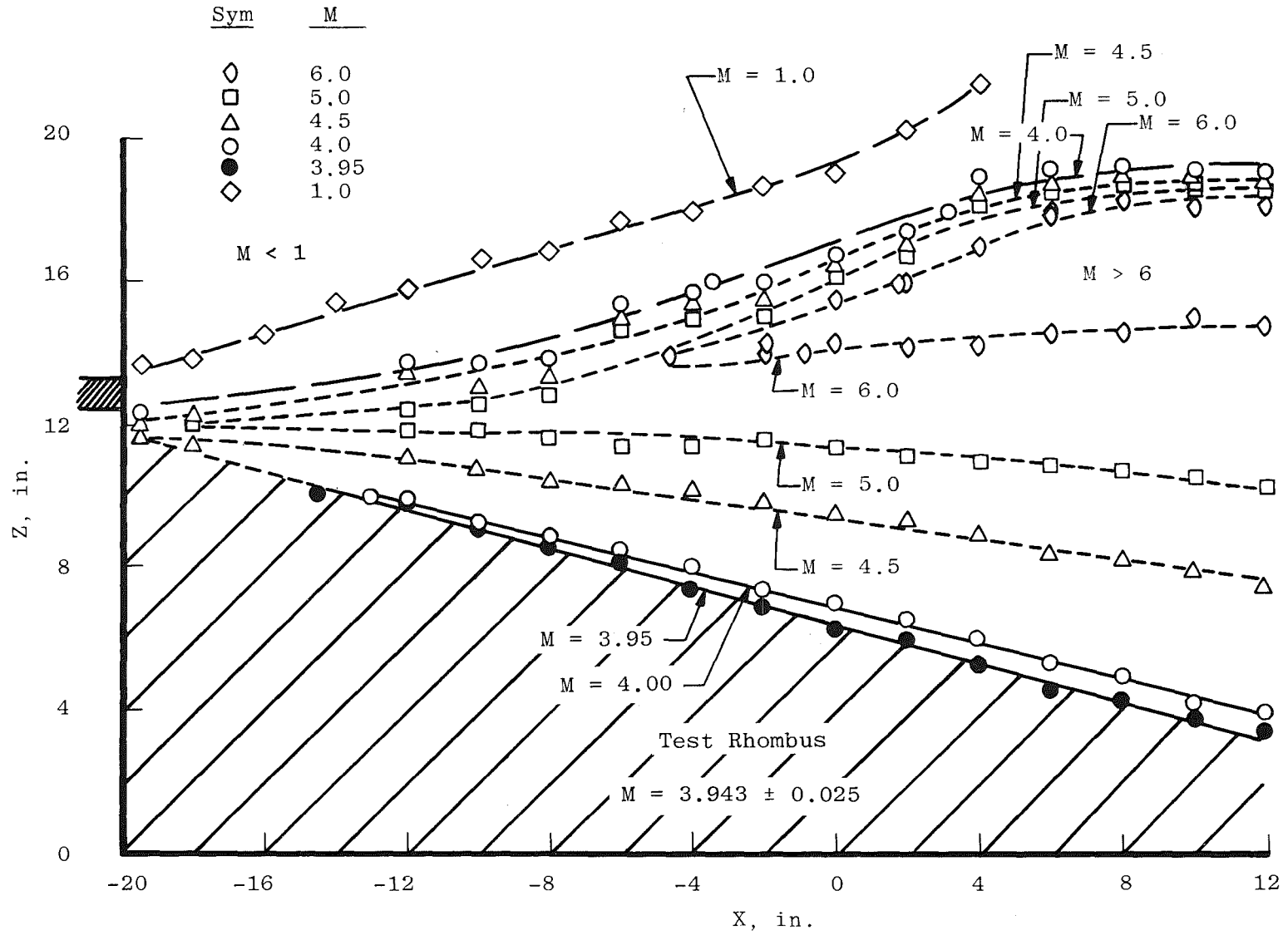


c. $PT = 179 \text{ psia}$, $TT = 1557^\circ\text{R}$, $RE/ft = 3.3 \times 10^6$
 Figure 18. Continued.

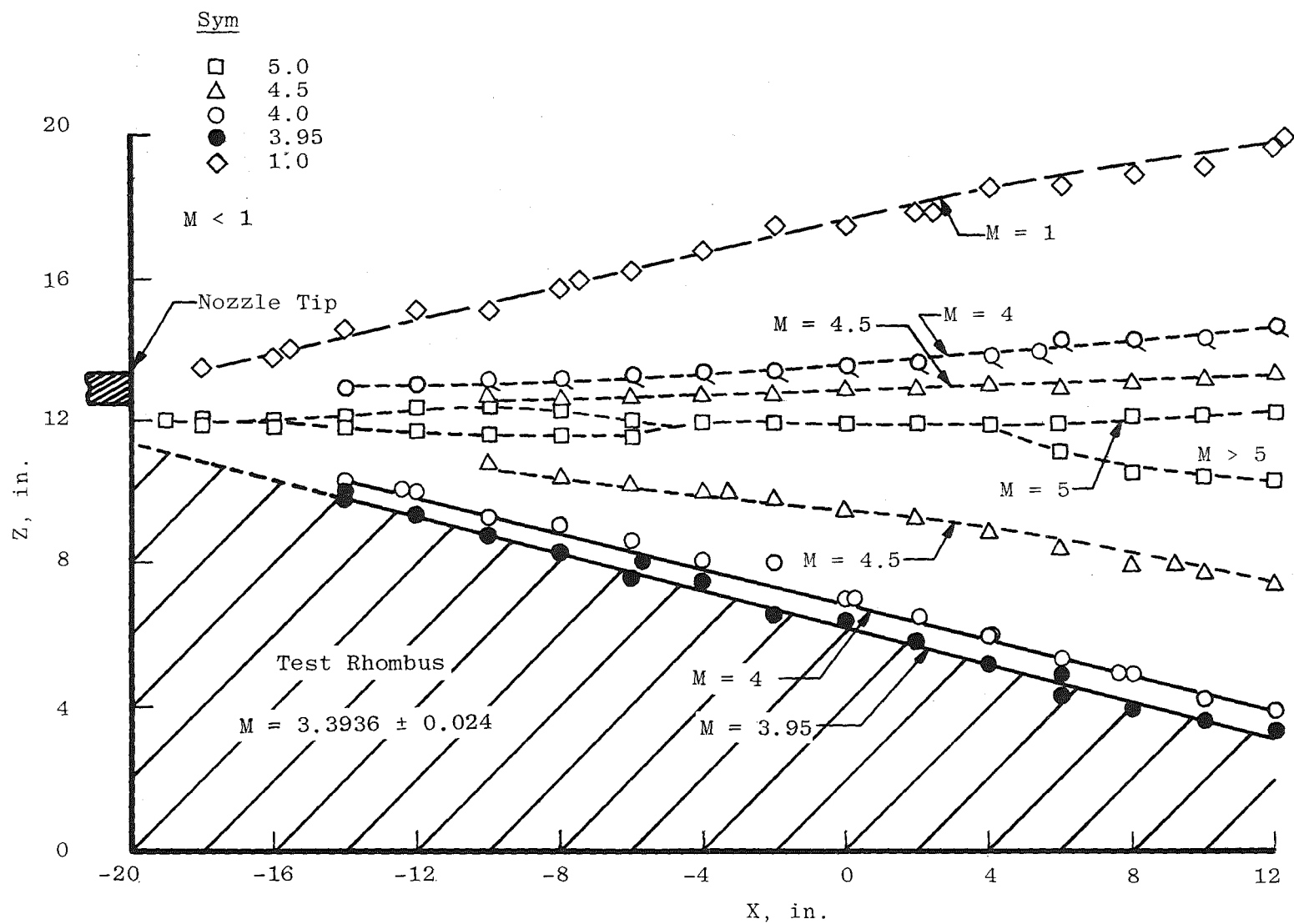


d. $PT = 99 \text{ psia}$, $TT = 1659^\circ\text{R}$ and $RE/ft = 1.7 \times 10^6$ (series heater circuit)

Figure 18. Concluded.



a. $PT/PD = 474$, $PT = 179$ psia, and $TT = 1560^\circ R$
 Figure 19. Lines of constant Mach number.



b. $PT/PD = 44$, $PT = 27$ psia, and $TT = 1470^\circ R$
 Figure 19. Concluded.

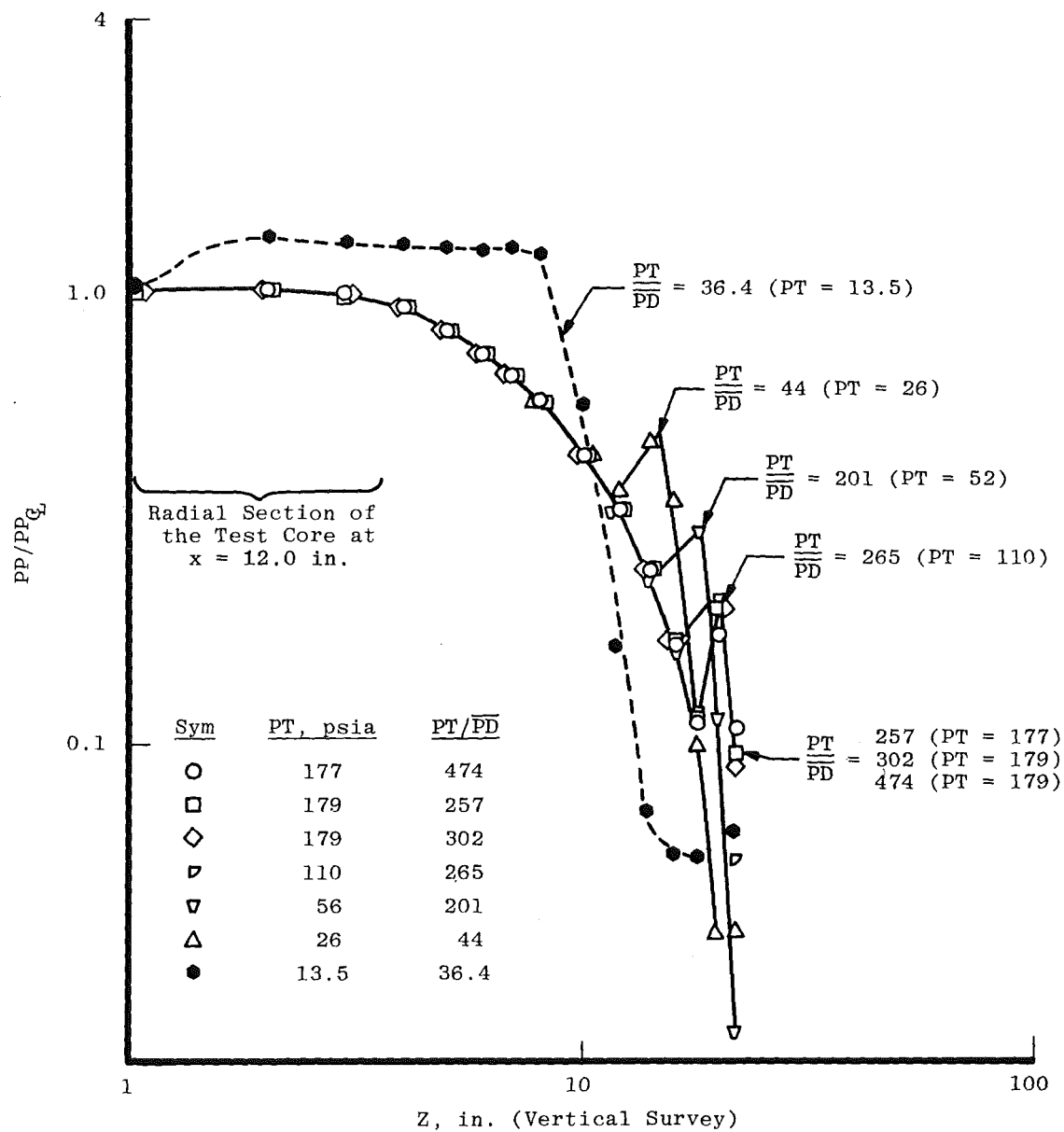
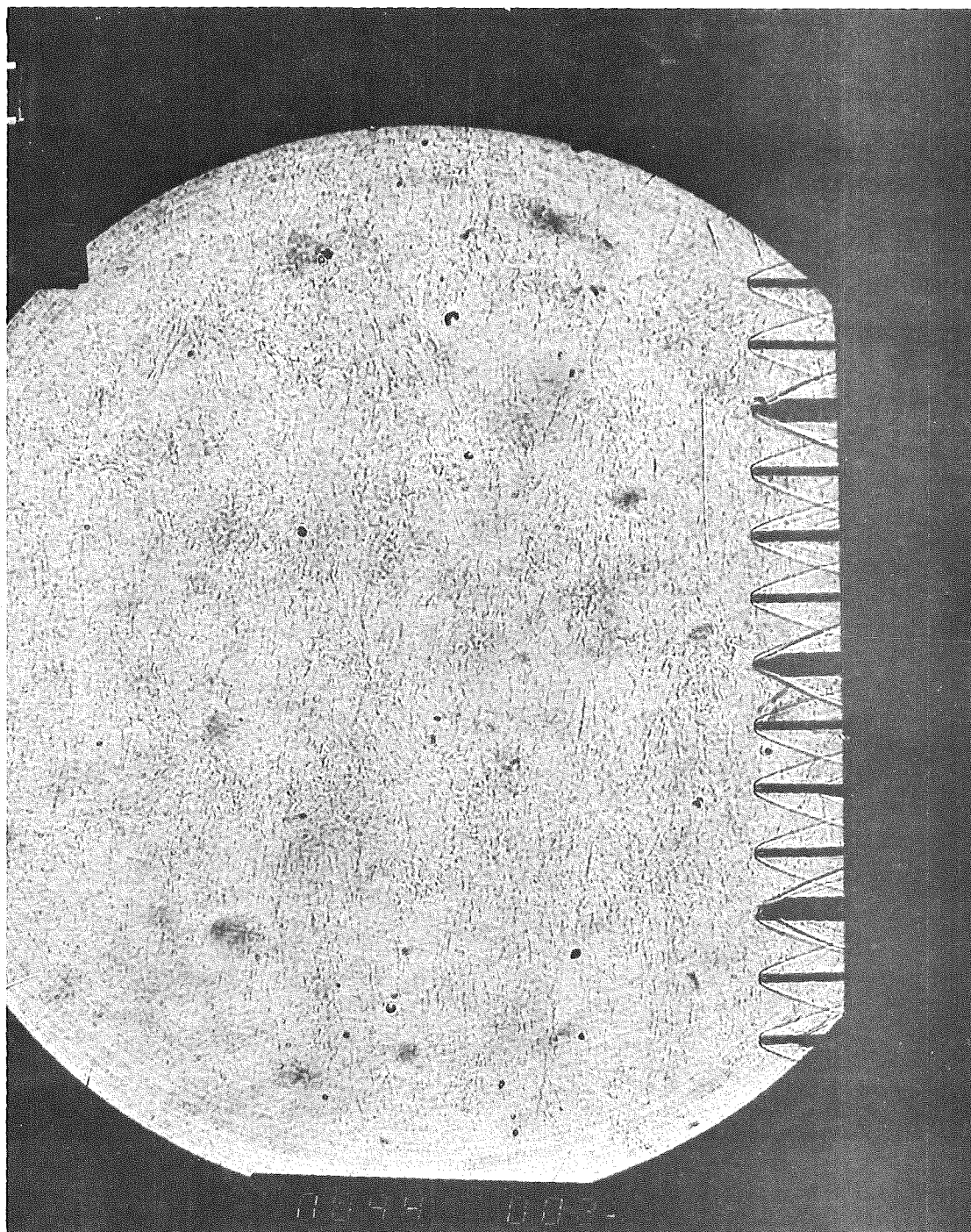
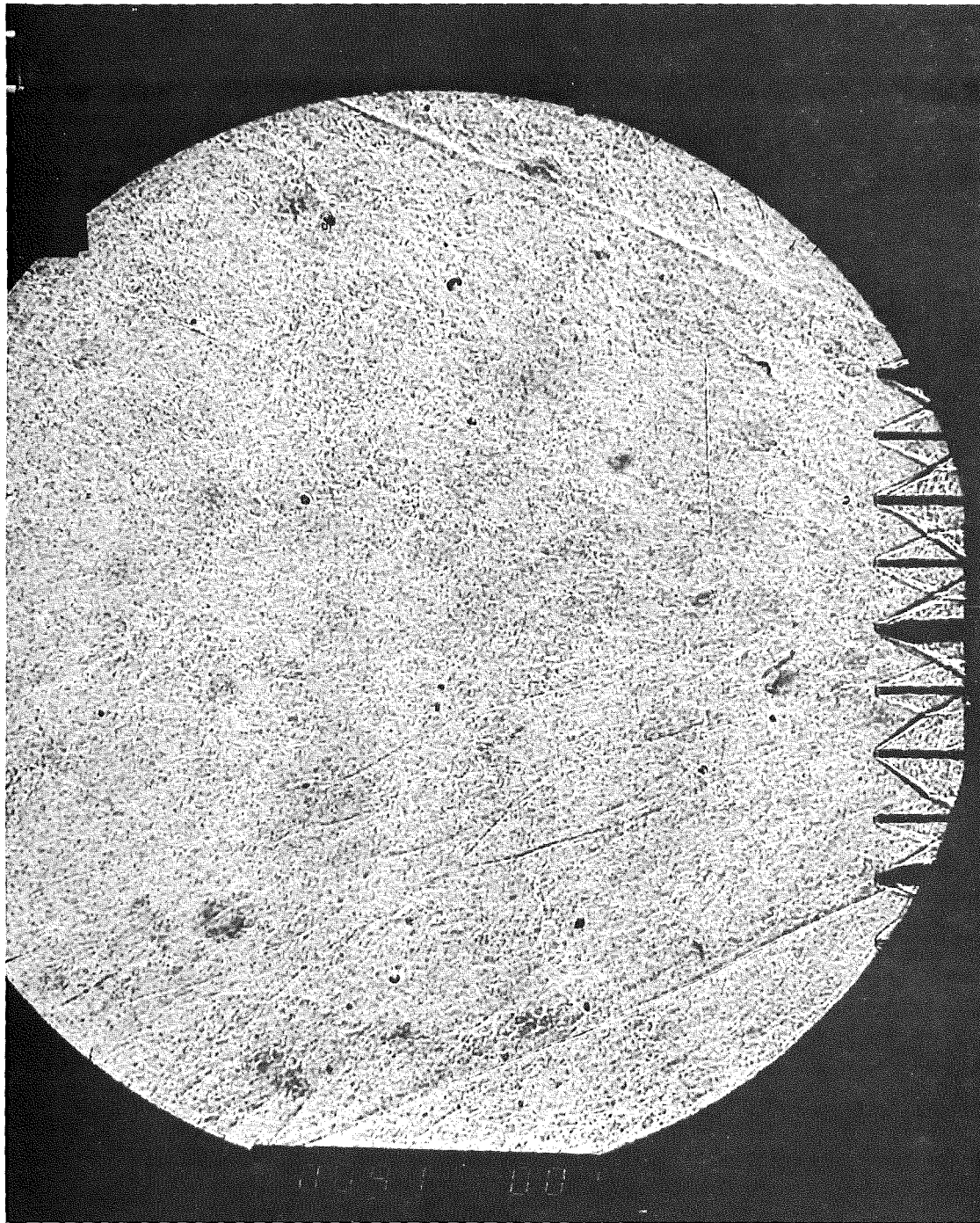


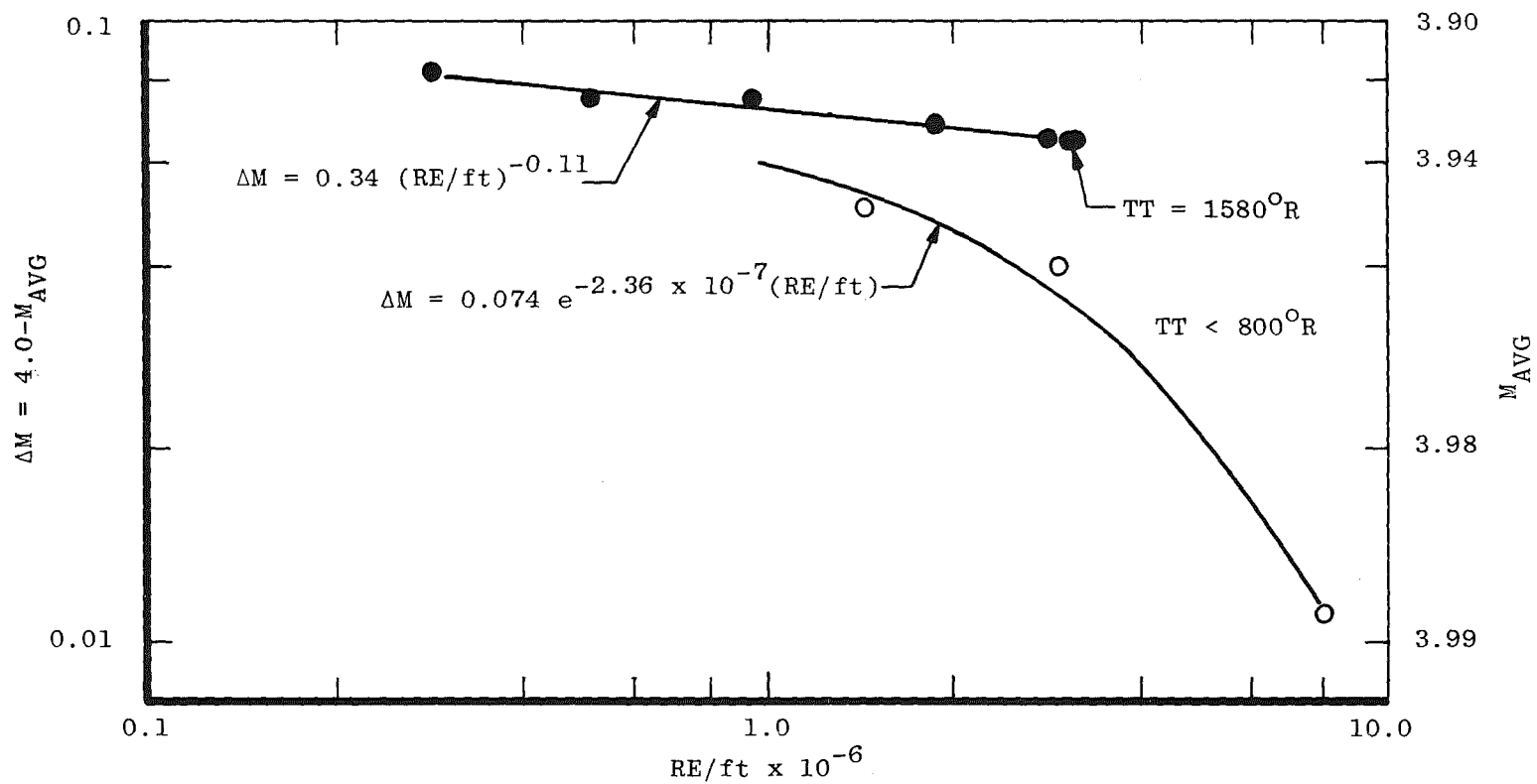
Figure 20. The effect of $\frac{PT}{PD}$ on the test section rhombus at $X = 12$ in.



a. Flow established at $PT = 40$ psia, plant stages 1 through 7 (shadowgraph)
Figure 21. Typical flow-field pictures.

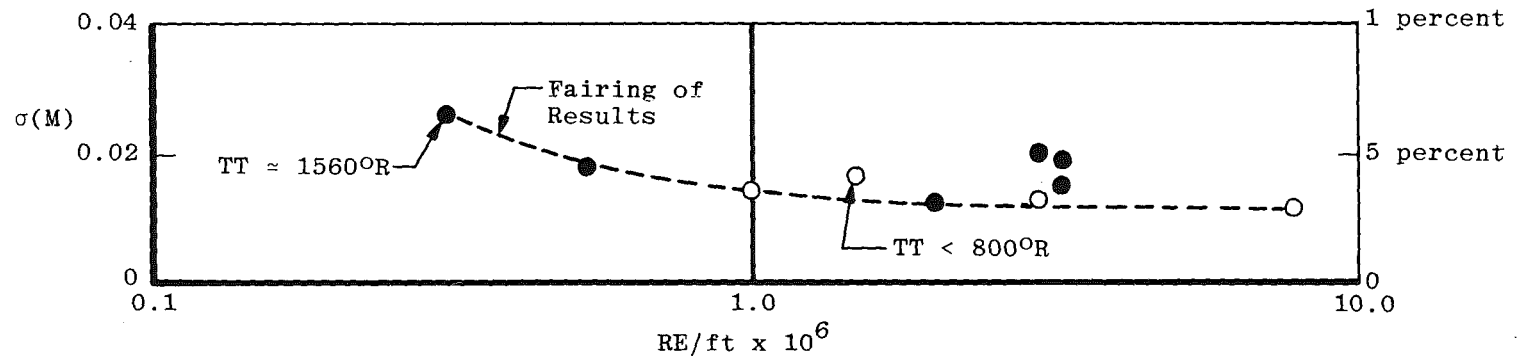


**b. Flow partially blocked or unstarted at $PT = 40$ psia,
plant compressor stages 2 through 7 (schlieren)
Figure 21. Concluded.**

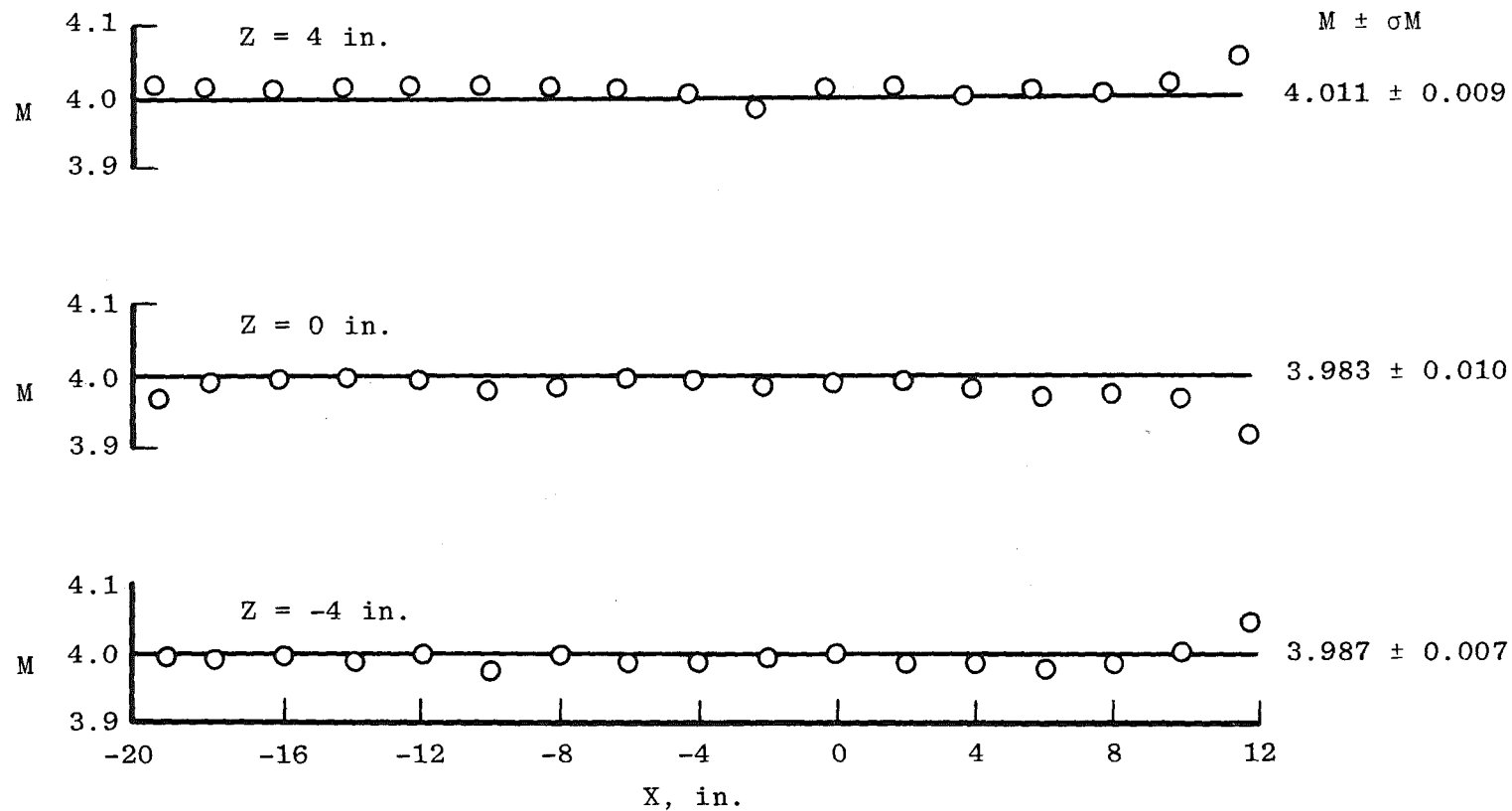


a. Average Mach number

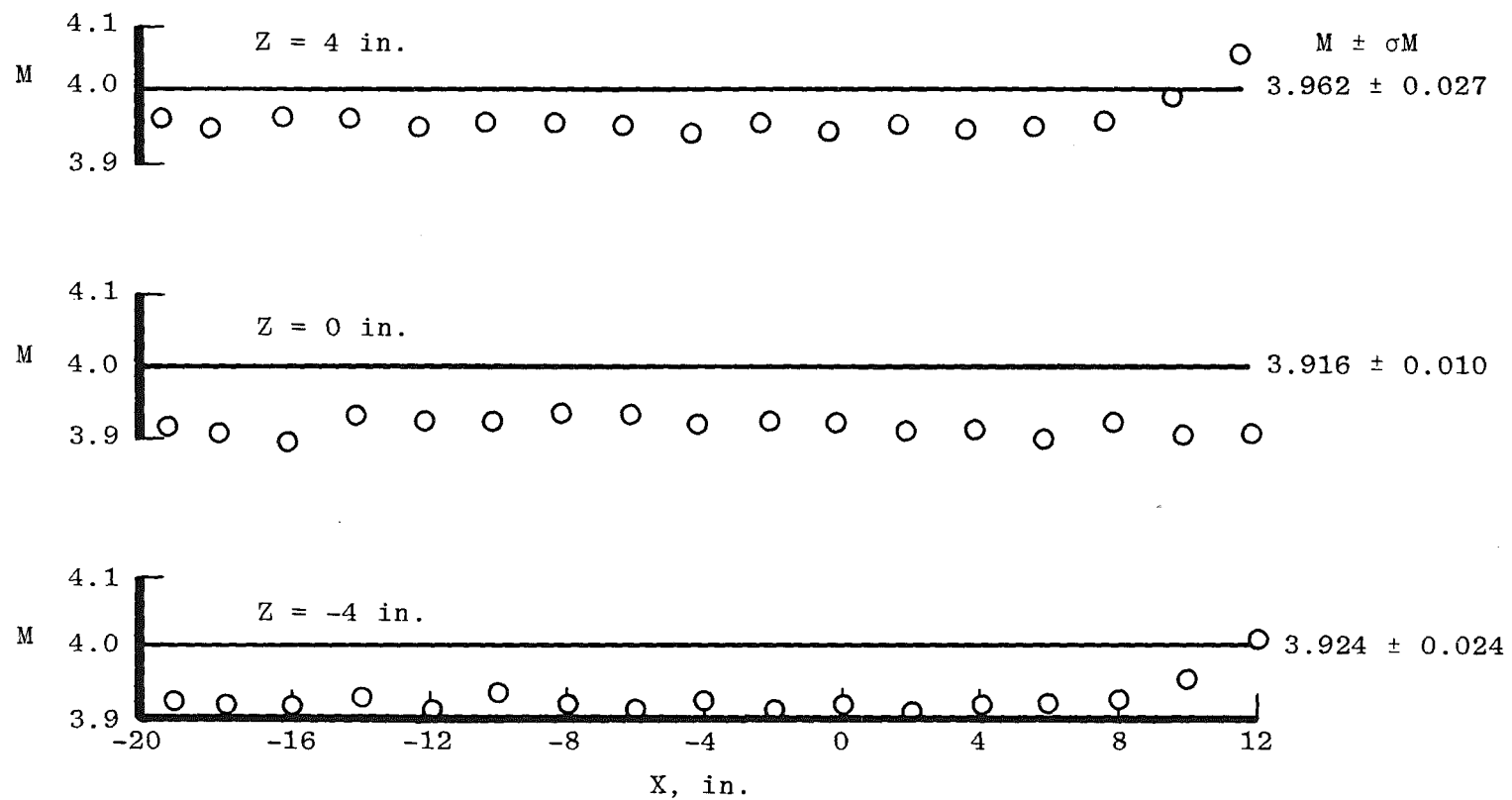
Figure 22. Test rhombus Mach number calibration as a function of free-stream Reynolds number.



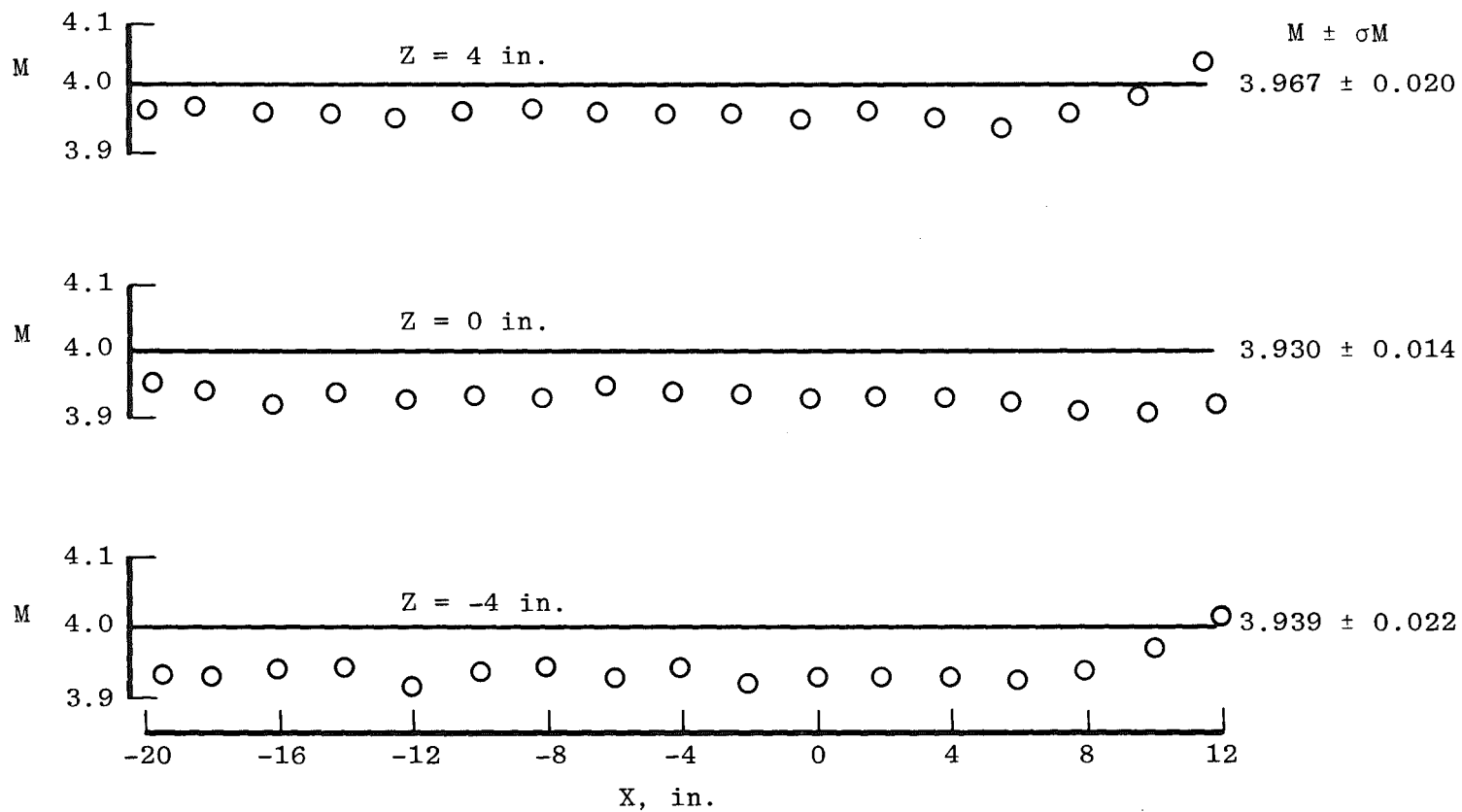
b. Mach number uniformity
Figure 22. Concluded.



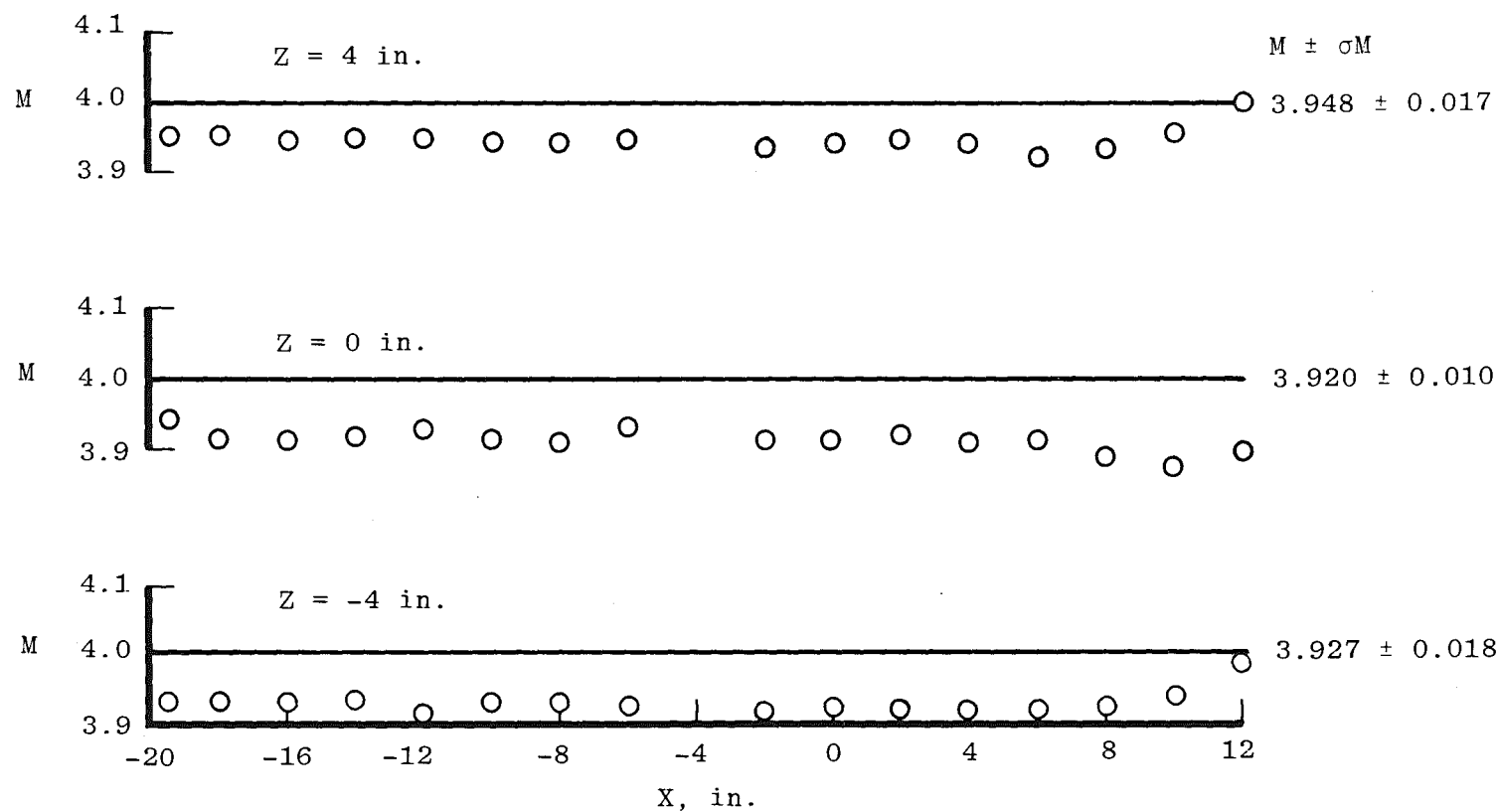
a. $PT = 132$ psia, $TT = 711^\circ R$, and $RE/ft = 8 \times 10^6$
 Figure 23. Free-stream Mach number axial distribution.



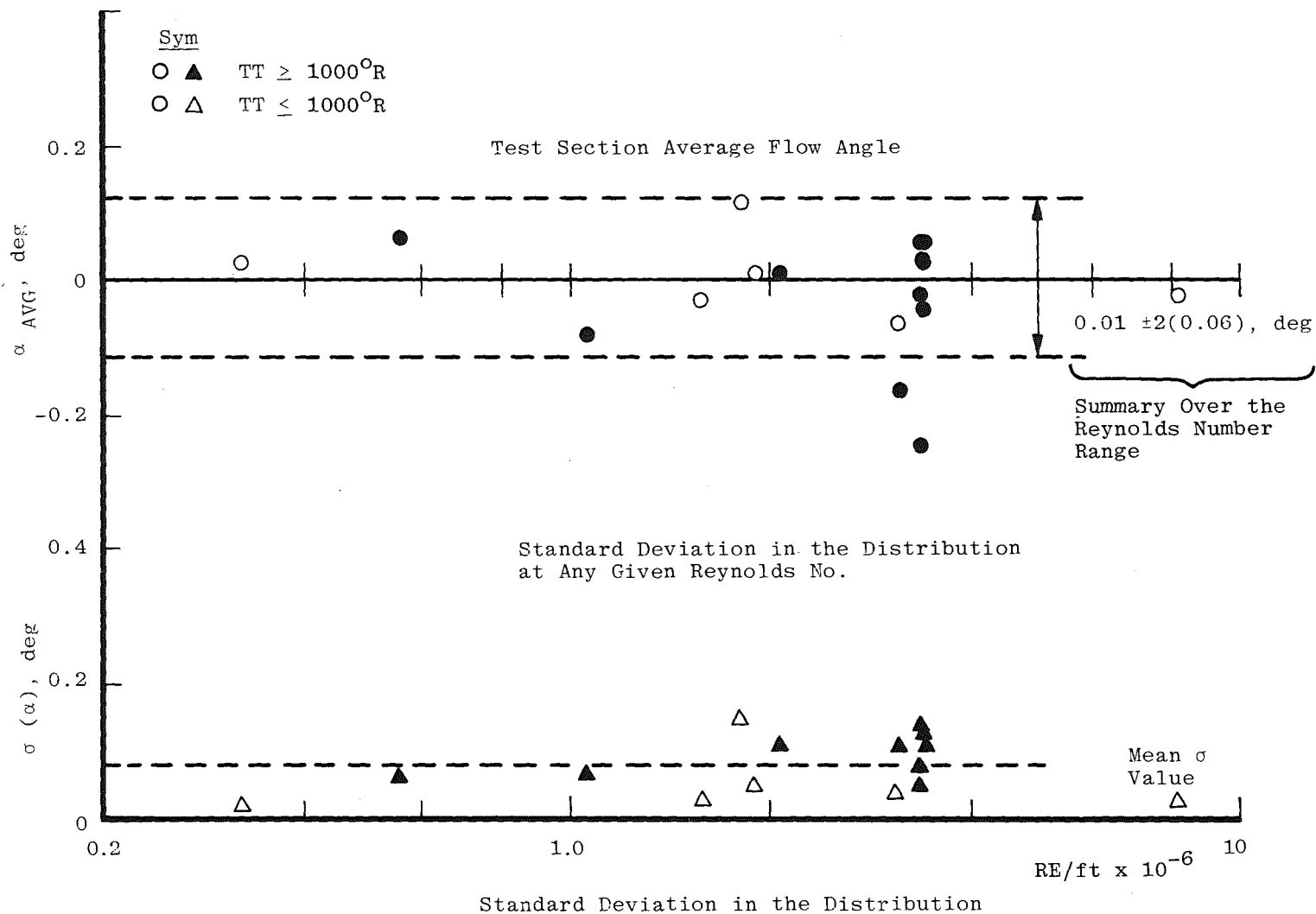
b. $PT = 26$ psia, $TT = 1461^\circ R$, and $RE/ft = 0.54 \times 10^6$
 Figure 23. Continued.



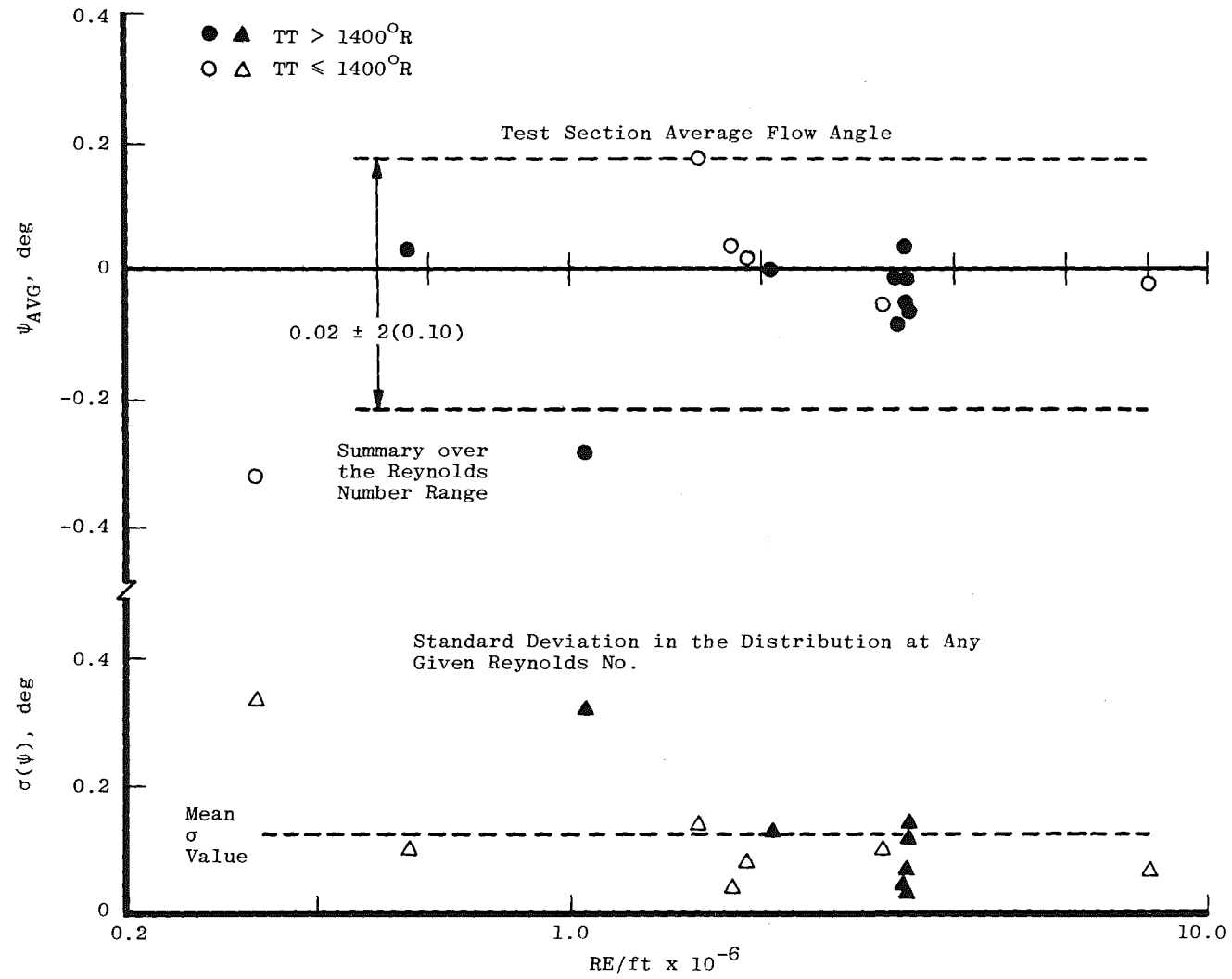
c. $PT = 179$ psia, $TT = 1557^\circ R$, and $RE/ft = 3.3 \times 10^6$
Figure 23. Continued.



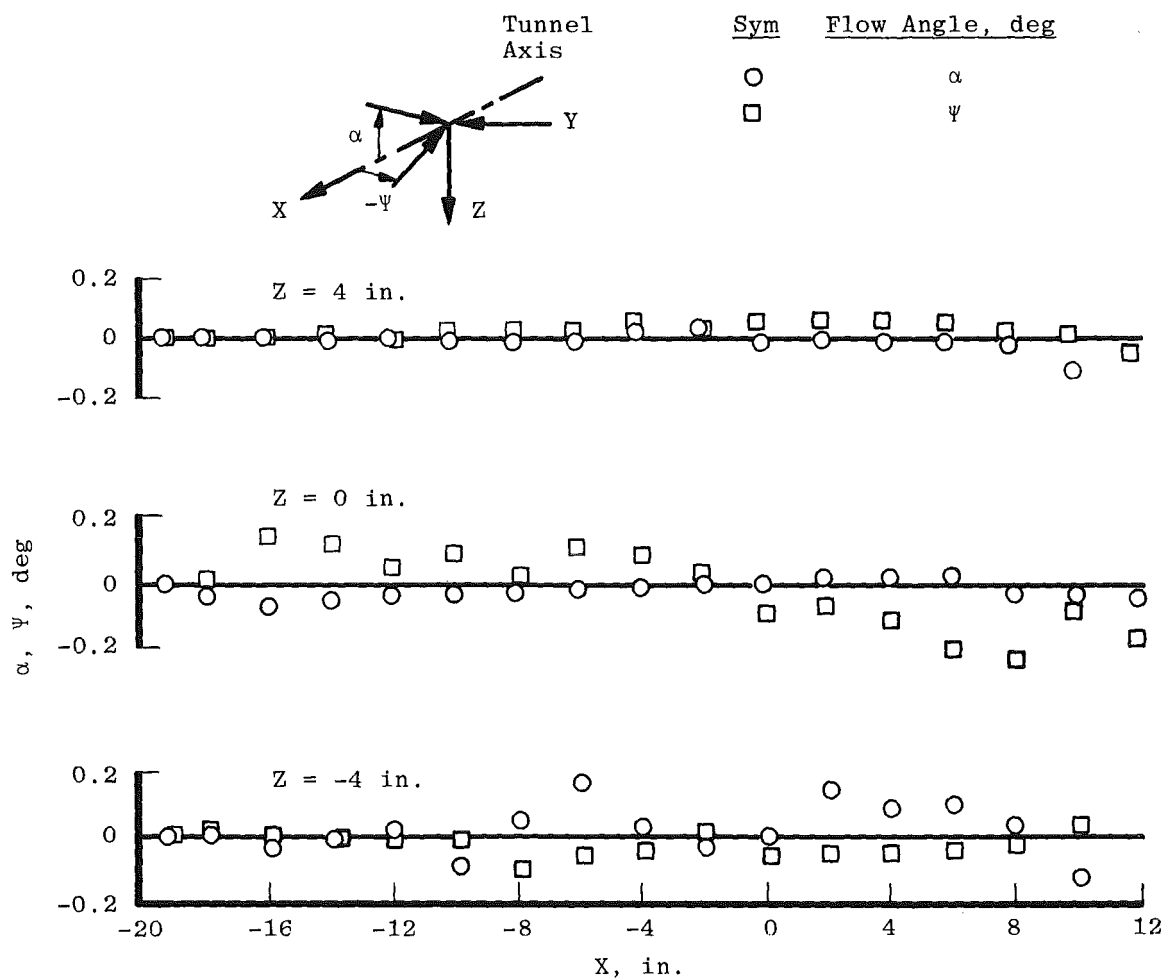
d. $PT = 99$ psia, $TT = 1659^\circ R$, and $RE/ft = 1.7 \times 10^6$ (series heater circuit)
Figure 23. Concluded.



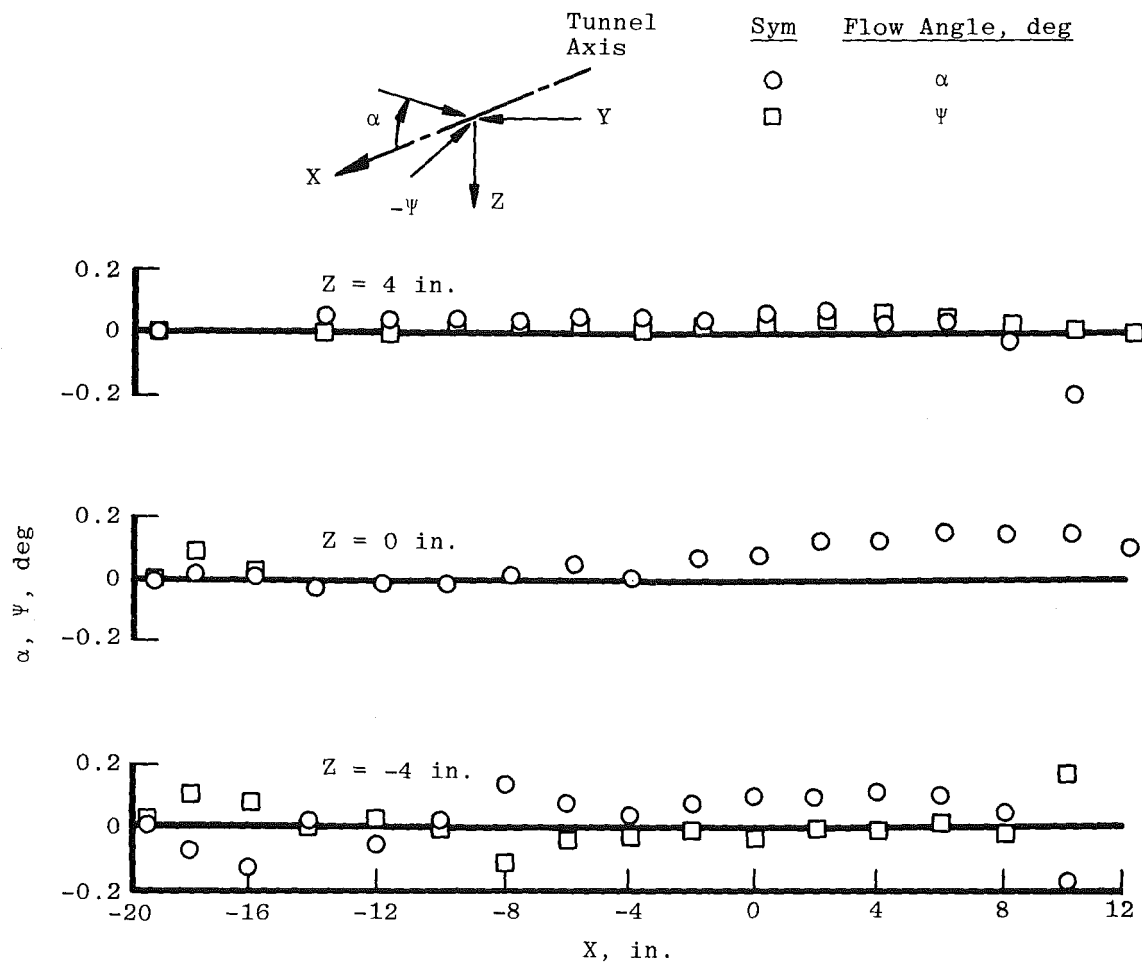
a. Pitch angle
Figure 24. Mach/flow angularity probe results.



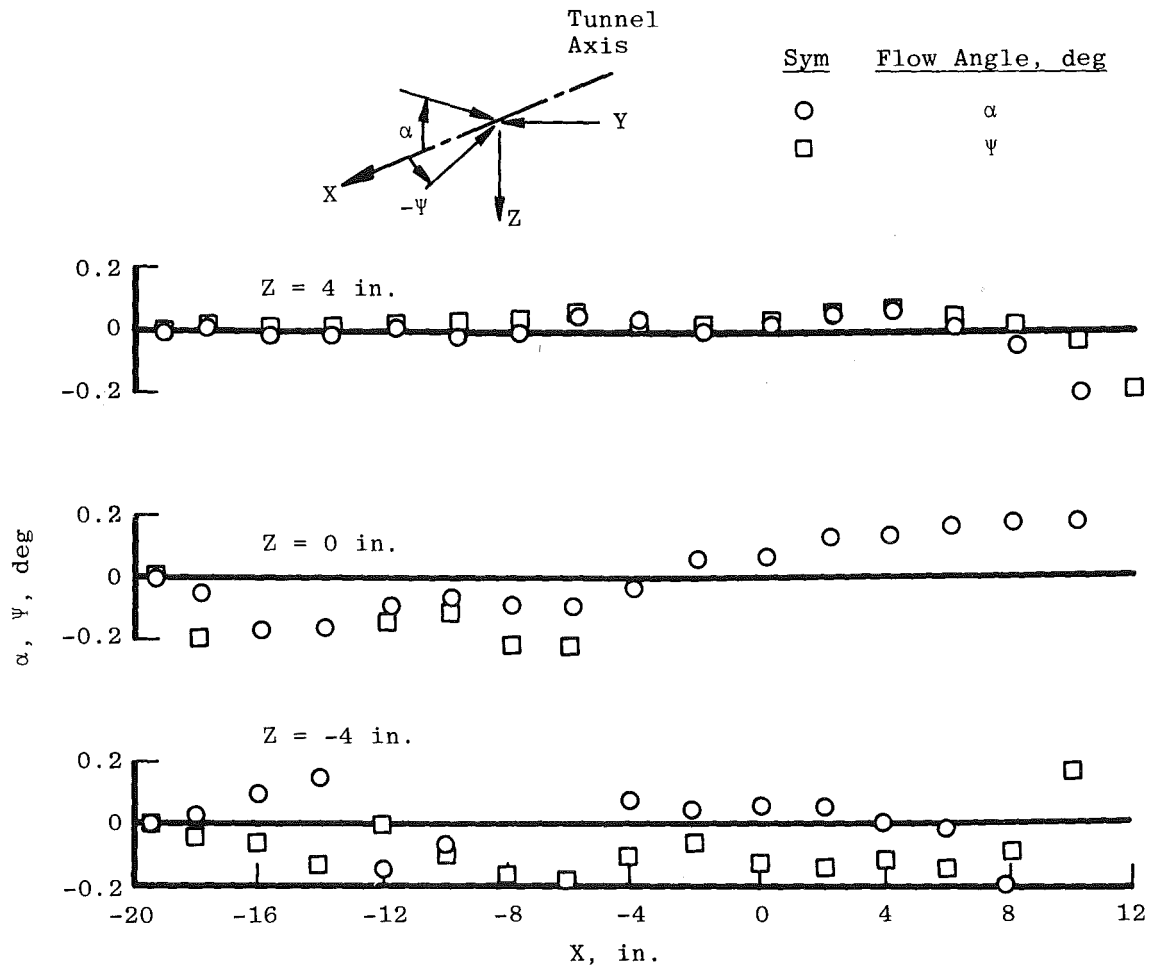
b. Yaw angle
Figure 24. Concluded.



a. $PT = 132$ psia, $TT = 711^\circ R$, and $RE/ft = 8 \times 10^6$
Figure 25. Flow angle variations.



b. $PT = 26$ psia, $TT = 1,461^\circ\text{F}$, $RE/ft = 0.54 \times 10^6$
 Figure 25. Continued.



c. $PT = 179$ psia, $TT = 1557^\circ R$, $RE/ft = 3.3 \times 10^6$
Figure 25. Concluded.

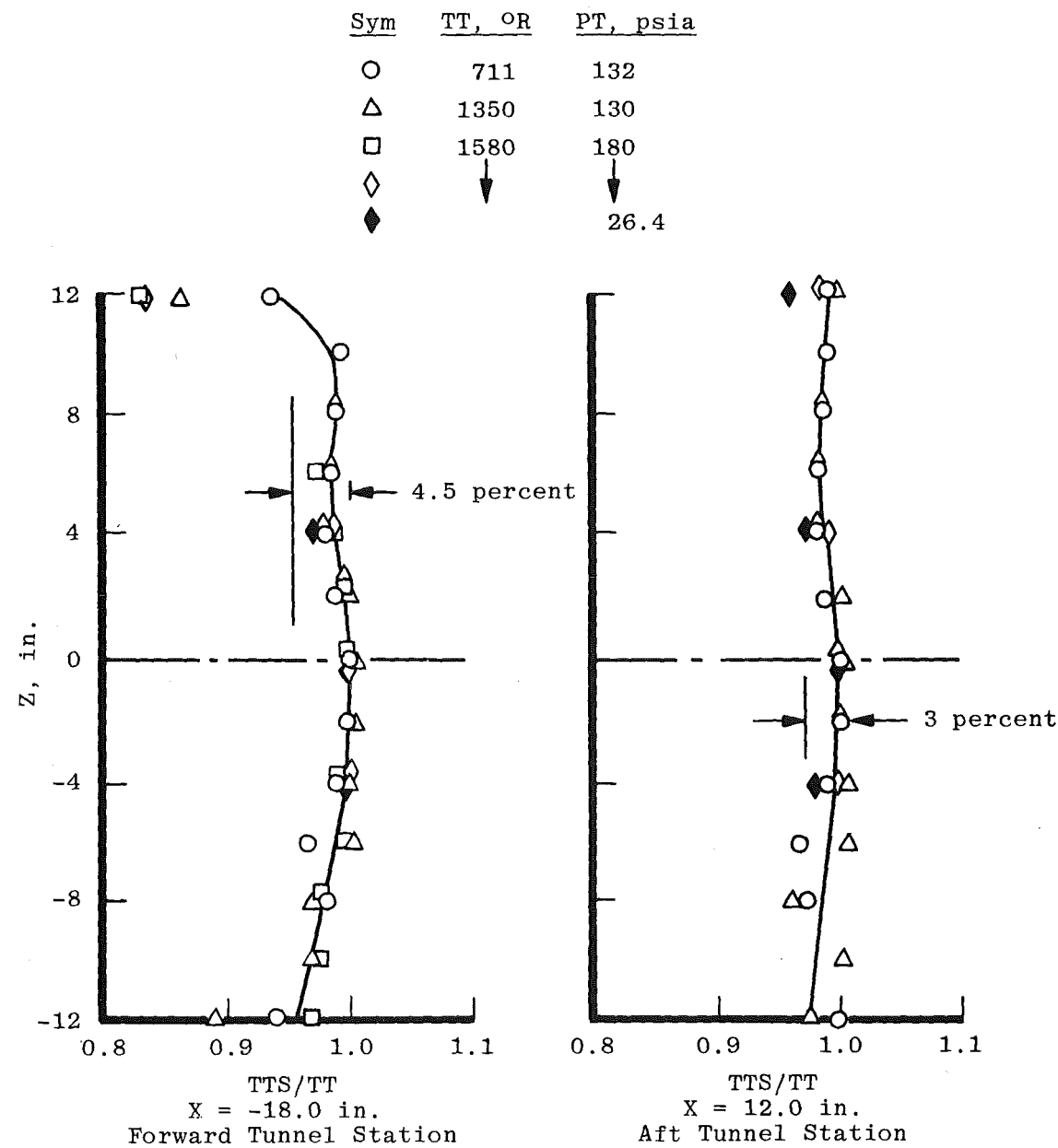


Figure 26. Vertical distribution of the total temperature distribution in the test section.

Typical:

Open Symbol - Initial Survey at $Z \geq 0$
 Flagged Symbol - Second Survey at $Z \geq 0$
 Solid Symbol - $Z < 0$

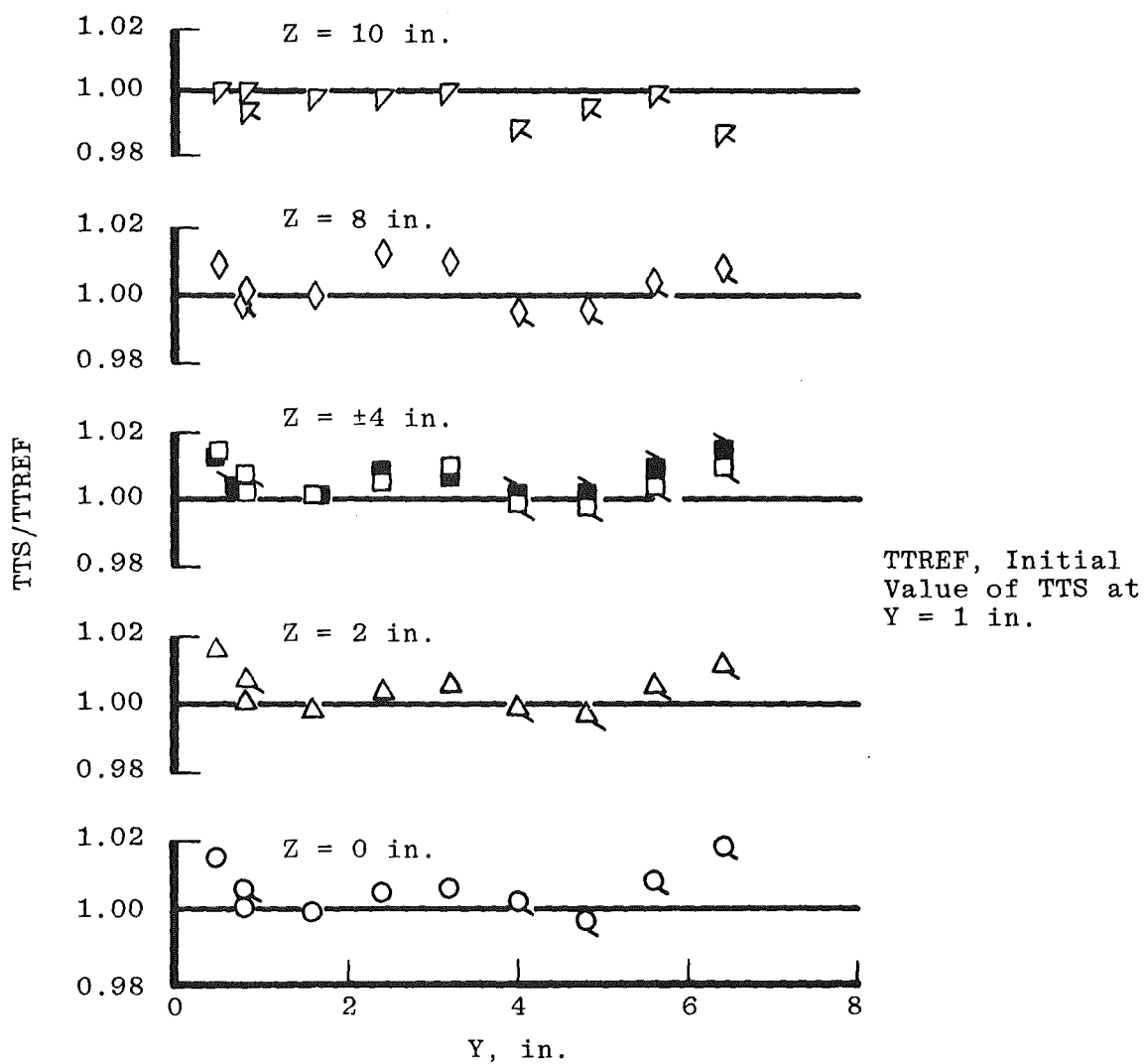


Figure 27. Lateral survey of the total temperature variation at $X = -18$ in., $M = 4.0$, $PT = 180$ psia, and $TT = 1580^\circ R$ ($RE/ft = 3.3 \times 10^6$)

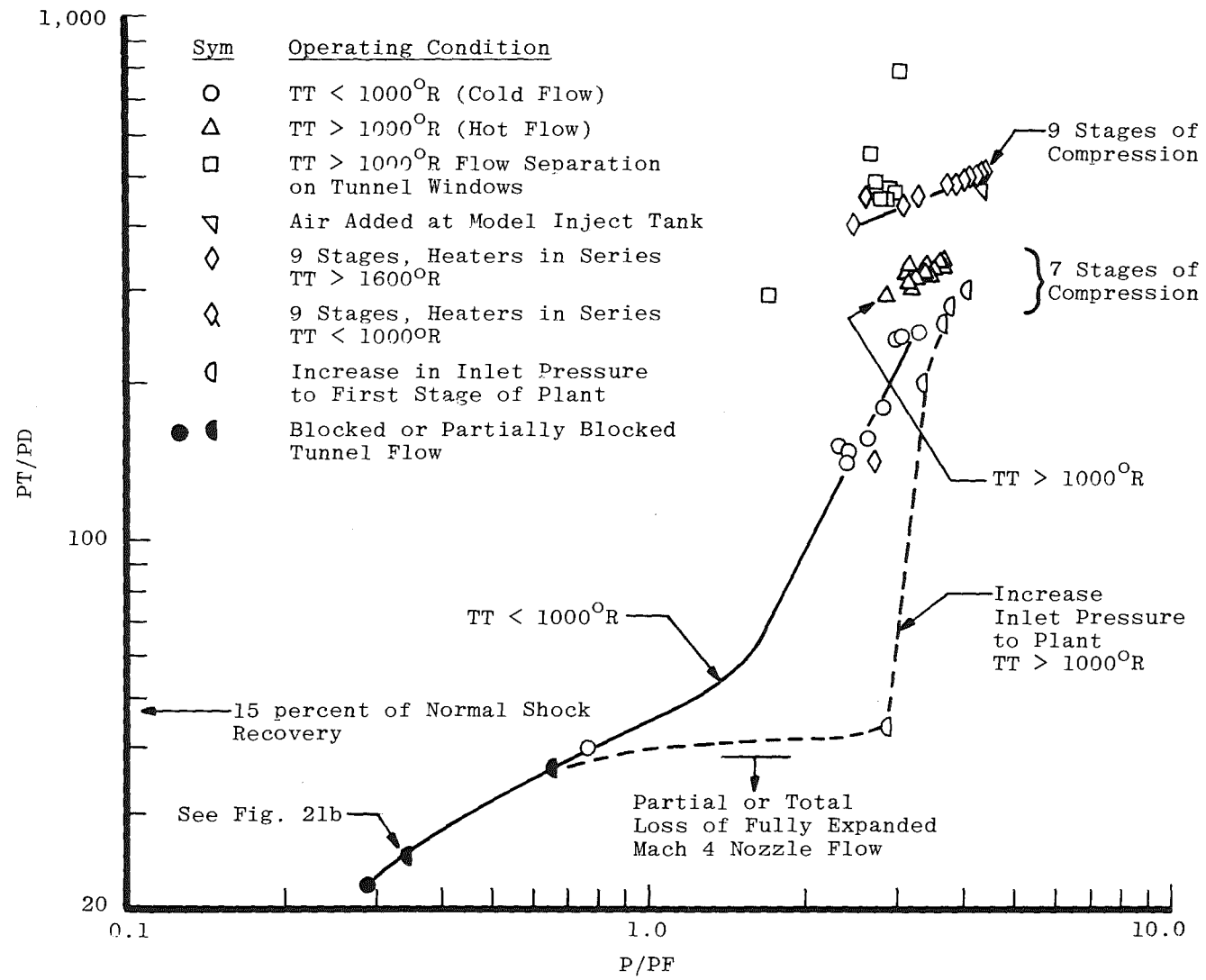


Figure 28. Aerothermal (Tunnel C) diffuser performance.

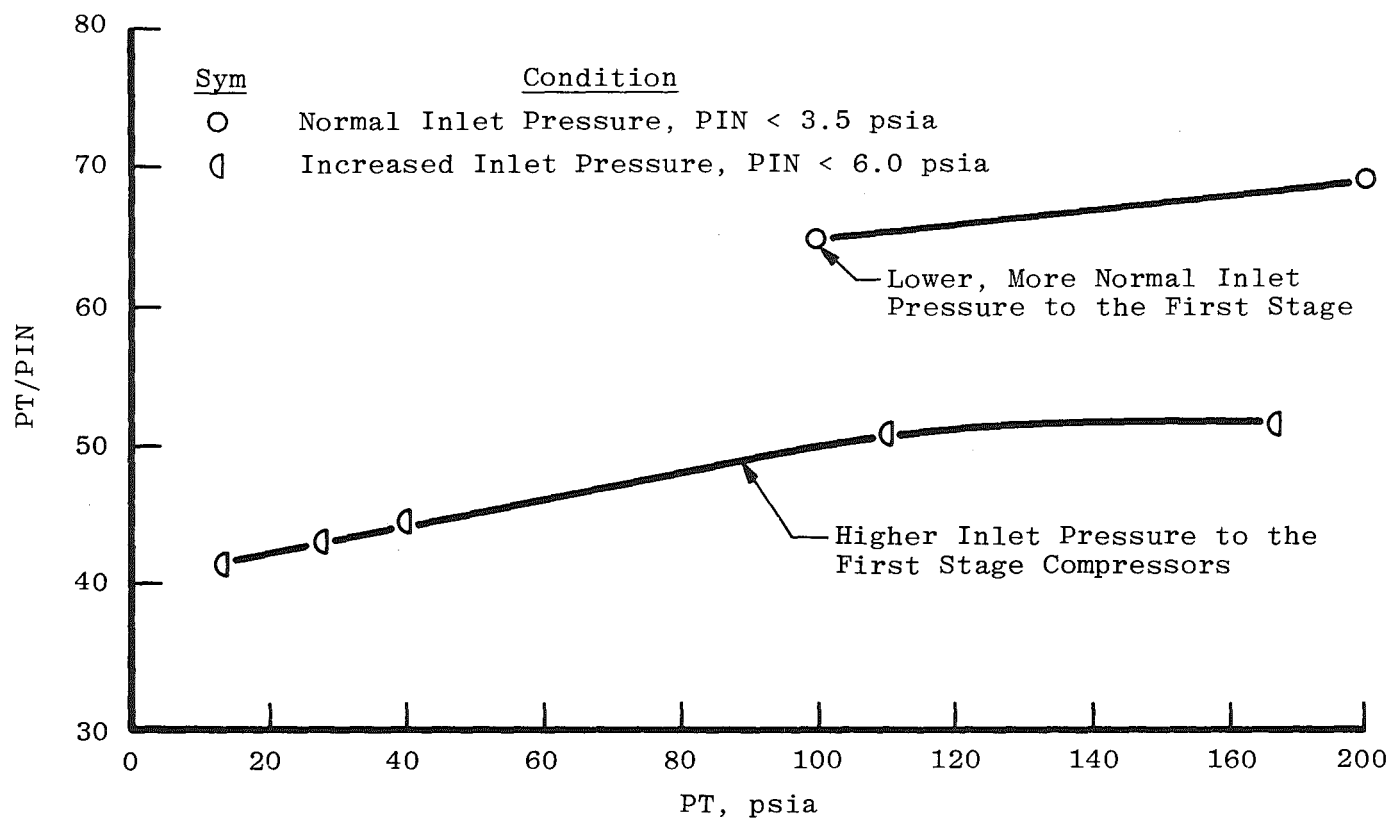


Figure 29. Variation of pressure ratio across the aerothermal wind tunnel as a function of PT.

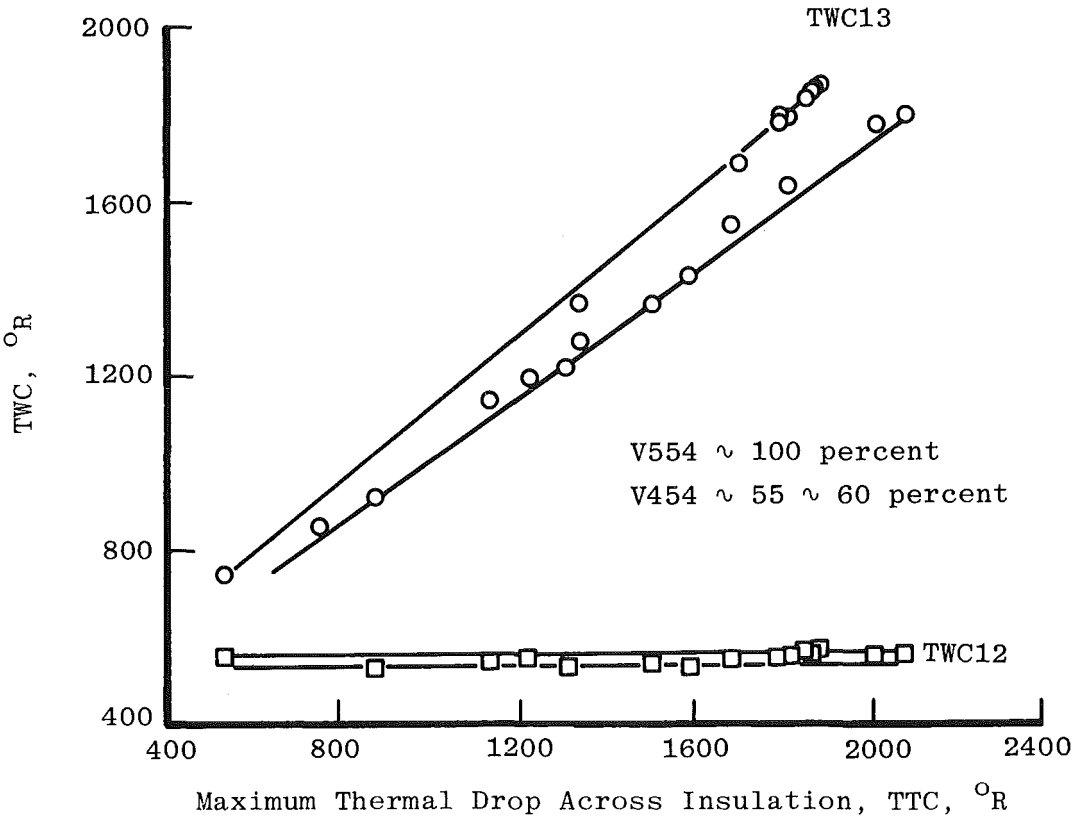


Figure 30. Effectiveness of the thermal insulation in the mixing chamber.

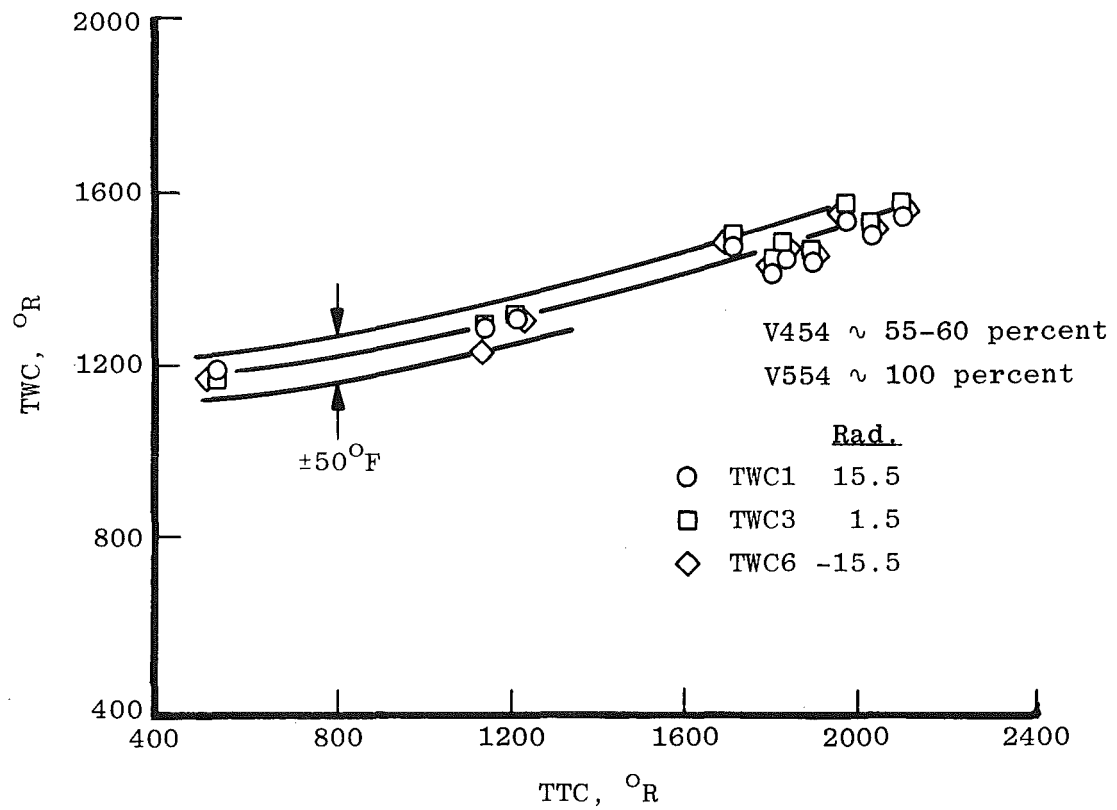
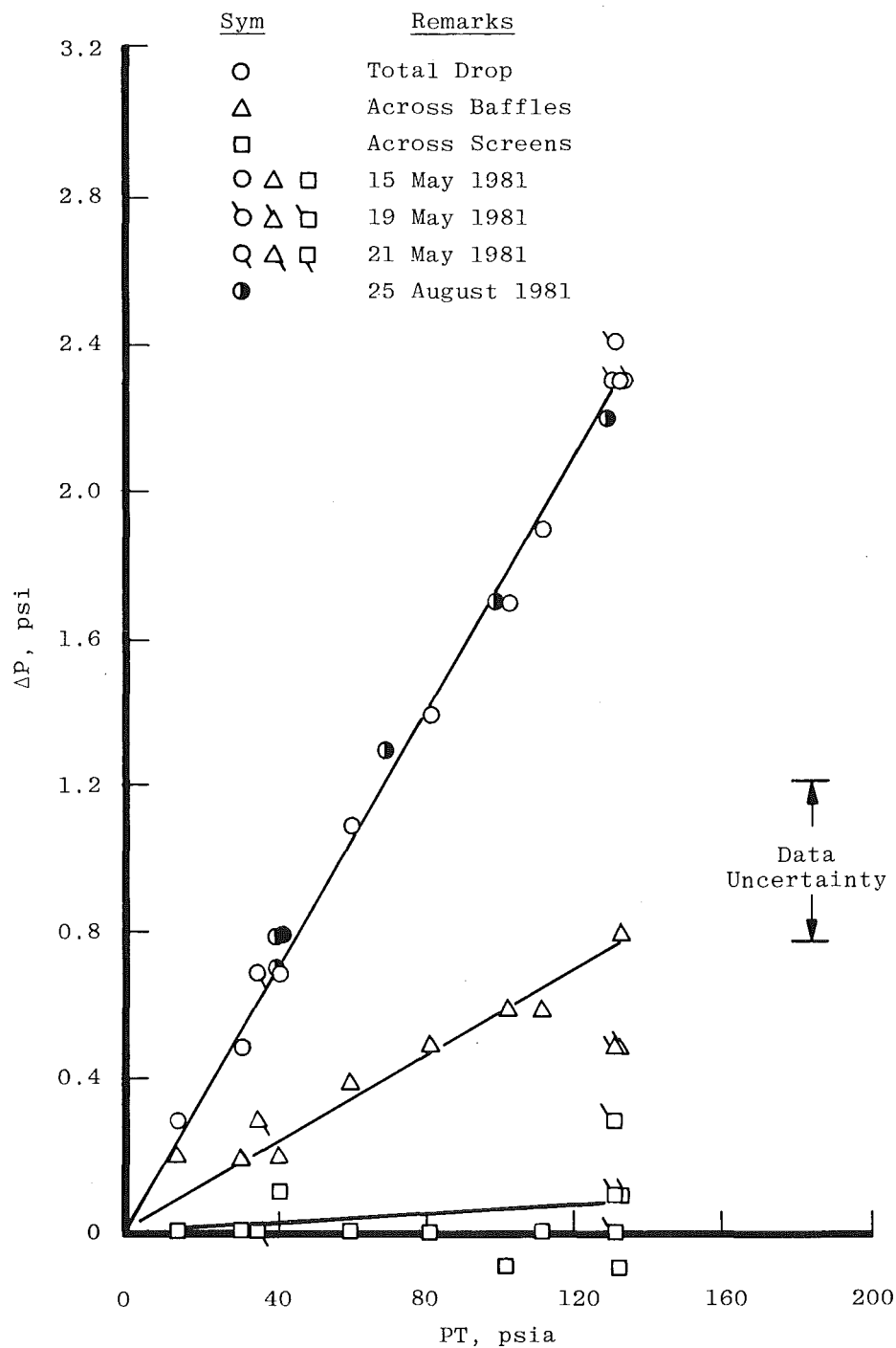
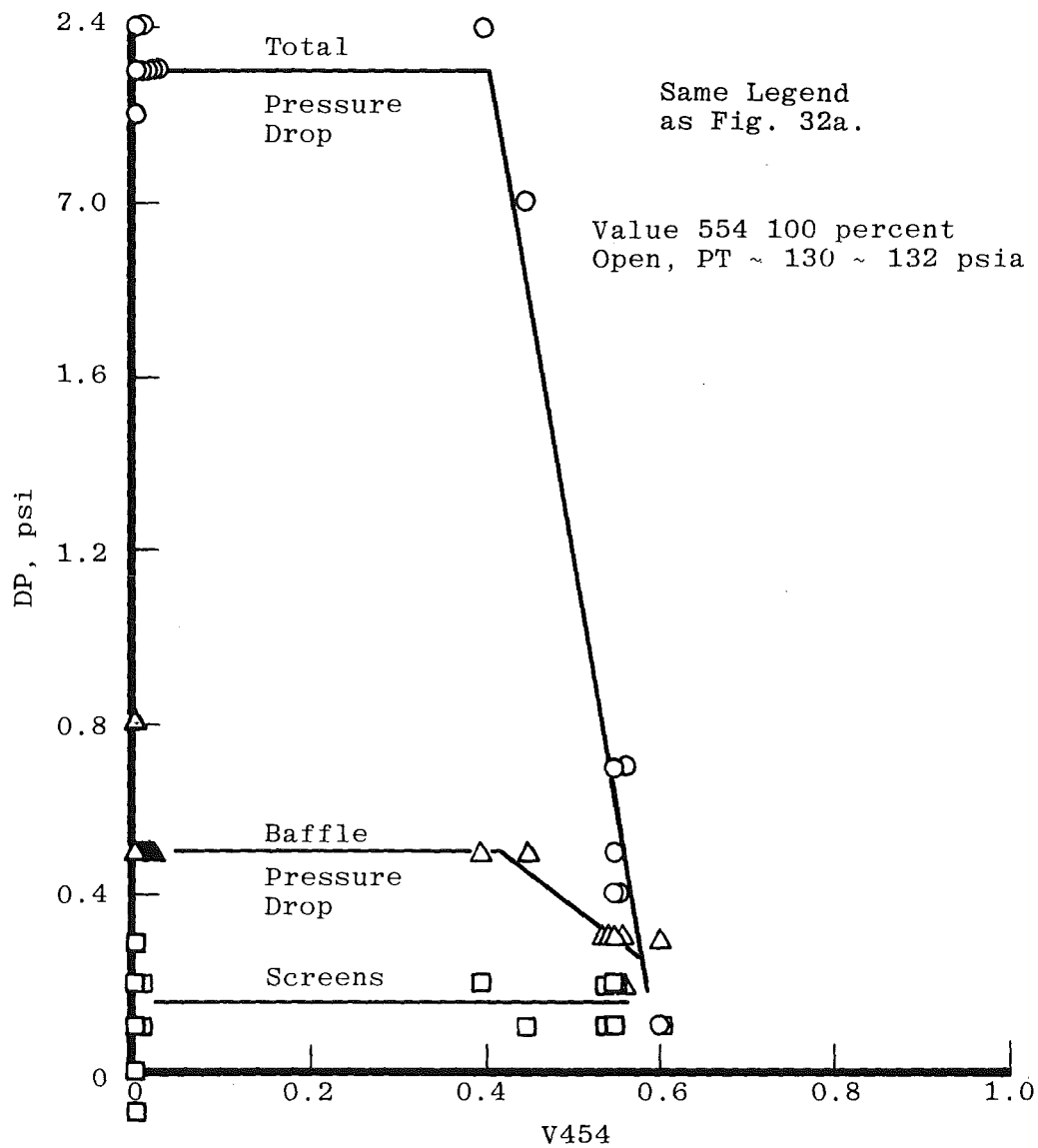


Figure 31. Correlation between mixing chamber baffle temperature and the HB-3 air discharge temperature.

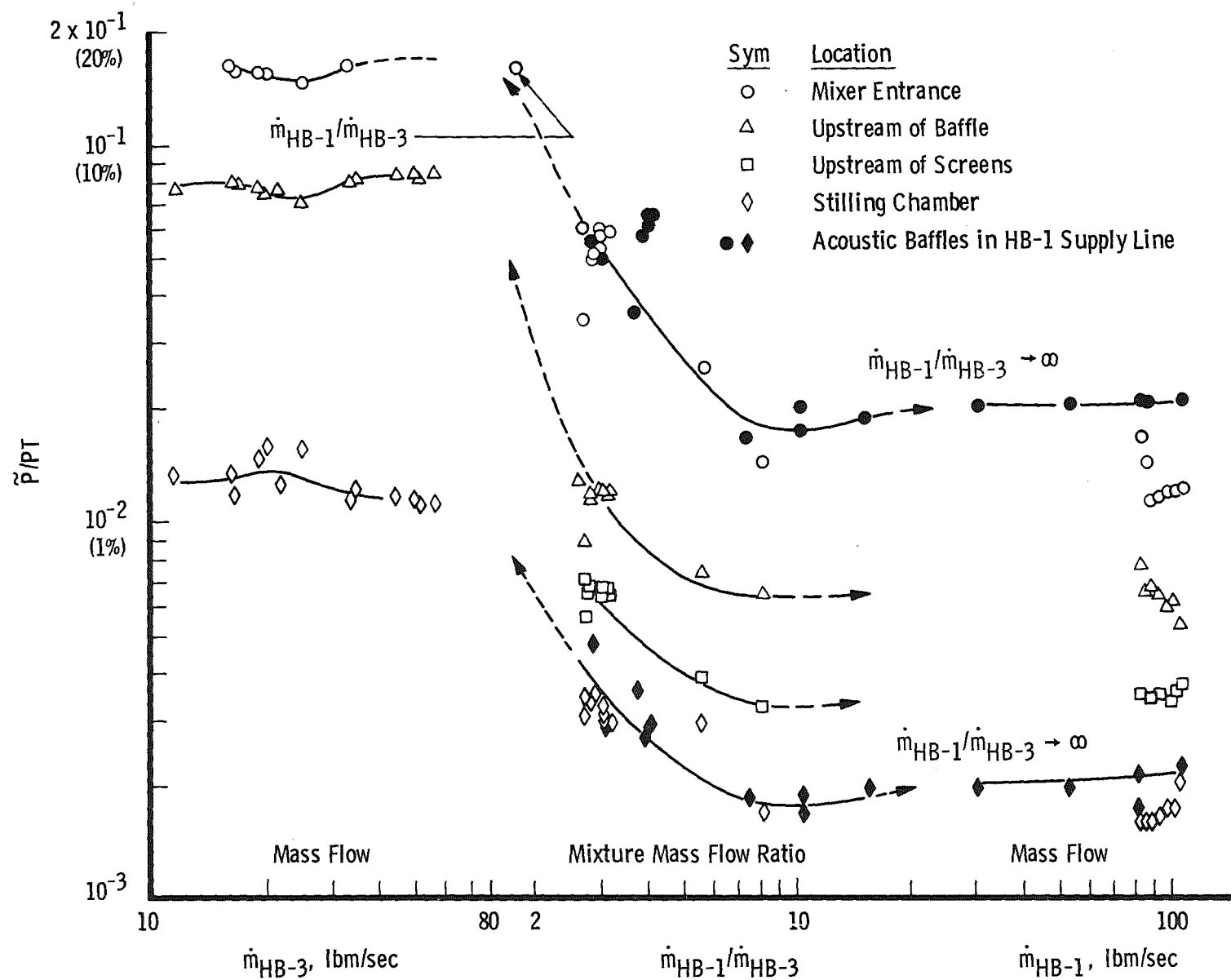


a. Pressure drop measurements made during May and August tunnel entries; V454, 0 percent and V554, 100 percent

Figure 32. Pressure drops through the mixing chamber.



b. The effect of primary flow on pressure drop through the mixing chamber
Figure 32. Concluded.



a. Hot flow, $TT > 900^\circ R$

Figure 33. Mixing chamber dynamic pressure fluctuations.

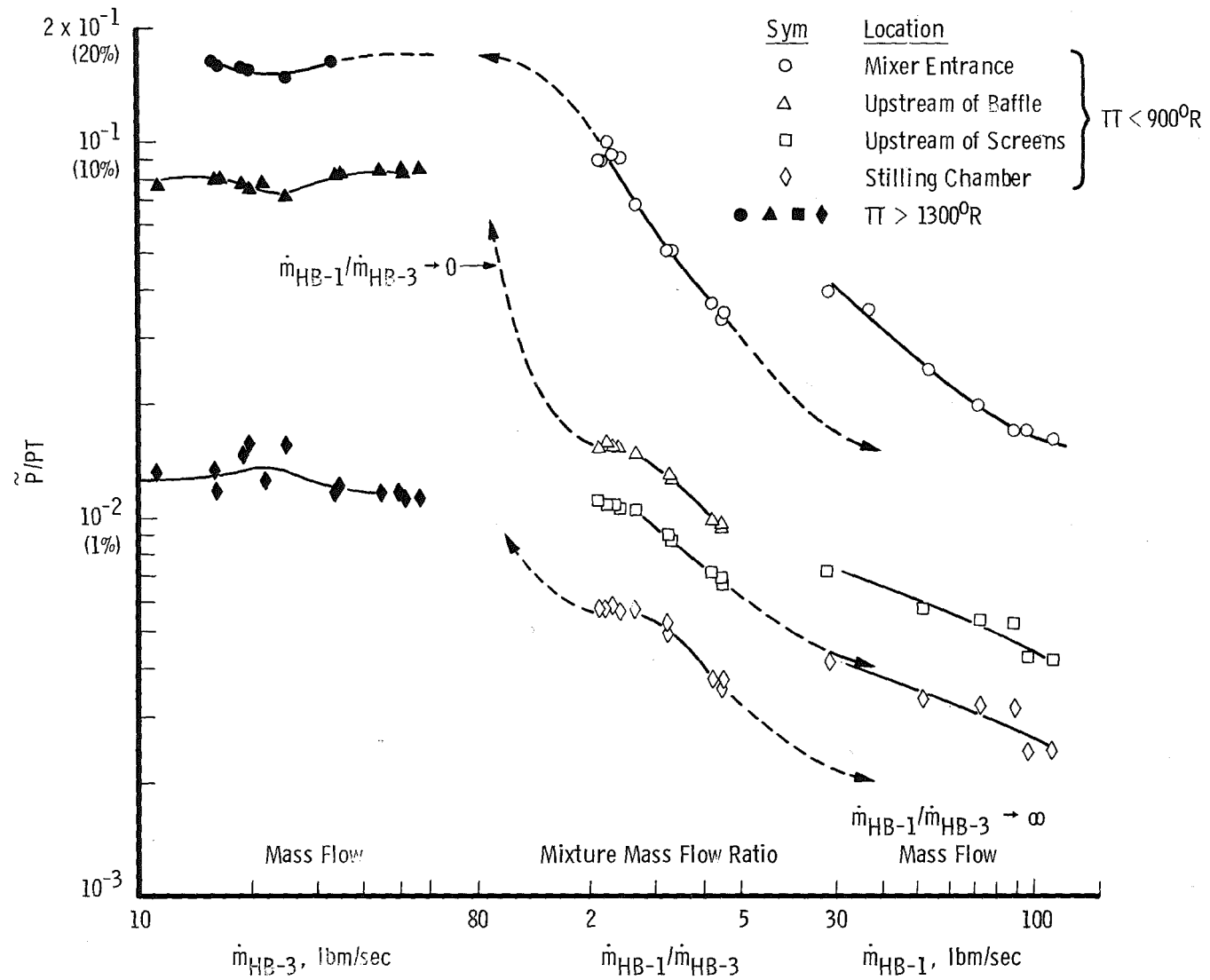
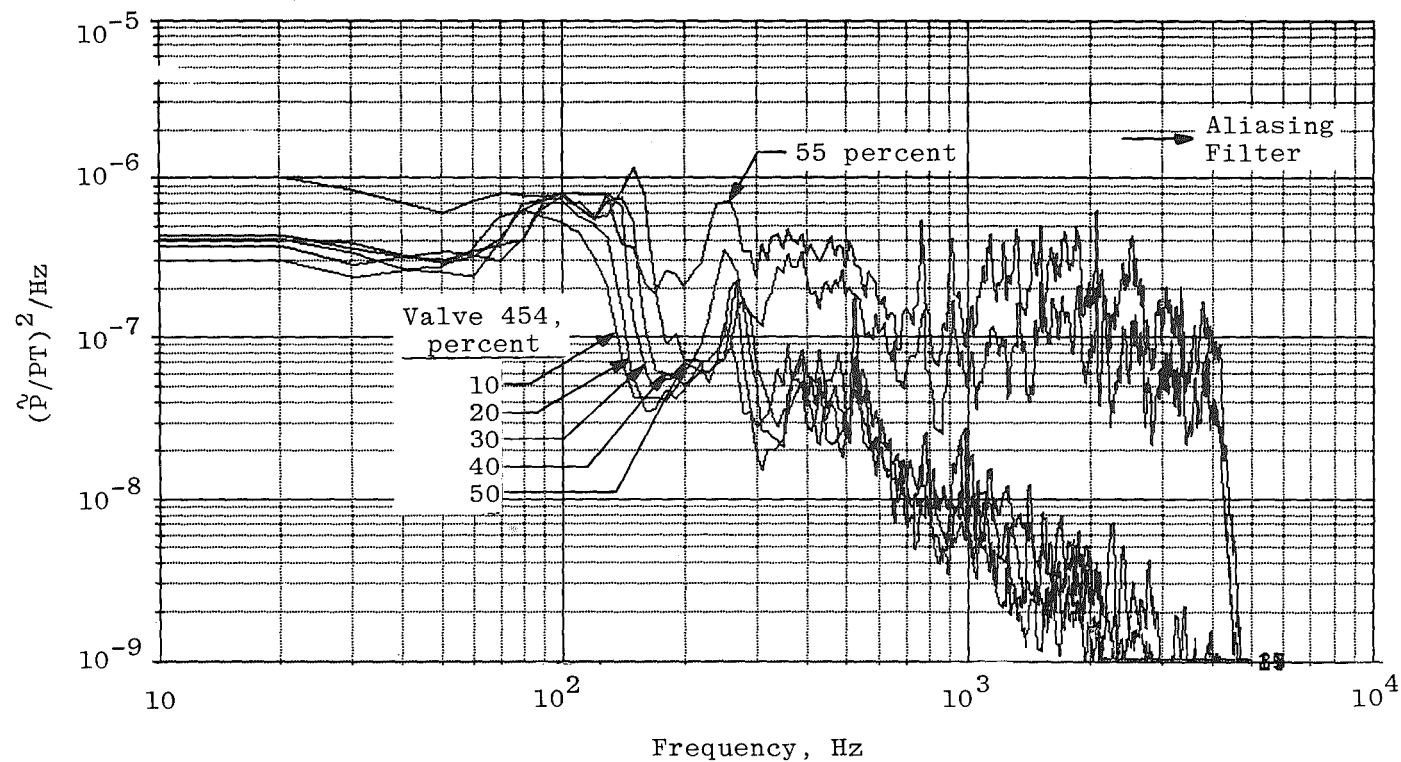
b. Basically cold flow results ($TT < 900^{\circ}R$)

Figure 33. Concluded.

Valve 454, percent	$\frac{\dot{m}_{HB-1}}{\dot{m}_{HB-3}}$	RMS, percent	F(NED = 0.99)	
10	45.7	1.14	2.28 KHz	BW = 5 KHz
20	19.1	1.06	2.00	G = 12.2
30	10.1	1.00	1.82	SF = 20.0
40	7.3	0.97	3.38	PT = 132 psia
50	3.8	1.99	4.14	
55	2.9	3.01	4.16	



a. Entrance to the mixer

Figure 34. Power spectral density distribution of a typical set of mixing chamber pressure fluctuation measurements.

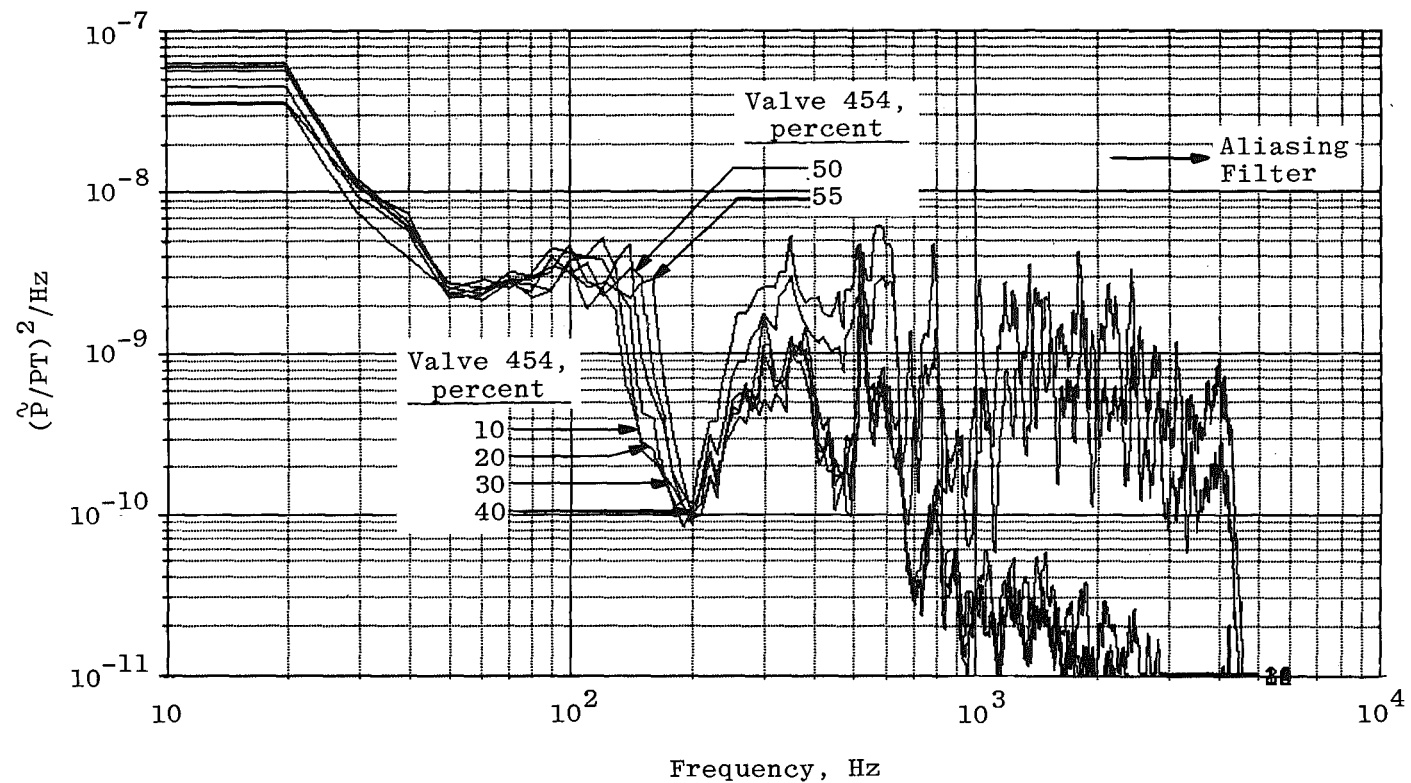
Valve 454, percent	$\frac{\dot{m}_{HB-1}}{\dot{m}_{HB-2}}$	RMS, percent	F(NED = 0.99)
10	45.7	0.14	1.30 KHz
20	19.1	0.14	1.29
30	10.1	0.12	1.52
40	7.3	0.14	2.10
50	3.8	0.18	4.08
55	2.9	0.24	4.18

BW = 5 KHz

G = 12.2

SF = 24.3

PT = 132 psia



b. Stilling chamber
Figure 34. Concluded.

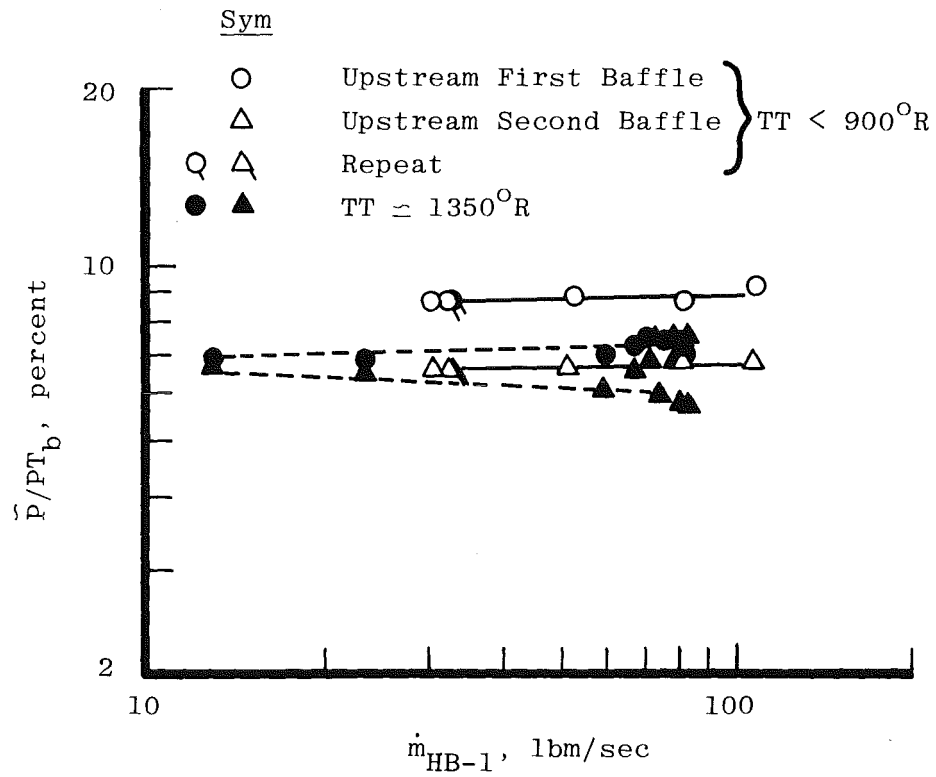
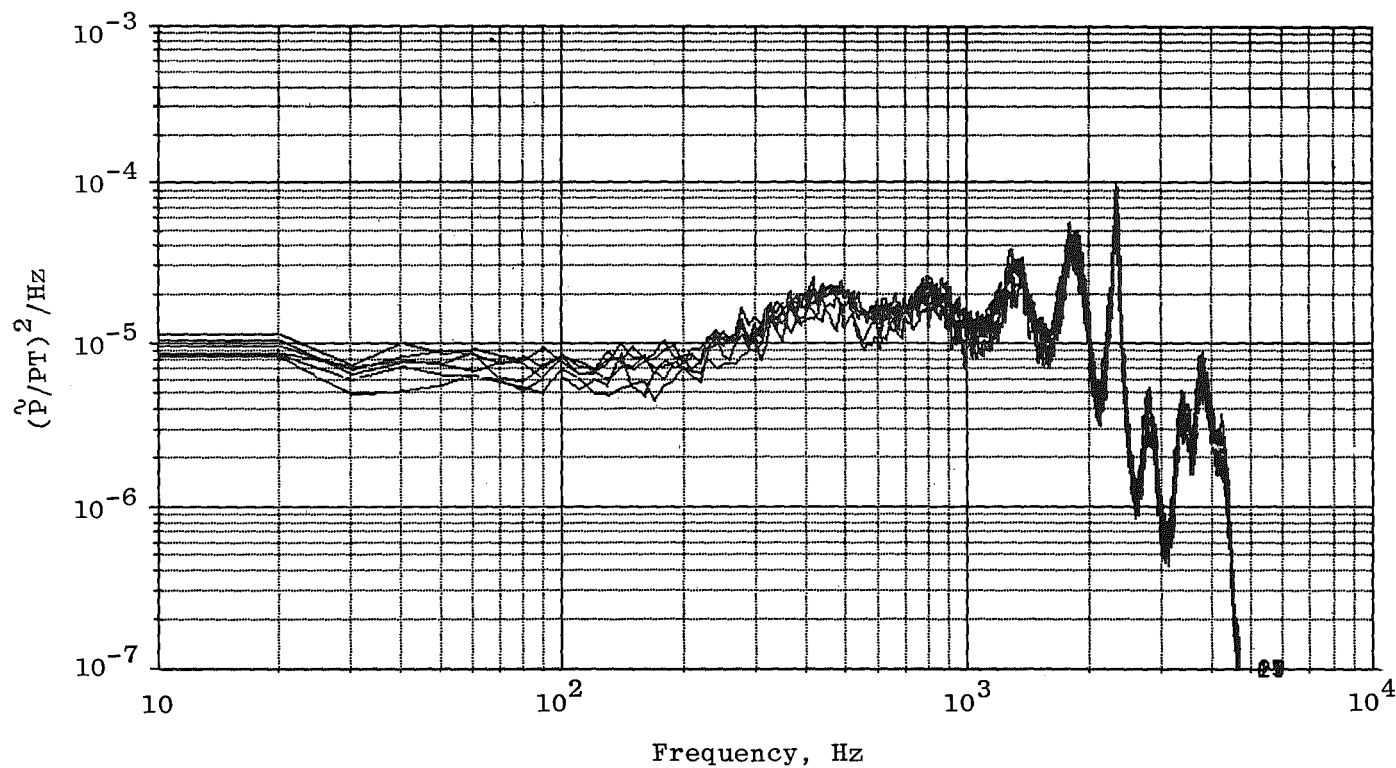


Figure 35. Pressure fluctuations in HB-1 bypass air supply line.

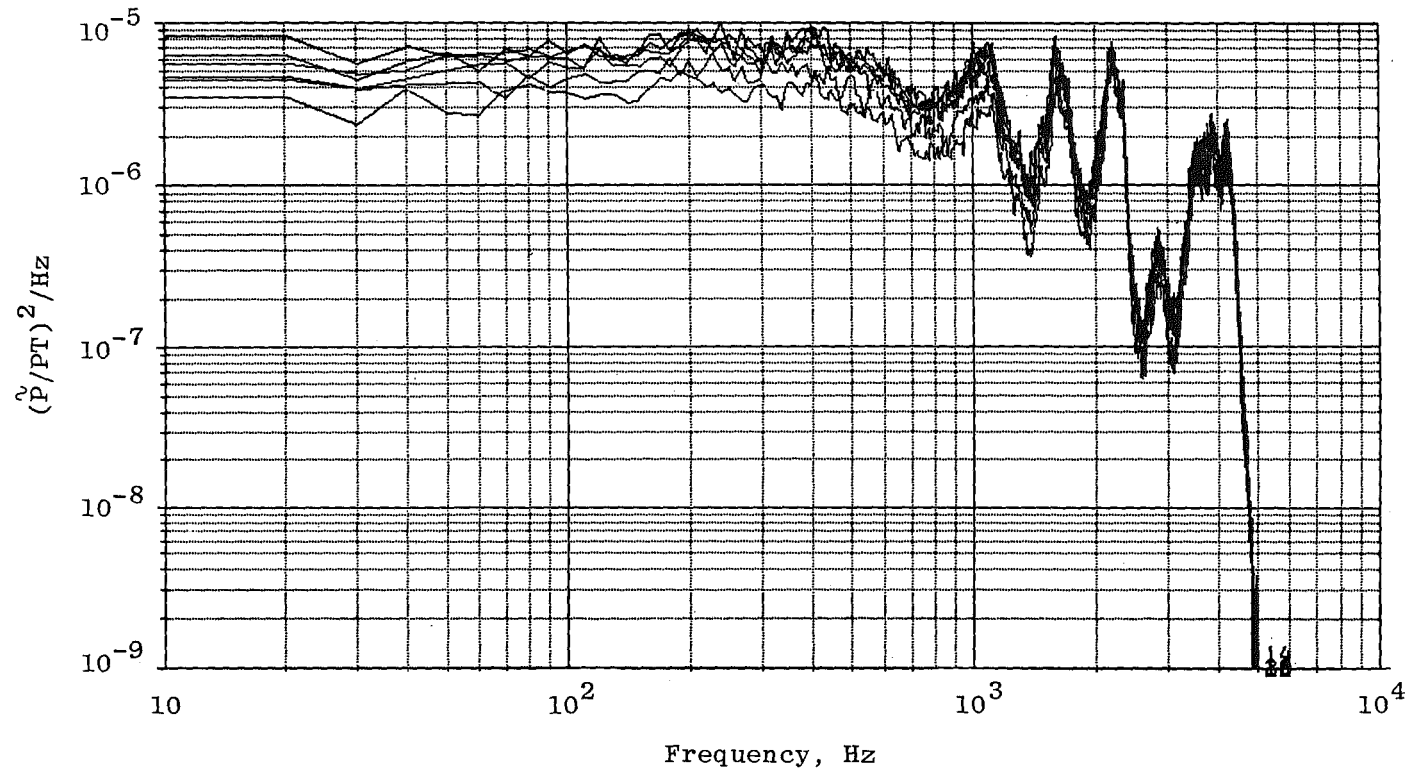
Valve 454, percent	$\frac{\dot{m}_{HB-1}}{\dot{m}_{HB-3}}$	\dot{m}_{HB-1} , lbm/sec	RMS, percent		
10	45.7	81.2	23.0	BW = 5 KHz	
20	19.1	80.6	22.9	G = 0.1	
30	10.1	78.4	22.4	SF = 20.2	
40	7.3	77.4	22.0	PT = 132	
50	3.8	72.2	20.4	394 < PT _b < 444 psia	
55	2.9	68.4	19.2		



a. Upstream of the first baffle

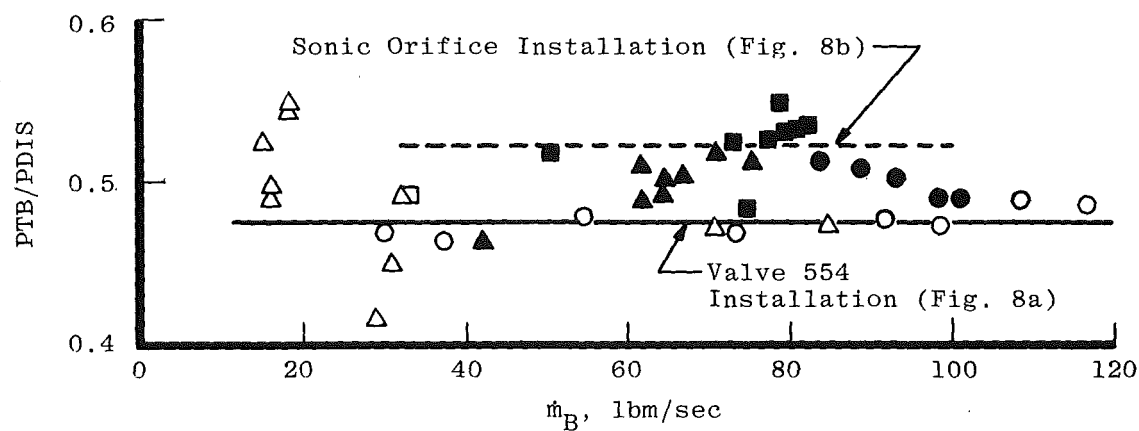
Figure 36. Power spectral density of the pressure fluctuations recorded in the bypass line downstream of valve 554.

Valve 454, percent	$\frac{\dot{m}_{HB-1}}{\dot{m}_{HB-3}}$	\dot{m}_{HB-1} , lbm/sec	RMS, percent	BW = 5 KHz	
10	45.7	81.2	11.1	G = 1.2	
20	19.1	80.6	11.0	SF = 18.9	
30	10.1	78.4	10.7	PT = 132	
40	7.3	77.4	10.2	180 < PT _b < 202 psia	
50	3.8	72.2	9.1		
55	2.9	68.4	8.2		

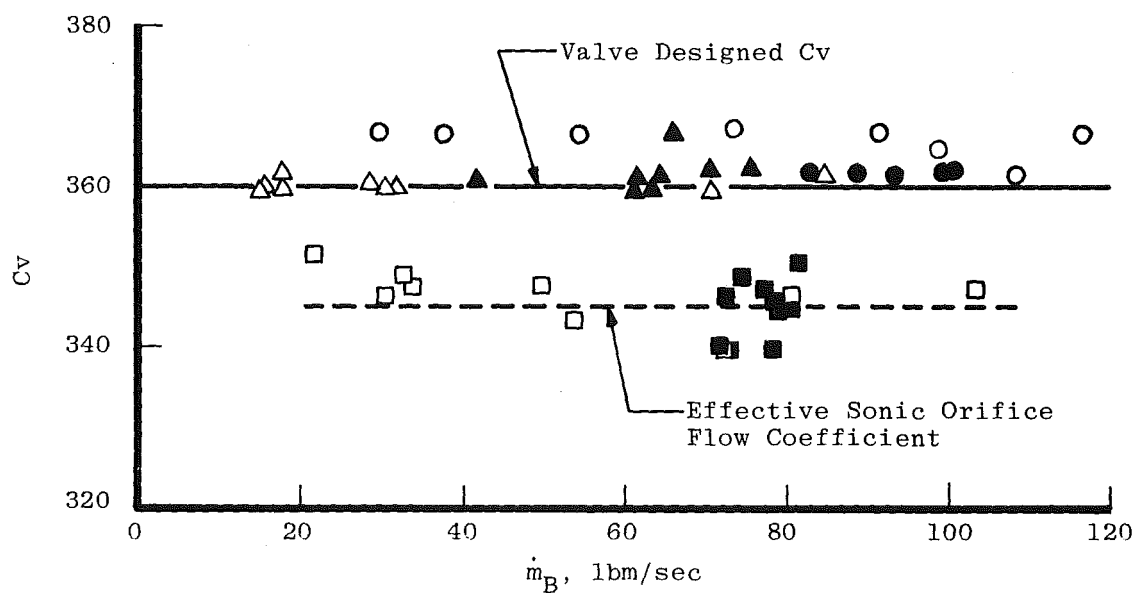


b. Upstream of the second baffle
Figure 36. Concluded.

Sym	V554	V454	TTB, °R
○	100	0	< 1000
△	100	Vary	< 1000
● ▲	100	---	> 1000



a. Pressure drop from plant to valve 554 location



b. Flow coefficient at valve 554 location
Figure 37. Bypass line and valve characteristics.

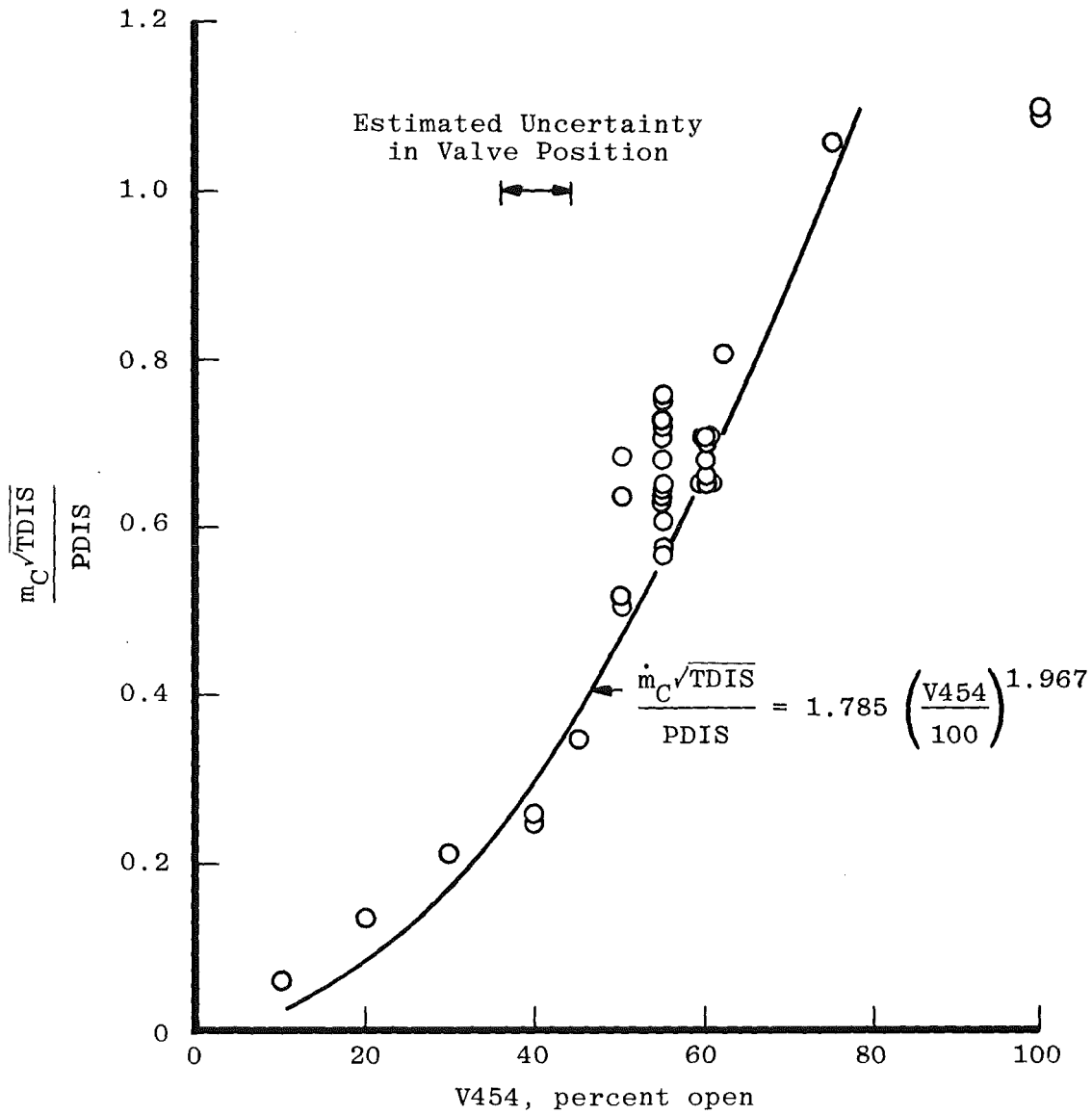


Figure 38. Valve performance in the primary flow line upstream of electric heater HB-3.

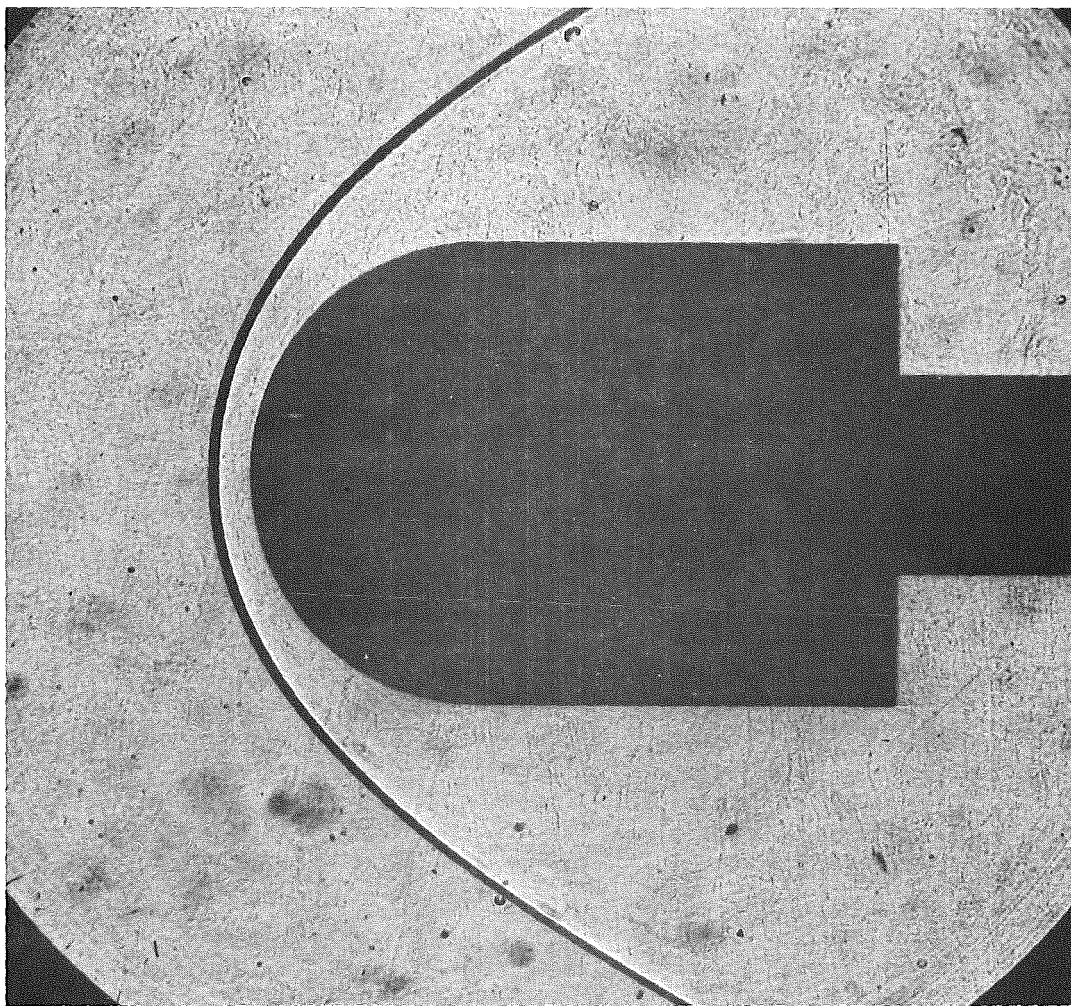


Figure 39. Shadowgram of the hemisphere, $M = 3.95$, $PT = 180$ psia, and $TT = 1570^{\circ}R$.

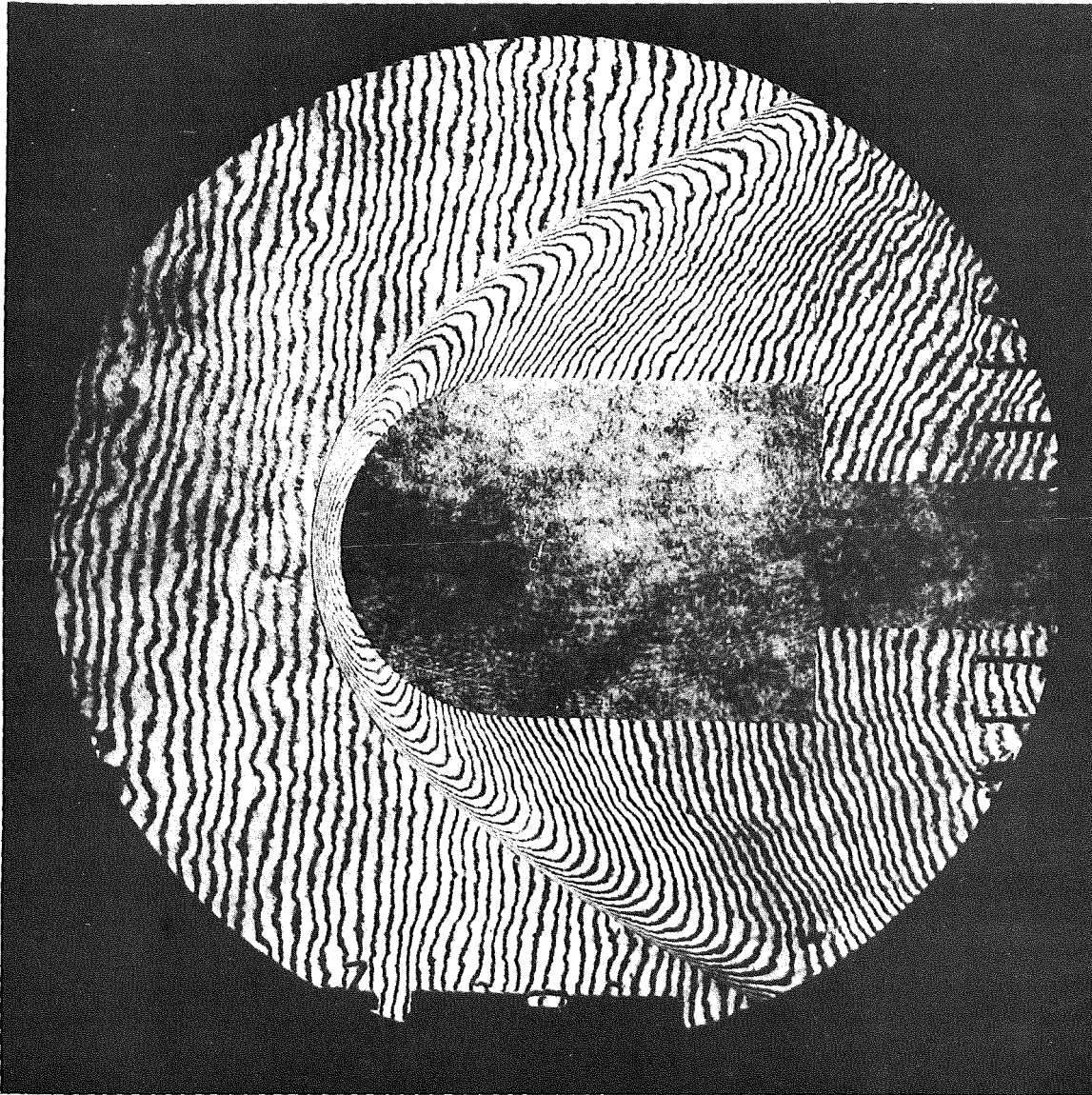


Figure 40. Interferogram of the hemisphere, $M = 3.95$, $PT = 180$ psia, and $TT = 1570^{\circ}R$.

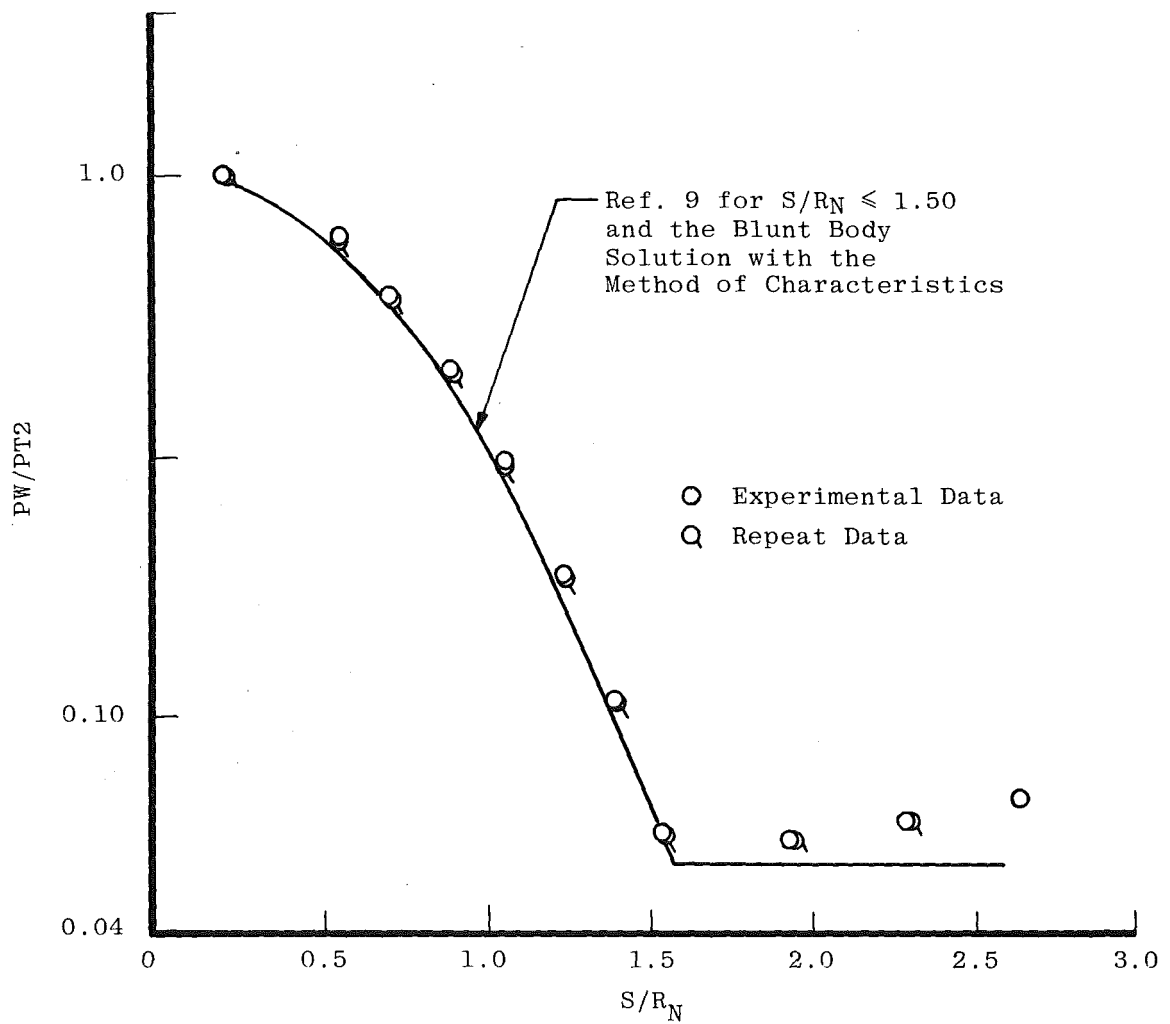


Figure 41. Hemisphere cylinder pressure distribution, Mach No. 3.95, $P_T = 180$ psia, $T_T = 1570^\circ R$, and $RE/ft = 3.3 \times 10^6$.

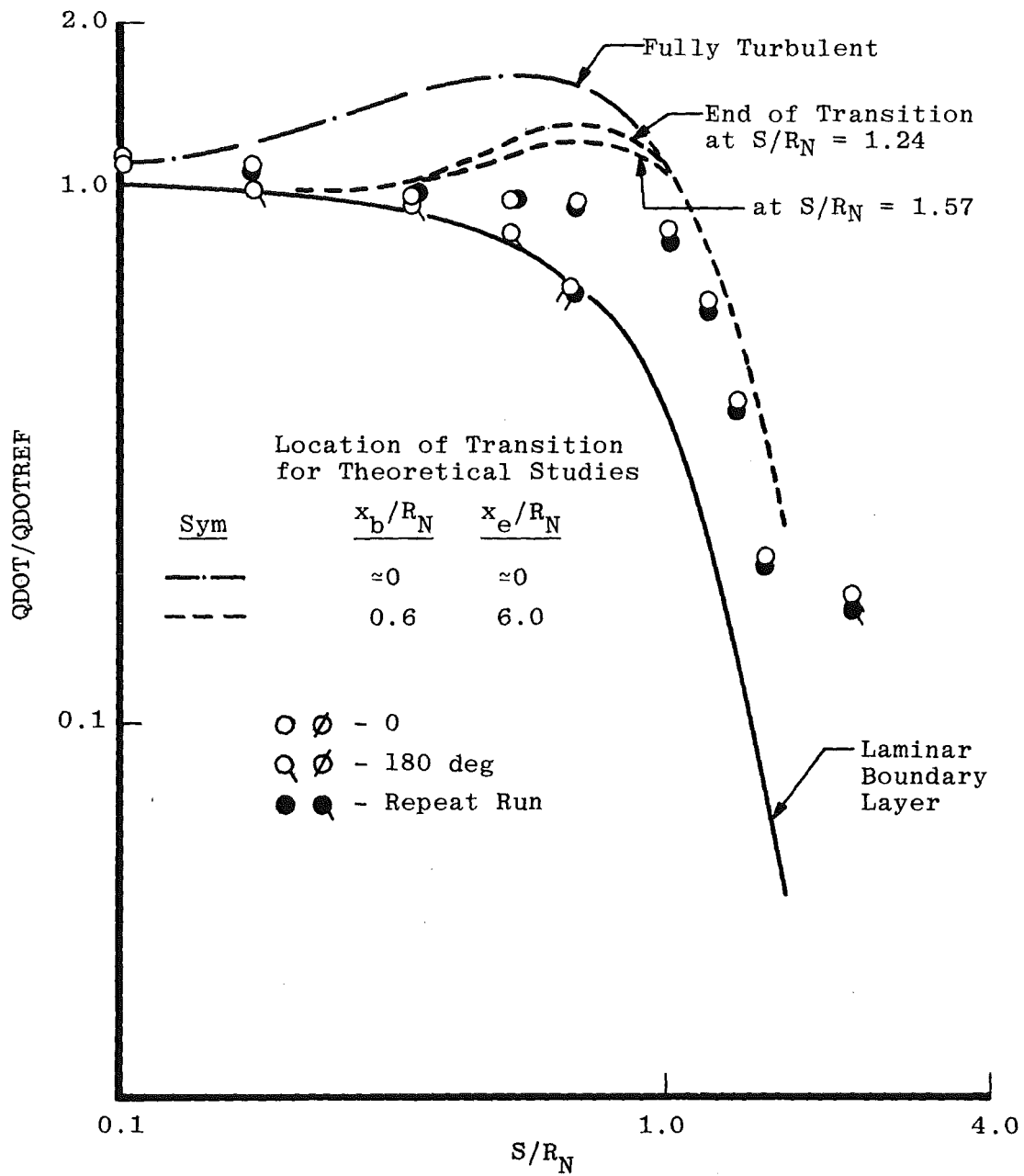
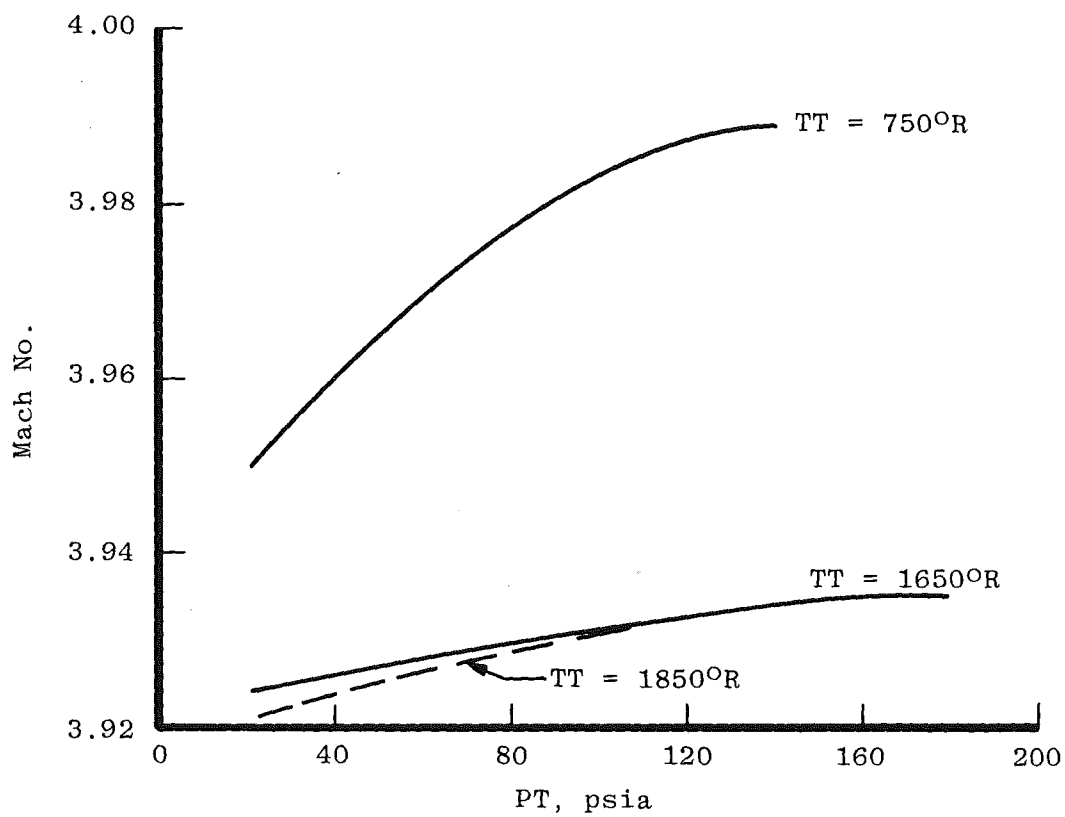
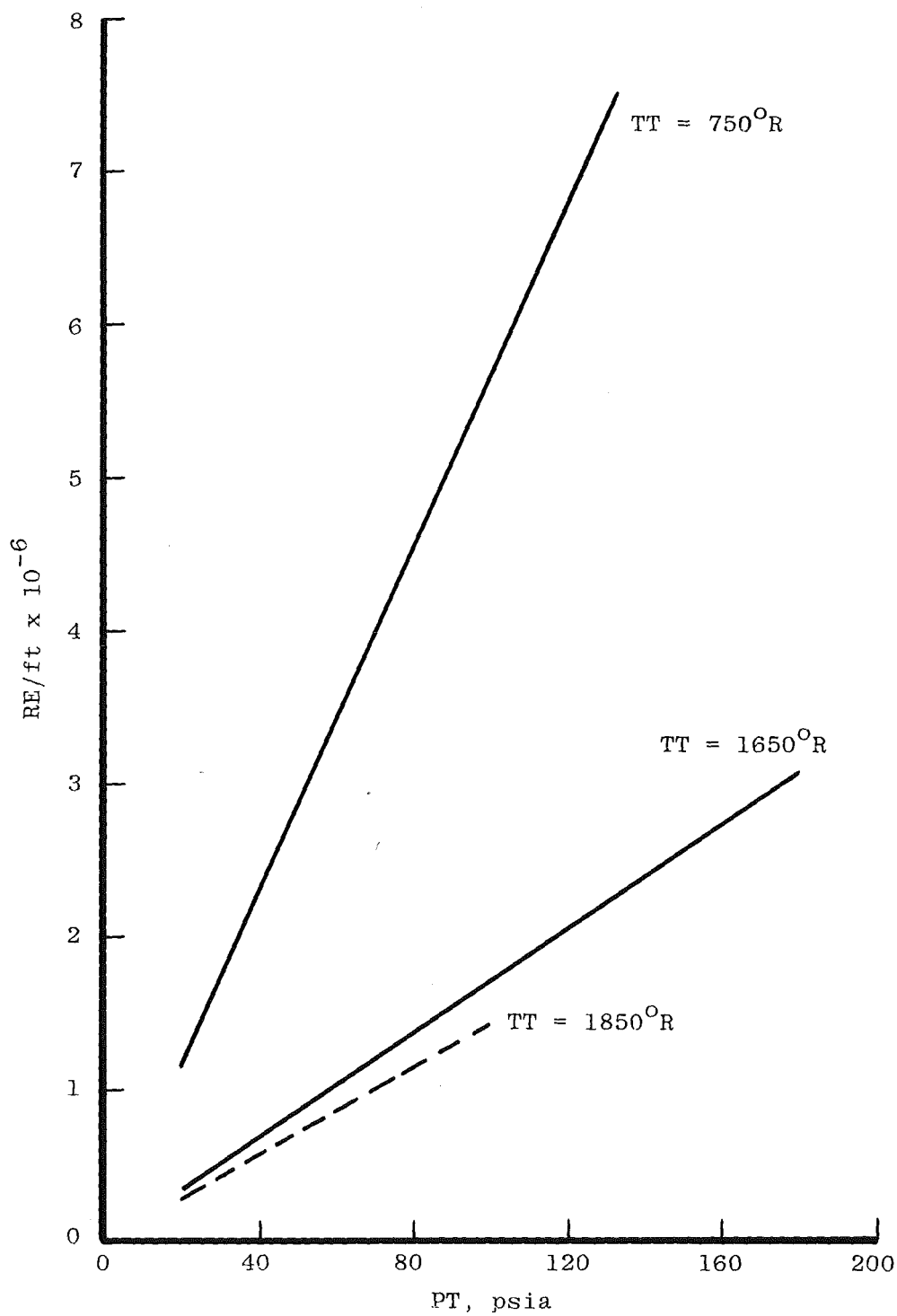


Figure 42. Hemisphere cylinder heat transfer distribution, Mach No. 3.95, PT = 180 psia, TT = 1570°R, and RE/ft = 3.3×10^6 .

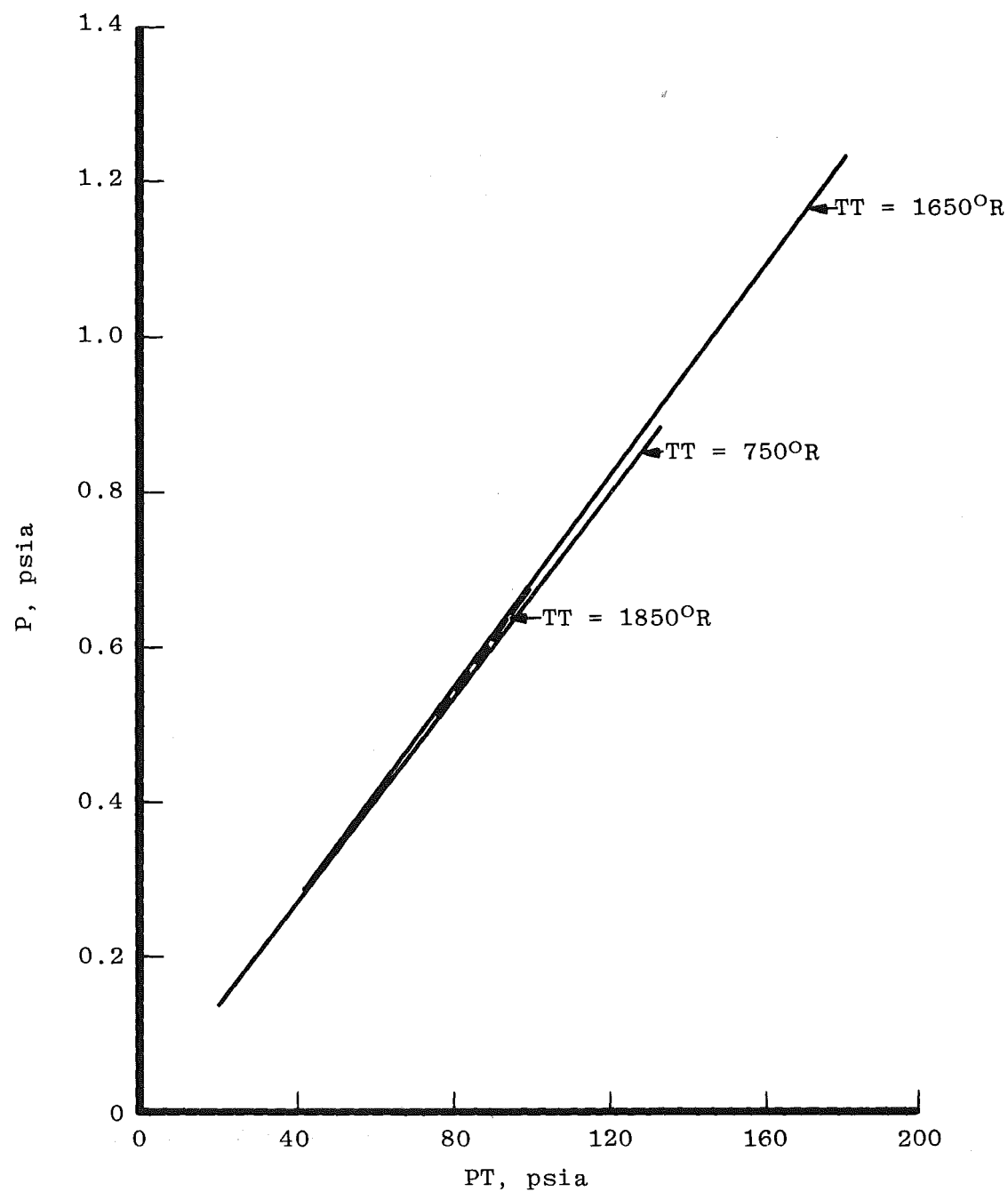
Appendix A
Test Section Free-Stream Properties



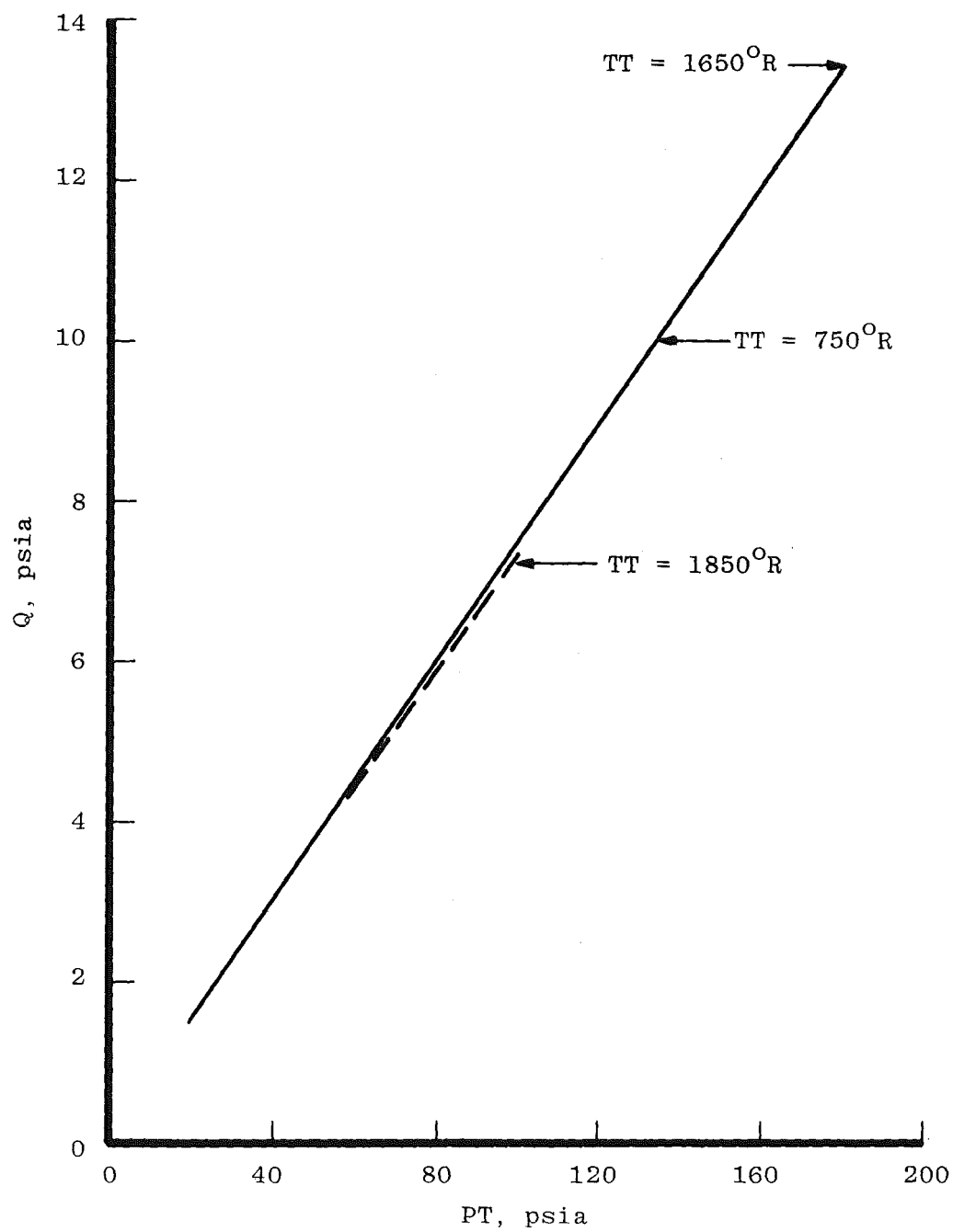
a. Average test section rhombus Mach number
Figure A-1. Test section rhombus properties.



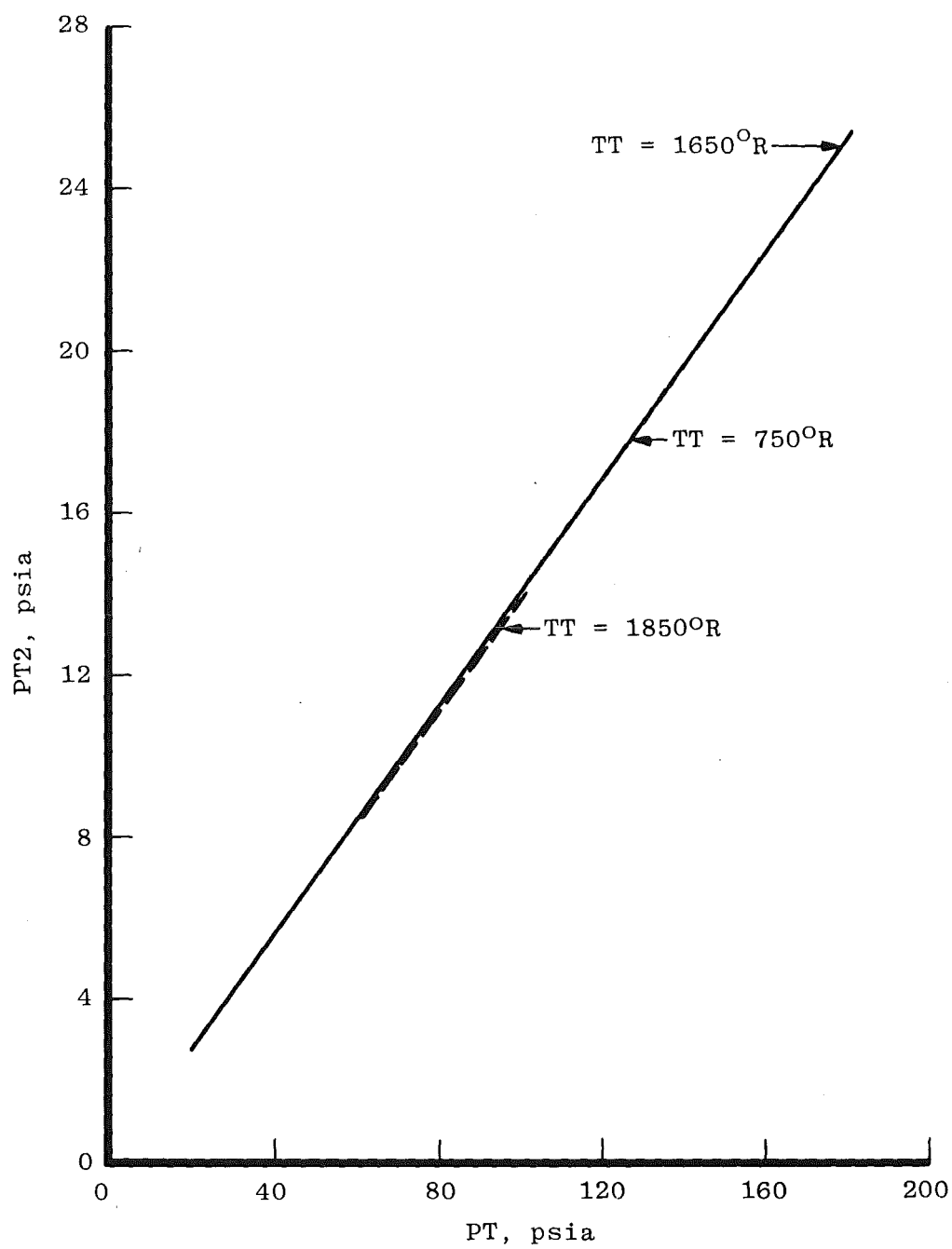
b. Free-stream Reynolds number per foot
Figure A-1. Continued.



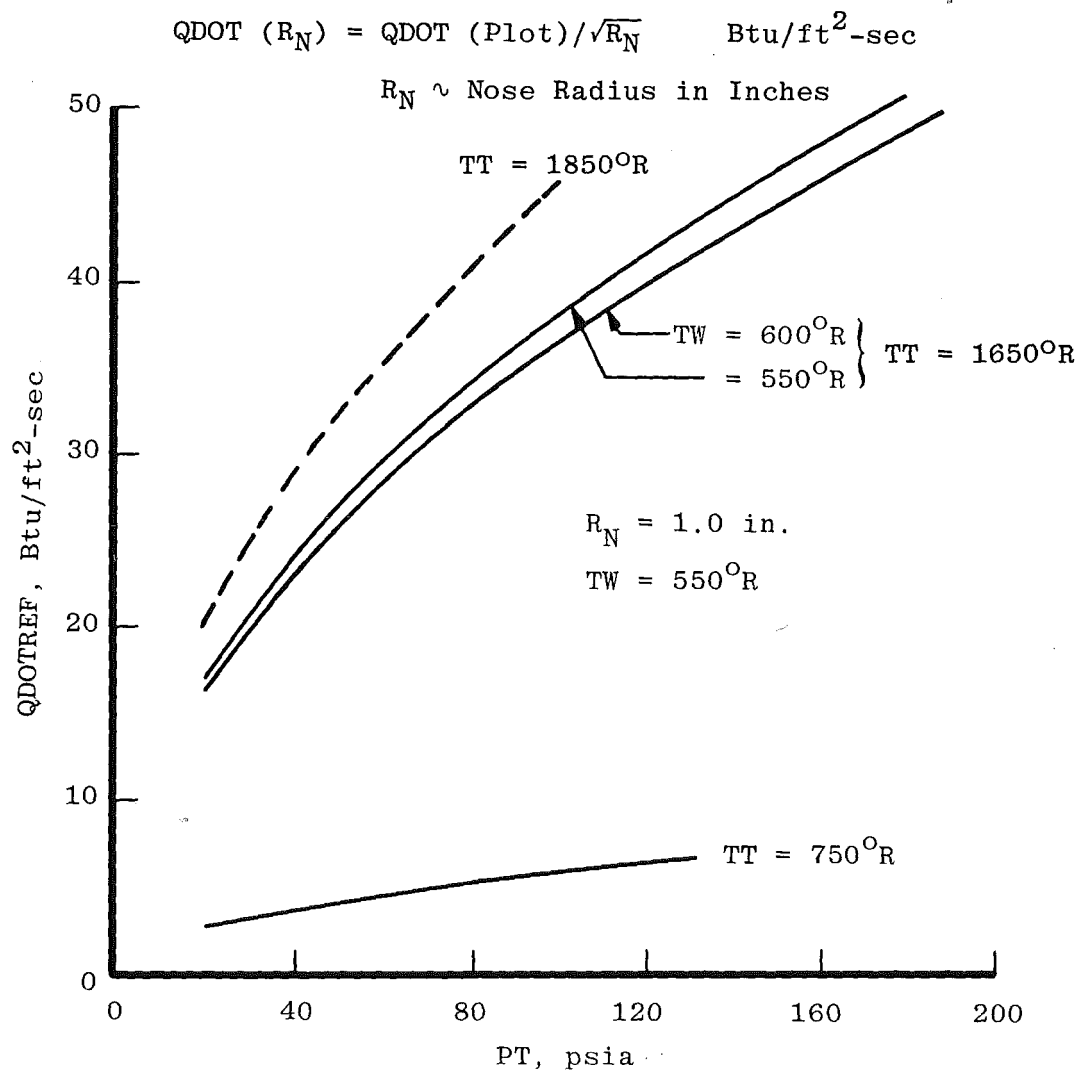
c. Free-stream static pressure
Figure A-1. Continued.



d. Free-stream dynamic pressure
Figure A-1. Continued.



e. Test section pressure downstream of a normal shock
Figure A-1. Continued.



f. Estimate of stagnation heat transfer rate based on $R_N = 1.0 \text{ in.}$ and $TW = 550^\circ R$
 Figure A-1. Concluded.

Appendix B
Real-Gas Correction Factors

Real-Gas Adiabatic Flow Coefficients

General Form

$$R(PG) = \sum_{i=1}^{j=2} \sum_{j=1}^{i=2} A_{ij} P T^{i-1} T T^{j-1}$$

A _{ij}	PG		
	P/PT	T/TT	PT ² /PT
A ₁₁	0.985060	1.000316	0.984694
A ₂₁	1.3141 × 10 ⁻⁵	-3.6631 × 10 ⁻⁵	-1.5145 × 10 ⁻⁵
A ₁₂	4.561 × 10 ⁻⁵	-1.270 × 10 ⁻⁵	4.546 × 10 ⁻⁵
A ₂₂	3.500 × 10 ⁻⁸	5.300 × 10 ⁻⁸	7.230 × 10 ⁻⁸
A ₁₃	-3.630 × 10 ⁻⁸	2.020 × 10 ⁻⁸	-3.500 × 10 ⁻⁸
A ₂₃	-1.750 × 10 ⁻¹¹	-1.750 × 10 ⁻¹¹	-2.500 × 10 ⁻¹¹

In general:

$$P/PT(\text{Real Gas}) = R\left(\frac{P}{PT}\right) \cdot \frac{P}{PT} (\text{Perfect Gas}).$$

The correlation between this curve fit and the real-gas properties based on the Beattie-Bridgeman equation of state for air is shown in the figures included in this appendix.

Real-Gas Enthalpy

General Forms

The following approximation is independent of pressure, but is applicable for air over the range of 500 to 2000°R for pressures less than 2,000 psia:

$$H = 4.875 + 0.2235 \cdot T + 1.35 \times 10^{-5} T^2$$

$$T \sim ^\circ\text{R}$$

$$H \sim \leftarrow \text{enthalpy, btu/lbm}$$

This expression does not deviate by more than 0.5 percent from the following real-gas curve fit which includes the effects of pressure:

$$H = C_{p_0} \sum_{i=1}^{j=3} A_{ij} P^i T^{j+1}$$

$$A_{11} \quad 0.994581$$

$$A_{21} \quad -7.8102 \times 10^{-5}$$

$$A_{12} \quad 9.41585 \times 10^{-7}$$

$$A_{22} \quad 9.60560 \times 10^{-8}$$

$$A_{13} \quad 1.40885 \times 10^{-8}$$

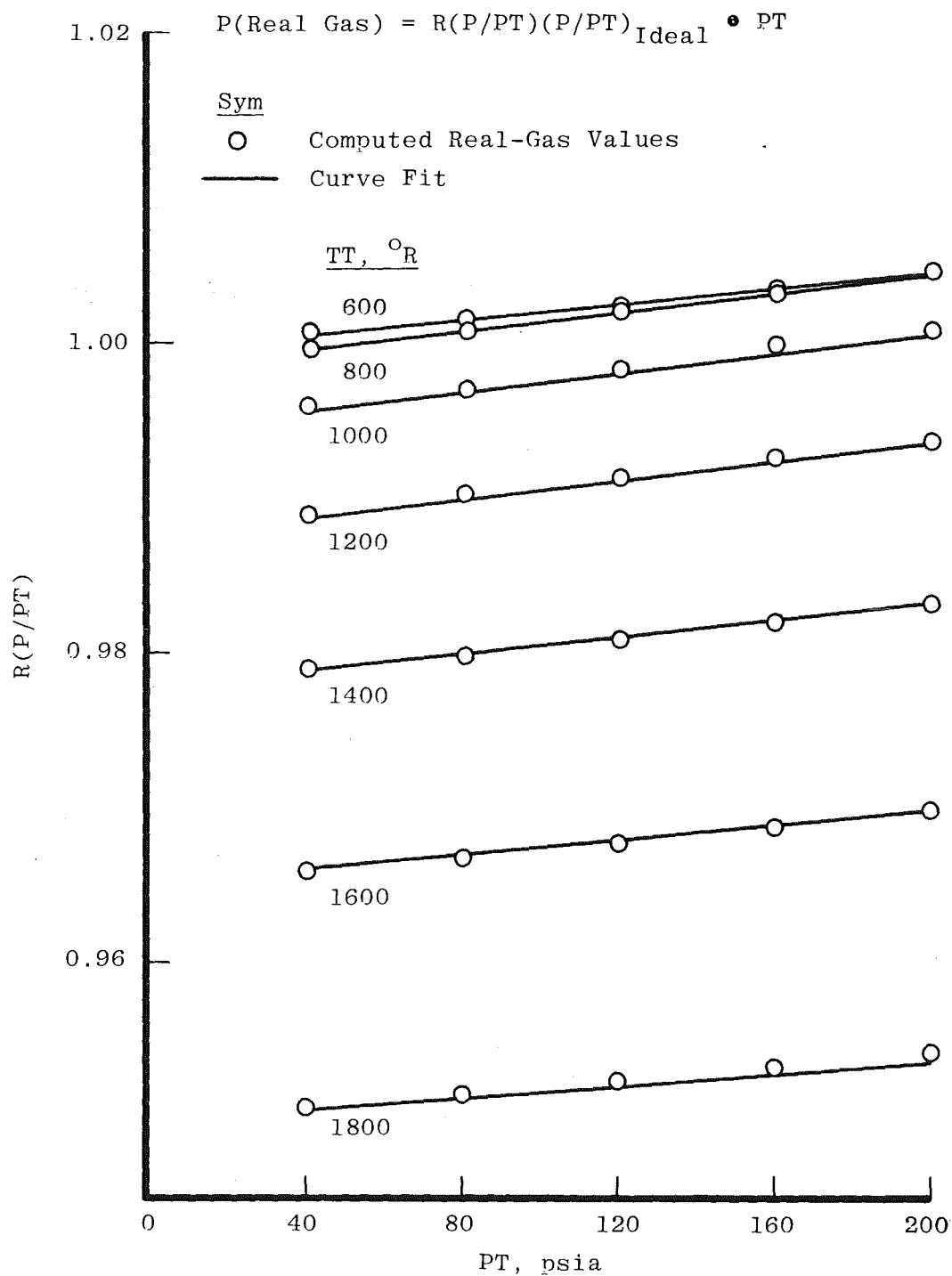
$$A_{23} \quad -2.77356 \times 10^{-11}$$

$$C_{p_0} = 0.239974 \text{ Btu/lbm} - ^\circ\text{F}$$

$$P \sim \text{psia}$$

$$T \sim ^\circ\text{R}$$

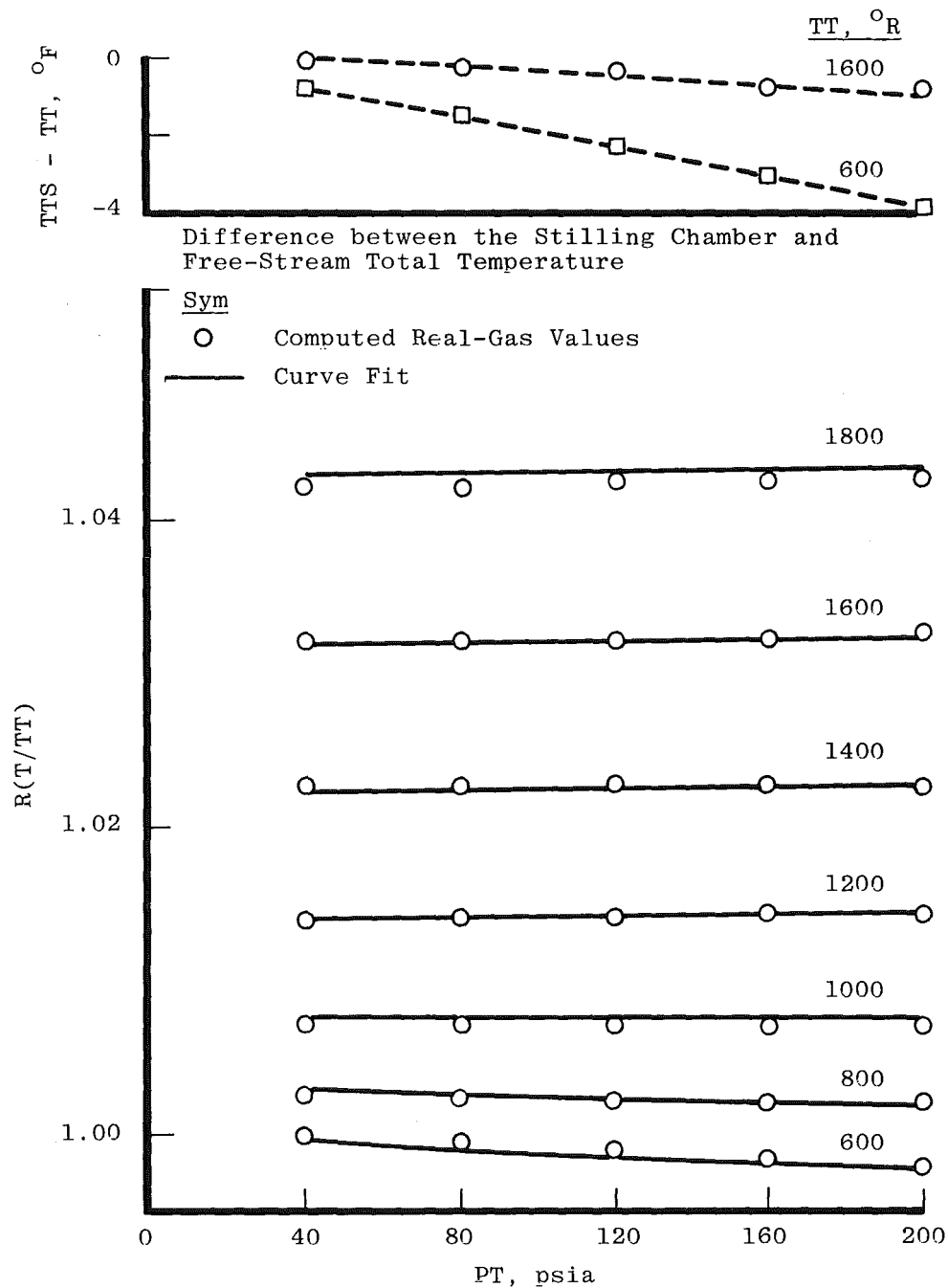
This curve fit agrees to within ± 0.15 percent in most cases and at the extreme pressures (approaching 2,000 psia) to within ± 0.5 percent of the real-gas computations based on the Beattie-Bridgeman equation of state for air.



a. Free-stream static pressure (P)

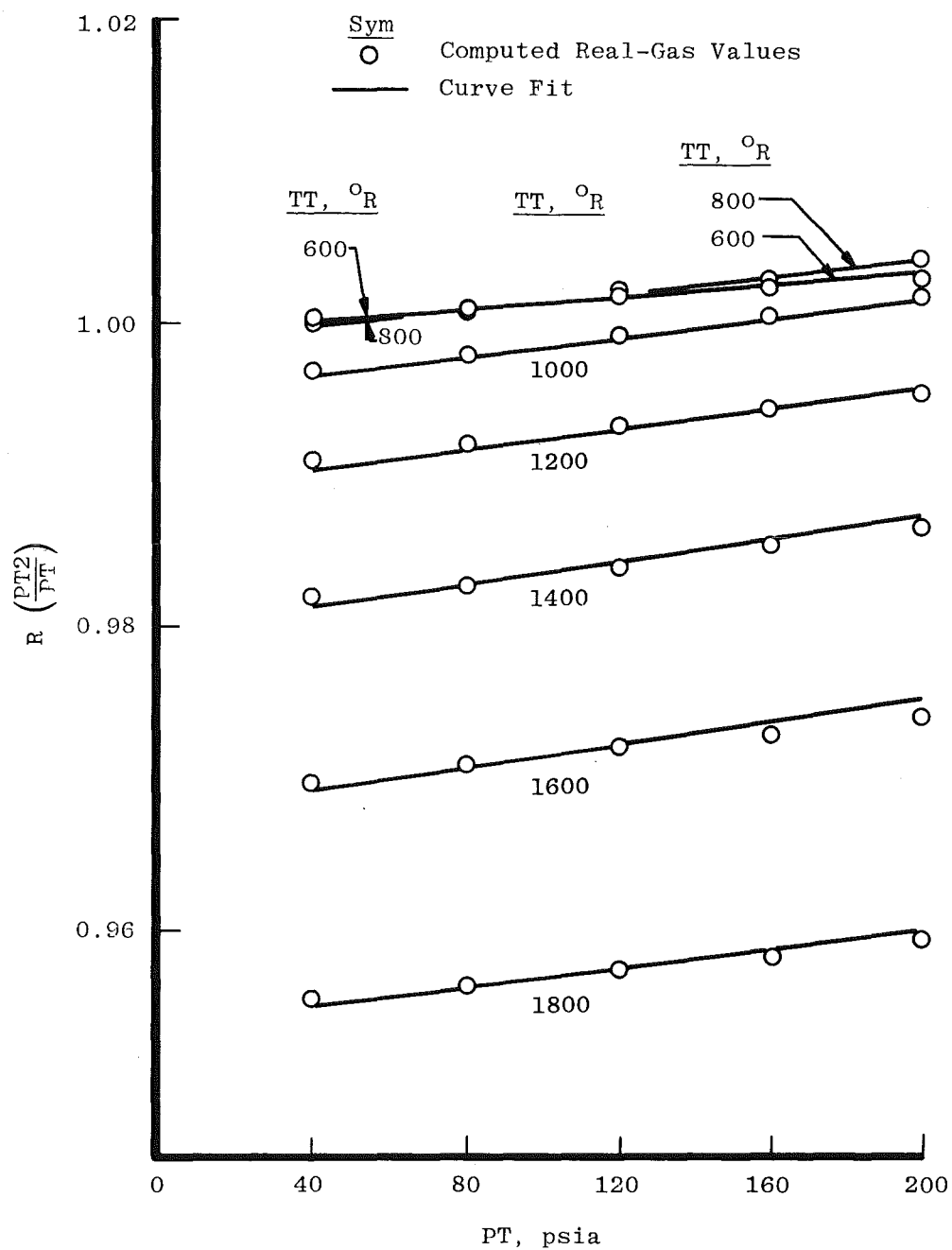
Figure B-1. Aerotherm test section properties real-gas effects.

$$T \text{ (Real Gas)} = R \left(\frac{T}{TT} \right) \cdot \left(\frac{T}{TT} \right)_{\text{Ideal}} \cdot TT$$



b. Free-stream static temperature (T)
Figure B-1 Continued.

$$PT_2 = R \left(\frac{PT_2}{PT} \right) \left(\frac{PT_2}{PT} \right)_{\text{Ideal}} PT$$



c. Normal shock pressure (PT_2)
Figure B-1. Concluded.

NOMENCLATURE

A	Maximum test core area, sq in.
A*, AREA	Geometric, effective nozzle throat or valve cross-sectional area, in.
A _{ij}	Coefficients
ALPHAO	Local flow angle in the pitch plane as defined by the probe at the first point in the surveys, deg
ALPHAF, α	Change in the local flow angle in the pitch plane relative to the first point, ALPHAO, in the surveys, deg
BW	Total spectral bandwidth of the analysis, KHz
C _p , C _{p0}	Specific heat at constant pressure, Btu/lbm-°F
C _v	Valve V554 flow coefficient
D	Diameter, in.
ETA	Rate of change of the pressure differential across the cone with local flow angle, per deg
F(NED.99)	Frequency bandwidth including 99 percent of the dynamic signal energy, Hz
G	Gain
H	Enthalpy, Btu/lbm
HB-1	Gas-fired air heater designation
HB-3	Electric air heater designation
ℓ	Distance from the center of the chamber, Fig. 10, in.
MACH, M	Mach number
\dot{m}	Mass flow rate, lbm/sec
P	Static pressure, psia
PD	Diffuser wall surface static pressure, psia
\overline{PD}	Average diffuser static pressure, psia
PDIS	Plant discharge pressure, psia

PE	Nozzle exit static pressure, psia
PF	Flange surface (free-jet cavity) pressure, psia
PIN	Inlet pressure to first compressor stage of the plant, psia
PP	Free-stream pitot pressure, psia
PSIF, Ψ	Change in the flow angle in the yaw plane relative to the first point, PSIO, in the survey, deg
PSIO	Local flow angle in the yaw plane as defined by the probe at the first in the surveys, deg
PT	Mach 4 nozzle stilling chamber pressure, psia
PTB	Discharge pressure of the gas-fired heater and pressure upstream of the location of V554, psia
PT _b	Pressure upstream of either the first or second baffle in the bypass line
PTC	Discharge pressure of the electric air heater (Mach 10 stilling chamber pressure), psia
PT2	Computed total pressure downstream of a normal shock, psia
PW	Model surface pressure, psia
\tilde{P}	Fluctuating pressure, psi
Q	Dynamic pressure, psia
QDOT	Local heat transfer rate, Btu/ft ² -sec
QDOTREF	Fay-Riddell stagnation point heat transfer rate, Btu/ft ² -sec
R	Radius, in.
RE	Free-stream Reynolds number
RMS	Root-mean-square
R _N	Nose radius, in.
R()	Ratio of real-gas property () to the corresponding perfect gas property

S	Surface length from the stagnation point on a blunt body, in.
SF	Scale factor, mv/psi
T	Static temperature, °R
T.C.	Thermocouple
TDIS	Plant discharge temperature, °R
TF	Internal flange temperature, °R
TT	Local or average Mach 4 nozzle stilling chamber temperature, °R
TTB	Discharge temperature of gas-fired heater and total temperature upstream of V554 location, °R
TTC	Discharge total temperature of the electric air heater (Mach 10 stilling chamber total temperature), °R
TTREF	Reference total temperature, °R
TTS	Test section total temperature, °R
TW	Model wall temperature, °R
TWC	Mixing chamber wall temperature, °R
V454, V554	Valve opening, fractional or percent value
X,Y,Z	Tunnel coordinates referenced to the midpoint between the test section windows, or as specified (see Fig. 7), in.
x	Model surface distance, in.
x_b , x_e	Beginning and end of transition, measured along surface from stagnation point, in.
Δ ()	Difference in parameter ()
σ ()	Standard deviation in the uniformity of the distribution ()
ϕ	Roll angle, deg

SUBSCRIPTS

AVG	Average value
B	Bypass line
C	Primary line
C	Centerline